Volume 1:

Literature Review

Flow Slide Failure

of

Excavated Subaqueous Slopes

A study of the prediction of liquefaction potential and the retrogressive nature of flow slide failure prepared by:

Tim Helbo

February - August 1996

Delft University of Technology / Fugro Ingenieursbureau b.v.

"Über die Ursachen und das Wesen der Schwimmsanderscheinung gehen die Meinungen auch heute noch recht weit auseinander"

Karl Terzaghi (1925)

"I urge you to think originally and not be bound by any standing versions of explanations"

Victor H. Torrey III (1996)

Preface

Although flow slides have been studied intensively for a long time, the fundamental mechanisms leading to this kind of soil (structure) failure are still, at least partly, a mystery.

In September, 1995, Fugro Ingenieursbureau b.v. in Leidschendam suggested to study subaqueous slope failures resulting in a flow slide, within the framework of my graduate study program. I accepted in December, 1995, and started my research, conducted in partial fulfilment of the requirements for the degree Master of Science in the Delft University of Technology, on February 1st, 1996.

The report lying before you contains the results of a literature review on previously conducted research, related to flow slide failure. Apart from this Literature Review, a Directive for Engineering Practice (Volume 2) and Case History Study / Appendix (Volume 3) have been prepared, as part of the graduate study program.

I wish to extend my sincere thanks to J.L. Lindenberg[1], J.W. Heijting[2], J.D. van Rheenen[3], I. Herle[4], V.H. Torrey[5], J. Brouwer[6] and J. de Koning for their effort to help me further knowledge of theory and practice related to flow slide problems.

This graduate study program has been supervised by a graduate committee. The following advisors were seated in this committee:

A. Verruijt	Delft University of Technology
K. d'Angremond	Delft University of Technology
G.L.M. van der Schrieck	Delft University of Technology
M.Th.J.H. Smits	Fugro Ingenieursbureau b.v.

I wish to thank my graduate committee for its assistance.

Leidschendam, 12 September 1996,
Tim Helbo.

---

1 Ministry of Transport and Public Works (RWS), Department of Road and Hydraulic Engineering (DWW)

2 Heijting Aannemersbedrijf en Handelsonderneming bv

3 Province of Gelderland

4 Institut Für Bodenmechanik und Felsmechanik (IBF), Universität (TH) Fridericiana Karlsruhe, Germany

5 US Army Waterways Experiment Station, Vicksburg, MS, USA

6 Delft University of Technology, Faculty of Mechanical and Marine Engineering

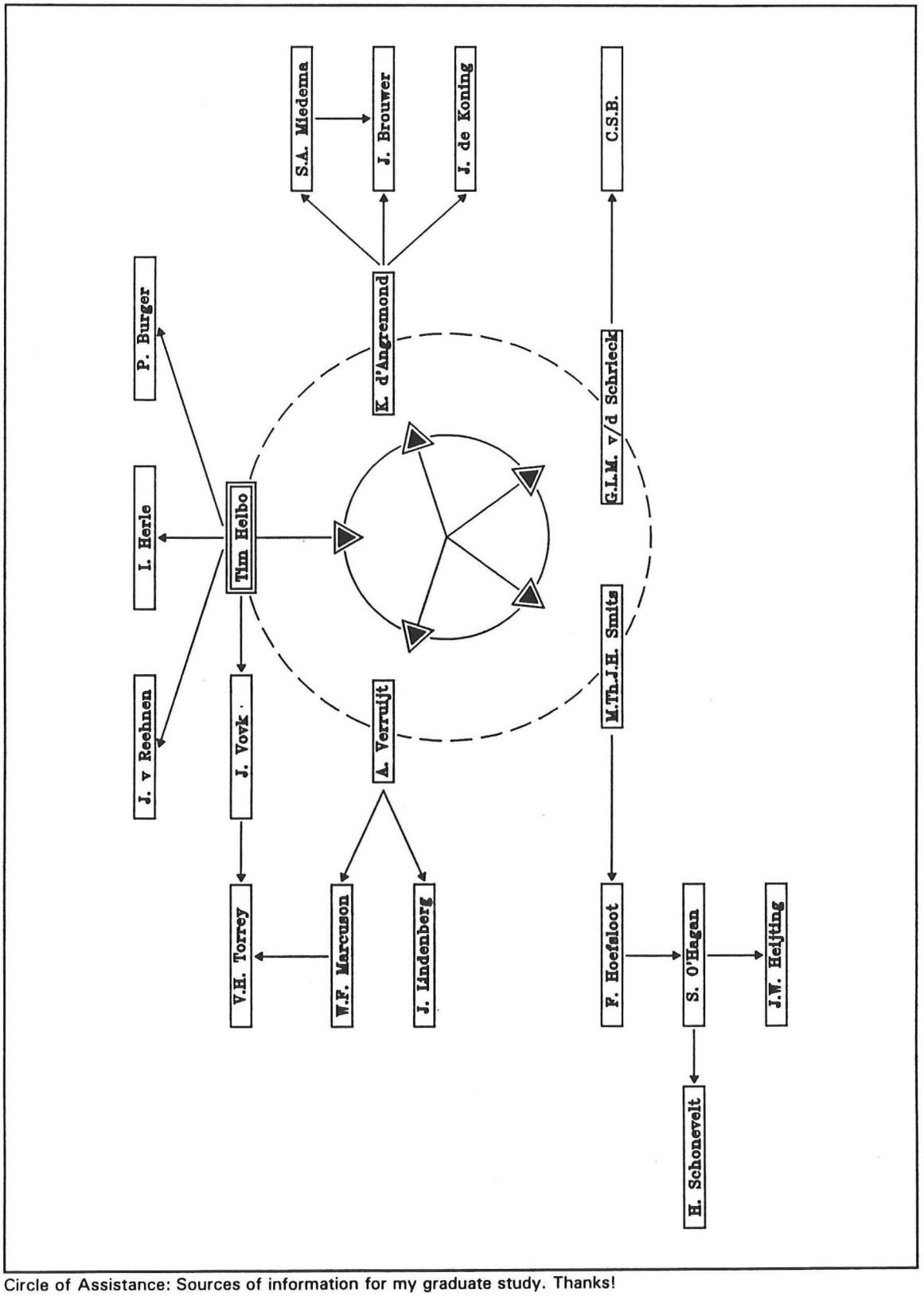

Circle of Assistance: Sources of information for my graduate study. Thanks!

Contents

Scope of Flow Slide Study

Introduction

Flow slides occur around the globe in deltic areas, along rivers and during dredging activities, like sand fill construction or sand mining. Many of these flow slide failures, which may involve the movement of millions of cubic meters of soil, pass and have passed unnoticed by mankind because they take place under water, according to Terzaghi (1956).

However, if flow slide failures cause changes in the morphology of rivers and coastlines, they do become known. Sometimes even uncomfortably, when they bring damage to our flood protection works, newly reclaimed land or other structures. The province of Zeeland in The Netherlands has a rich history in - sometimes destructive - flow slides, as mentioned by Lindenberg (1986a).

In the next few paragraphs, the general idea of what a flow slide is will be discussed, followed by the problem definition and formulation of the main aims of this flow slide study as well as the set-up of this Volume 1: Literature Review.

The Cause of Flow Slides

Generally, it is assumed that the cause of flow slide failures lies in the liquefaction of (part of) a sloping body. However, this explanation can be made plausible only when loose to very loose fine sand layers are encountered in the subsoil, over substantial depths. This is likely to be the case in areas where young marine sands have been deposited relatively fast and along (former) river beds where erosion and sedimentation of sand are continuously taking place.

Sometimes, flow slide failures are encountered in areas where the above does not hold, or at least does not give a credible explanation. Therefore, there is a tendency toward developing alternative explanations for the exact mechanisms, leading to flow slide failure. One of those alternative mechanisms may be the development of active banks, after initial oversteepening at the toe of a slope.

Because the actual mechanism, leading to flow slide failure, is not fully understood, the term "flow slide" is used to refer to the consequences of the failure, rather than to the cause of it. The distinctive features of flow slide failures are large soil displacements, very flat resulting subaqueous slope angles and embankments which have caved in. The fact that the term "flow slide" always has been related to the consequences of the failure, has lead the attention away from the actual causing phenomena. Thus, the misleading thought that liquefaction can be the only mechanism to be held responsible, could strike root.

Problem Definition and Formulation of Main Aims

Unexpected failure of subaqueous excavated slopes in the form of flow slides is considered in this graduate study. Excavated slopes are not the same as slopes constructed by means of hydraulic fill. Several recent flow slide failures in sand borrow pits, together with qualms in engineering practice about not knowing exactly what fundamental mechanism causes flow slide failure, gave cause for this study.

The knowledge that flow slide failure may be caused by either static liquefaction of (part of) a sloping body (also called spontaneous collapse)[7], or by the development of active banks, is taken as a point of departure. Liquefaction due to dynamic loading will be left out of consideration. Special attention will be paid to the geological circumstances of The Netherlands.

Herewith, the central problem of this flow slide study becomes: "How, from an engineering point of view, can we understand and predict flow slide failure of excavated (or being excavated) slopes, better?". To be able to answer the question at issue, we need to understand the fundamental mechanisms, leading to flow slide failure. Then, the soil properties may be related to the mechanisms and specific circumstances may be taken into account.

The main aim of this graduate study is to obtain insight in different mechanisms, possibly triggering flow slide failure and causing its retrogressive nature. Since the extent of a flow slide can be very large, and seems hard to predict, the prediction of the potential for failure will be the pith of the study, not the consequences of failure (Volume 1: Literature Review). The possible ways to model failure potential are investigated and their prediction values are evaluated on the basis of case histories (Volume 3: Case History Study / Appendix). With the insights obtained, an effort has been made to formulate a practical guideline for flow slide analyses, which should lead to improvements in engineering practice (this Volume 2: Directive for Engineering Practice).

Set-up of this Volume 2: Directive for Engineering Practice

As stated in the above, one of the main aims of this graduate study was to formulate a practical guideline for engineering and consultancy practice. This is how the report lying before you should be looked upon. Chapter 1 serves as an introduction to soil properties and phenomena, related to flow slide failure. The main aim of this chapter is to offer the reader some basic knowledge and to avoid semantics in the following chapters.

Chapter 2 describes the recommended static liquefaction potential analysis for engineering practice. It may serve as a directive in future analyses of the stability of subaqueous (to be) excavated slopes, as well in slope design as in failure reconstruction. Chapter 3 comprises a qualitative discussion on construction aspects and the dangers of the development of active banks. This chapter is meant to familiarize the reader with the possible contribution of active banks to flow slide failure. Conclusions and recommendations are summarized thereafter.

---

[7] Static liquefaction occurs as a result of contraction of the soil under a monotonically increasing shear stress level (see Chapter 1)

1 Liquefaction Potential Modelling

§ 1.1 Introduction

Flow slides may be caused by the static liquefaction of sand in a sloping body. The soil tendency to decrease in volume, when subjected to monotonically increasing shear stress, is a necessary condition for static liquefaction to occur. If soil has no tendency to decrease in volume, the soil has no *static liquefaction potential*. So, in order to be able to predict whether static liquefaction may occur - and hence whether there is a chance of a flow slide occurring - it seems logical to try to determine the susceptibility of the soil to static liquefaction, first.

The determination of the susceptibility of granular soils consists of two parts. Part one concerns the description of the soil behaviour by some constitutive law. Part two concerns the formulation of a stability criterion to test the soil behaviour. Given the in-situ conditions, static liquefaction potential may be predicted by subjecting the predicted soil behaviour to the stability criterion. Different approaches to liquefaction potential modelling may differ in their way of predicting the soil behaviour or in their formulation of a stability criterion.

§ 1.2 Methods Based on the Theory of Steady-State Soil Mechanics

§ 1.2.1 Introduction

Instability and *failure* are two different aspects in the behaviour of soil. However, instability may lead to failure. Therefore, in the steady-state approach, the point from where typical stress states may cause instability, is taken as the criterion for liquefaction potential.

The common statement of the group of researchers, that follow the steady-state theory, is that, even before any research is done on the contractive behaviour and the development of excess pore pressure, something may be said about the susceptibility of soils to liquefaction. They state that the analysis to determine static liquefaction potential is an ordinary stability analysis, not a deformation problem. Their approach bears no relation between soil deformation and the change in void ratio or settlements that may occur. The steady-state shear strength is the residual shear strength of soils, after continued deformation. Poulos (1981) defined the steady state of deformation as follows:

> "THE STEADY STATE OF DEFORMATION FOR ANY MASS OF PARTICLES IS THAT STATE IN WHICH THE MASS IS CONTINUOUSLY DEFORMING AT CONSTANT VOLUME, CONSTANT NORMAL EFFECTIVE STRESS, CONSTANT SHEAR STRESS, AND CONSTANT VELOCITY. THE STEADY STATE OF DEFORMATION IS ACHIEVED ONLY AFTER ALL PARTICLE ORIENTATION HAS REACHED A STATISTICALLY STEADY STATE CONDITION AND AFTER ALL PARTICLE BREAKAGE, IF ANY, IS COMPLETE, SO THAT THE SHEAR STRESS NEEDED TO CONTINUE DEFORMATION AND THE VELOCITY OF DEFORMATION REMAIN CONSTANT.".

The *steady-state line* is an approximately straight line in the void ratio - (log) stress plane, that connects all combinations of void ratios and stresses, measured during the steady state of deformation. In the following paragraphs, use and verification of the steady-state theory, with respect to static liquefaction potential prediction, will be clarified. The development of the work by various researchers, as studied here, is presented in the table below:

1936	1985		1987	1992	1995
CASAGRANDE	POULOS	SLADEN	KRAMER	LADE	DI PRISCO
	CASTRO	D'HOLLANDER	SEED		MATIOTTI
	FRANCE	KRAHN			NOVA

§ 1.2.2 A Liquefaction Evaluation Procedure by Poulos *et al.*

Poulos *et al.* (1985) state that liquefaction and flow slides may occur when the driving shear stress is greater than the minimum shear resistance of the soil, or steady-state shear strength, only. According to Poulos *et al.* (1985), the undrained steady-state shear strength, S_{su}, is a function of the soil properties (grain-size distribution and particle shape) and the in-situ void ratio, only. They state that as long as the driving shear stress, τ_d, is smaller than S_{su}, the soil has no liquefaction potential. Since S_{su} is the minimum strength a saturated contractive soil can have in undrained shear, no volume decrease tendency or excess pore pressure will develop. It is reasoned that no strength reduction, due to loss of effective stress, will occur.

Poulos *et al.* (1985) propose a liquefaction evaluation procedure in their paper that will be clarified here. The procedure is based on concepts from earlier work of Casagrande. The evaluation procedure consists of five steps:

1] Determine in-situ void ratio,
2] Determine steady-state void ratio as a function of effective stress,
3] Determine undrained steady-state strengths for 'undisturbed' specimens,
4] Correct the measured undrained steady-state strengths to the in-situ void ratio, and
5] Calculate in-situ driving shear stress and factor of safety.

The determination of the in-situ void ratio is, as in all other liquefaction evaluation procedures, the most sensitive step. It is very difficult to determine the in-situ void ratio, because disturbance, i.e. decreasing the in-situ void ratio[8], of the soil, during sampling, transportation to a laboratory or reconsolidation to in-situ stresses, is practically inevitable. Poulos *et al.* (1985) propose either *fixed piston sampling*, *freezing of the ground and coring*, or *sampling in test pits* to obtain the most accurate results possible.

[8] A very small increase in density - or decrease in void ratio - may convert a sample from a state in which it is liquefiable to a state in which it is not.

Next, the steady-state void ratio, as a function of effective stress, is determined by conducting five or six, strain-controlled[9], undrained triaxial tests, on reconstituted specimens. The specimens are tested under an initial void ratio - effective stress combination, well above the steady-state line. During the test, the contractive sample will follow a stress-strain path, showing a peak stress at a certain strain, and a stress fall thereafter, accompanied by large strains. The logarithm of the measured resulting minor principal stress is plotted against the corresponding void ratio.

The best fit through the points, obtained by the tests, is called the steady-state line. For stability analyses, it is convenient to plot the steady-state line in terms of the undrained steady-state shear strength. The following equations are used:

$$S_{su} = q_s \cos\phi_s$$

$$\sin\phi_s = \frac{q_s}{\bar{\sigma}_{3s} + q_s} = \frac{q_s}{(\bar{\sigma}_{3c} - \Delta u_s) + q_s}$$

$$q_s = \frac{\sigma_{1s} - \sigma_{3s}}{2}$$

in which the factor $\sigma_{1s} - \sigma_{3s}$ = the principal stress difference at the steady state from the triaxial test, $\bar{\sigma}_{3s}$ = effective minor principal stress at the steady state, $\bar{\sigma}_{3c}$ = effective minor principal stress (or confining pressure) at the start of shear (after consolidation), Δu_s = pore pressure induced in the specimen at the steady state of deformation, and ϕ_s = steady-state friction angle (in terms of effective stress). The quantities q_s, $\bar{\sigma}_{3c}$ and Δu_s are obtained directly during the triaxial tests.

Step 3 comprises the determination of the in-situ steady state, by conducting a series of *consolidated* undrained triaxial tests performed on 'undisturbed' samples, from the zone being evaluated. The resulting stresses and void ratios should be close to the steady-state line. The points may fall little above or below the steady-state line. Sufficient tests are needed to determine the average in-situ steady-state strength, reliably.

Thereafter, the in-situ shear strength is estimated. The procedure is presented in Figure 1. The trend of the in-situ steady-state line is assumed to be parallel to the steady state line, constructed from the tests on the compacted specimens. The shear strength, corresponding with the in-situ void ratio on the assumed steady-state strength line, through a particular steady-state point of one of the 'undisturbed' tests, is the estimated in-situ undrained steady-state strength.

The final step is to calculate the driving shear stress in the soil. This may be done by conventional limiting equilibrium approaches. If its average value is less than the estimated in-situ undrained steady-state strength, in all zones along the trial surface, then, it is postulated, liquefaction cannot occur.

---

9 Poulos *et al.* (1985) propose strain-controlled tests, but Sladen *et al.* (1985) report no significant difference between steady state parameters determined by stress or strain-controlled tests. Hence, they conclude that, for practical purposes, the critical state and steady state may be assumed one and the same for sands.

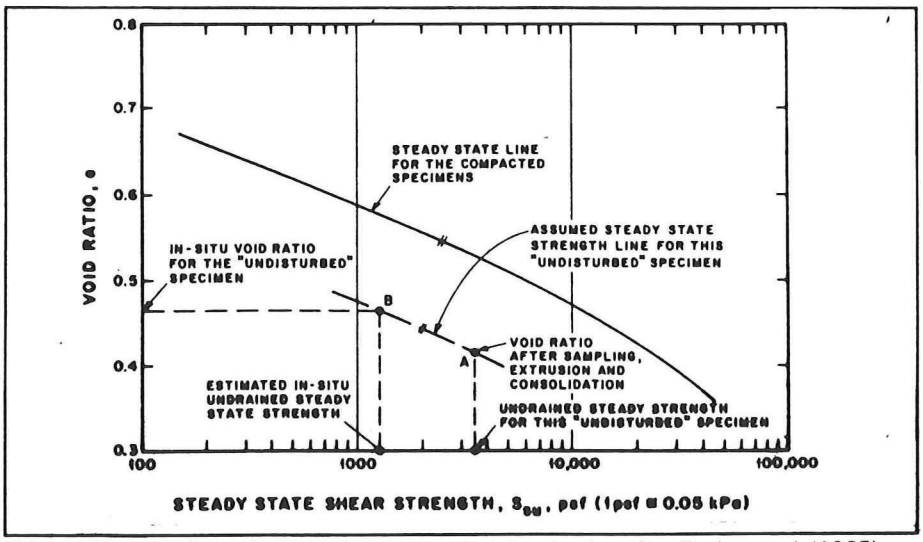

Figure 1 Undrained steady-state shear strength determination after Poulos *et al.* (1985)

The factor of safety against liquefaction is defined as:

$$F_l = \frac{S_{su}}{\tau_d}$$

According to Poulos *et al.* (1985), the entire mass is in *unstable equilibrium*, when the value of F_l is less than 1, or $\tau_d > S_{su}$. When this is the case, liquefaction and a flow slide may thus be triggered by any disturbance. They do add, however, that the disturbance must be large enough, and of sufficient duration, to indeed trigger liquefaction.

§ 1.2.3 A Collapse Surface Definition in the Void Ratio - Stress Space by Sladen *et al.*

Introduction:

The basis for the liquefaction failure analysis of Sladen *et al.* (1985), lies in large-scale flow slides during the hydraulic placement of an artificial island berm in the Beaufort Sea. However, the idea holds for excavated slopes as well.

Their main interest was to develop a method for back analysis of the slides. As such, it has a nature different from the steady-state method discussed before. Sladen *et al.* (1985) point out several shortcomings of the original reasoning of steady-state followers, and classify the original approach suitable for design purposes (as opposed to back analysis purposes), only. According to Sladen *et al.* (1985), the steady-state method makes no claim to explain the following observed features of the liquefaction phenomenon:

First, failure actually occurs at shear stress levels very much higher than the steady-state shear strength, as is evidenced by the extremely flat post-failure profiles encountered. Second, it incorrectly predicts deep failure planes to be more critical than shallow ones. Therefore it cannot explain the retrogressive nature of the liquefaction process. Third, no comment is made on the influence of the in-situ stress state on liquefaction potential.

In their work, Sladen *et al.* (1985) take the conclusion that the failed hydraulic fills must have been in a stress state where a very small undrained disturbance could lead to excess pore pressures and loss of shear strength, as a point of departure. They assume that this stress state relates to the peak deviator stress, measured in triaxial tests, and that this stress state may have developed under drained conditions. Because they consider liquefaction an equilibrium problem, they further state that the steady state is a condition of Mohr-Coulomb shear failure. As such, it follows that the effective normal stress and shear stress in the steady state are uniquely related by the angle of internal friction in the steady state.

Construction of the collapse surface:

The observation that the peak strengths, measured in undrained triaxial tests on loose samples, fall on a straight line in the q - p' stress plane, and that the position (not the slope!) of this line changes only with the void ratio, has given rise to the concept of a collapse surface in the three-dimensional void ratio-stress space.

To determine the shape of the collapse surface, a series of undrained load-controlled triaxial tests have been conducted, at different void ratios, according to the method proposed by Castro *et al.* (1982). The results (peak and steady-state stresses) of the tests were corrected for membrane penetration. Plotting the corrected results in the q - p' - e space yielded the collapse surface, as presented schematically in Figure 2 on page 8.

Use of the collapse surface:

Sladen *et al.* (1985) state that for (spontaneous) liquefaction to occur, the soil state has to reach the collapse surface (under drained conditions), before the shear stress suddenly exceeds the steady-state strength.

As it is possible to formulate the collapse surface in terms of parameters, directly analogous to a Mohr-Coulomb failure criterion, these parameters may be used in limiting equilibrium analysis to evaluate liquefaction potential[10]. To apply the proposed method as a design tool, it is *only* necessary to know the steady-state shear strength of a soil and the slope of the collapse surface.

Knowing the slope geometry and the likely range of ϕ_l, it is possible to estimate the steady-state shear strength prior to failure, and hence its state in the void ratio - shear stress - normal stress space, in back analysis.

---

10 For convenience it is assumed that the intermediate principal stress has no influence on shear strength, which can then be described in terms of a relationship between major and minor effective stress at failure, when applying data obtained from triaxial tests to limit equilibrium.

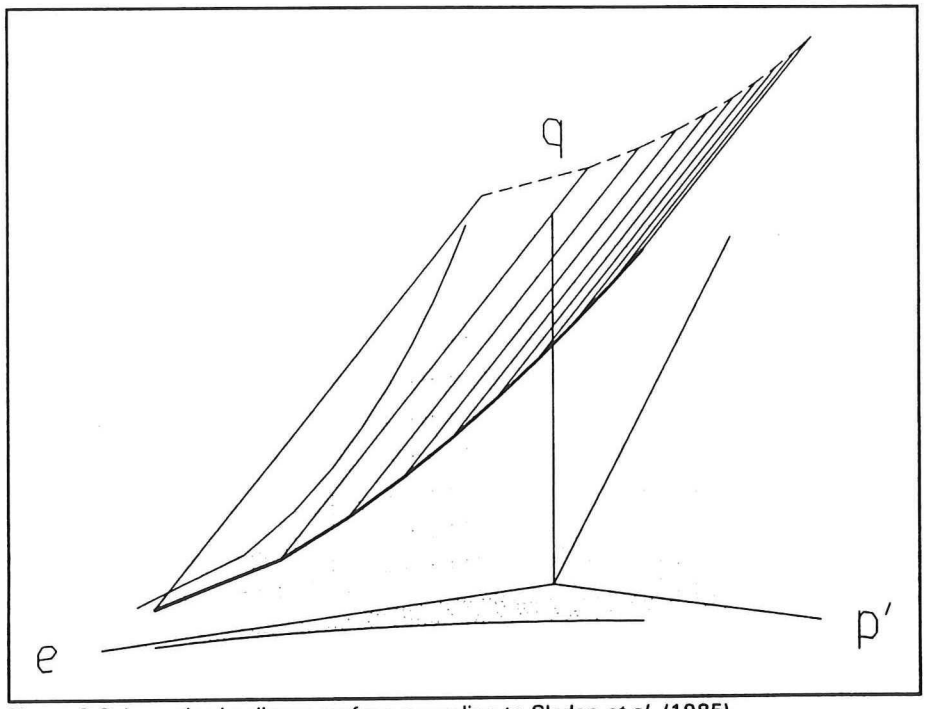

Figure 2 Schematized collapse surface according to Sladen *et al.* (1985)

§ 1.2.4 An Instability Line Definition in the Stress Surface by Lade

Definition of the instability line:

According to Lade (1992), commonly two criteria for failure of soil are employed in interpretation of results of triaxial tests. The first predicts failure when the principal stress difference, or deviator stress, $(\sigma_1 - \sigma_3)$, reaches a maximum. The second predicts failure when the principal effective stress ratio, (σ_1'/σ_3'), reaches a limiting value.

Lade (1992) prefers to refer to the steady state as the *ultimate state*. He formulates the ultimate-state instability definition as follows:

> "THE CONDITION OF MAXIMUM STRESS DIFFERENCE DOES NOT CORRESPOND TO A TRUE FAILURE CONDITION, BUT RATHER TO A CONDITION OF MINIMUM STRESS DIFFERENCE AT WHICH INSTABILITY MAY DEVELOP INSIDE THE TRUE FAILURE SURFACE. ...INSTABILITY MAY BE INDUCED ANYWHERE BETWEEN THE $(\sigma_1 - \sigma_3)_{max}$ CONDITION AND THE TRUE FAILURE SURFACE DESCRIBED BY $(\sigma_1'/\sigma_3')_{max}$.".

The line connecting all tops of a series of effective stress paths, in the q - p' plane, from consolidated undrained triaxial tests on loose soil provides the lower limit of the region of potential instability. This line represents Lade's instability line. Lade (1992) found from experiments that it is a straight line through the ultimate-state point. Because the ultimate strength of loose soils is very low, Lade (1992) states that, for practical purposes, the ultimate-state point can be assumed to be the same as the origin of the q - p' plane.

As the void ratio of the sand decreases, the instability line moves up and away from the origin, and it crosses the failure line at a point corresponding with the steady-state, or critical-state, value of p'. The instability line may be described as a linear function in the q - p' plane with slope ϕ_i and intercept c_i with the q axis. In his further analysis, Lade uses average values found by Sladen *et al.* (1985): $\phi_i = 17°$ and $c_i = 20\ kPa$, which he considers typical values for loose sands.

Construction of a region of potential instability in a subaqueous slope:

The method of analysis of potential instability of a slope, proposed by Lade (1992), comes down to the following steps:

1] Determine the failure line and the instability line for the given soil and void ratio, both in effective strength parameters, using consolidated undrained triaxial compression tests with pore pressure measurements,
2] establish the approximate states of stress in the slope from effective stress analyses, using a conventional slope-stability procedure and several slip surfaces,
3] compare the stresses with those required for potential instability, and
4] determine the region in the slope (if any) that may become unstable.

As an approximation, circular slip surfaces may be evaluated to determine the stress state in a slope. Taking the Mohr-Coulomb failure criterion as a point of departure and assuming that along a slip surface the factor of safety is constant, the stress states along a given circle are located on a straight line given by:

$$\tau = \frac{c' + \sigma' \tan\phi'}{F} = c_d' + \sigma' \tan\phi_d$$

For cohesionless soils $c' = c_d' = 0$. It may be observed that, for some circles in the slope, this line is located in a *region of potential instability*. To determine at which points on each slip circle the stress state enters the region of potential instability, the following criterion is evaluated and plotted as a function of the distance to the toe of the slope:

$$\frac{\tau - c_i'}{\sigma'} \geq \tan\phi_i$$

Plotting and connecting the calculated points of each of the slip circles in the slope, generates the region of potential instability. See for Lade's example Figure 9.

It is stressed that instability is not produced along a particular slip surface, but rather, in a volume of soil within the slope. Hence the term *region of potential instability*. The region of potential instability is specific to the slope inclination and soil parameters of the given soil type. The relative magnitude of the potentially unstable region increases with slope height. Lade (1992) further finds that the region of potential instability diminishes for a particular (low) slope hight, because then the stresses do not reach up into the critical stress region, between the instability line and the failure line.

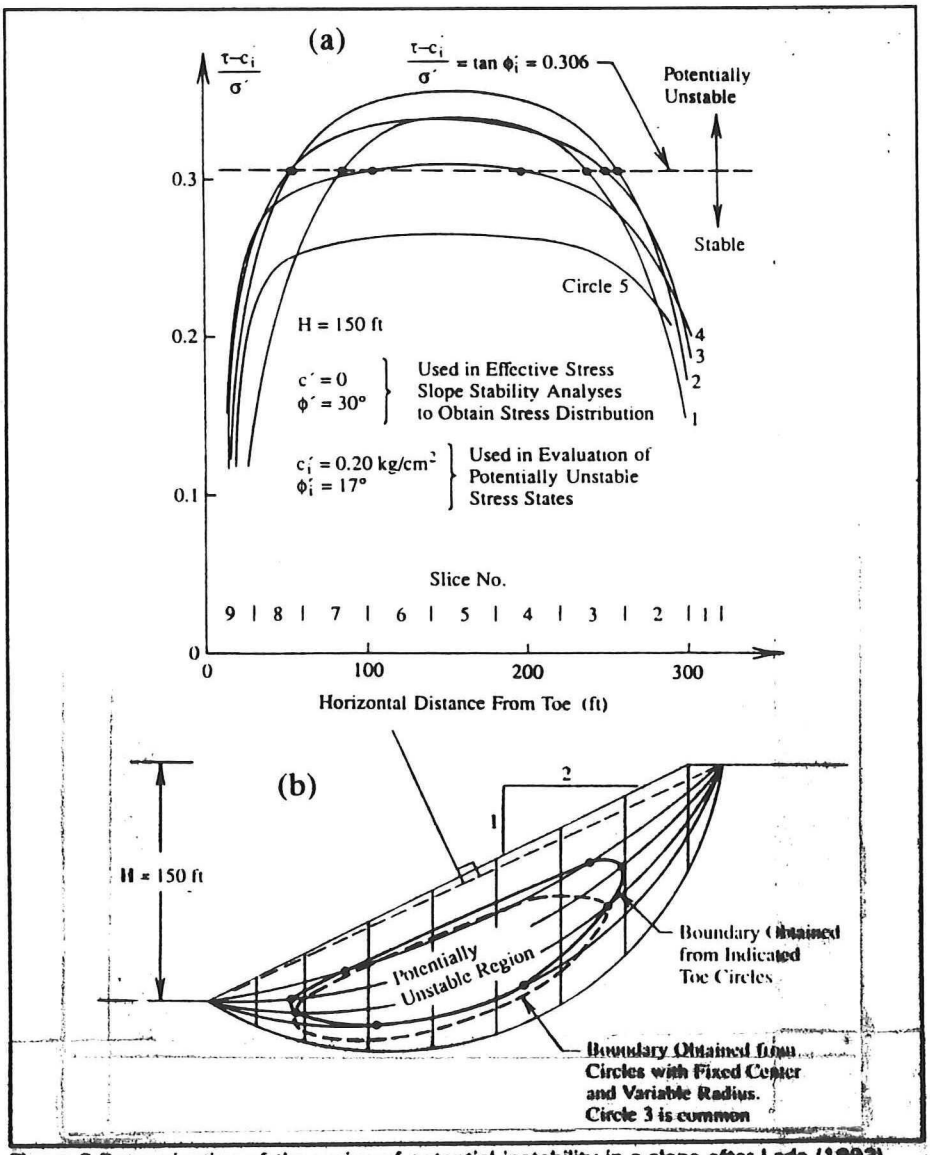

Figure 3 Determination of the region of potential instability in a slope after Lade (1992)

§ 1.2.5 Parametric Verification Study of Kramer *et al.*

Kramer *et al.* (1987) performed an extensive series of laboratory experiments to verify the validity of the steady-state liquefaction predictions. Also, they performed a parametric study to determine the effect of variations of the main parameters on the static liquefaction resistance. In short, they conclude that:

1] At relative densities greater than those corresponding to the steady-state line (see Poulos *et al.* (1985)), the soil will exhibit dilative behaviour (see also Lindenberg *et al.* (1981)), and there will be no potential for liquefaction. For soils that do display contractive behaviour, the static liquefaction resistance is found to decrease with decreasing relative density. Hence the potential for the initiation of liquefaction increases with decreasing relative density, or increasing in-situ void ratio,

2] The deviator stress under undrained conditions, required to initiate liquefaction, can be seen to increase as the confining pressure is increased. So, the static liquefaction resistance decreases with decreasing confining pressure and the potential for the initiation of liquefaction increases with decreasing confining pressure[11],

3] The static resistance of a sand decreases as the level of initial shear stress increases. Consequently, the potential for the initiation of liquefaction can be seen to increase with increasing initial shear stress level and may be very high at high levels of initial stress. This leads to the conclusion that the increase in shear stress, required to initiate liquefaction, should be seen as the difference between the static liquefaction resistance and any initial shear stress.

§ 1.3 The Classical Dutch Approach

§ 1.3.1 History of Dutch Flow Slide Research

In fact, there have been two factors of influence on the Dutch approach to liquefaction potential modelling in the Dutch soil mechanics history. First, a lot of practical data were available, mainly from liquefaction induced flow slides in the province of Zeeland. Second, several fundamental research programs conducted by Delft Geotechnics and Delft Hydraulics have brought insight in the basic phenomena.

Wilderom (1979) made an extensive inventory of the geometric characteristics of the geomechanical instabilities which, occurred in the province of Zeeland, and have been recorded since the second half of the 19th century. Lindenberg (1985) used Wilderom's result to sketch the state-of-the-art in flow slide consultancy.

Within the framework of Applied Research of the Ministry of Public Works (TOW), Begemann *et al.* (1977) and Lindenberg *et al.* (1981) studied the critical void ratio of sand, to verify the relationship between the initial void ratio of a sand body and its potential for liquefaction, as stated by Terzaghi (1925) (see also Volume 2: Chapter 1).

Large scale model tests on simulated flow slides have been conducted between 1973 and 1976 to stimulate the understanding of the flow slide phenomenon. In 1987 pore water pressure development during liquefaction and lateral spreading of liquefied soil was studied. The best flow slide recordings, yet, have been made in 1988, during the study of the construction of sand bodies under water. Bezuijen *et al.* (1988) and Mastbergen *et al.* (1988) reported on these tests.

§ 1.3.2 Critical Density Research and the Prediction of Undrained Sand Behaviour

Original definitions of critical density:

We can classify the classical Dutch liquefaction potential modelling as an attempt to find a correlation between pore pressure response and volume change tendency of dry soils. The basis for this approach lies in the research on the *critical density* of sand.

---

[11] On the other hand, the critical void ratio can be observed to decrease with increasing confining pressure.

The concept of critical density or critical porosity was first introduced by Casagrande in 1936. He supposed, based on the results of *direct shear* tests, that the final density attained by all samples of the same type of sand, with different initial densities, would be identical.

Two years later, in 1938, Casagrande formulated another definition of the critical density of sand because the former turned out to be unsuitable as a basis for criteria related to liquefaction and flow slide sensitivity. This second definition of Casagrande was based on ordinary drained triaxial tests. It was defined as the initial density for which, at the instant of applying the top deviator stress, no volume deformation of the sample occurs, in relation to the initial density. Casagrande's second critical density appeared smaller than the first. He concluded that the critical density is a function of the normal stress level (confining pressure).

In 1948, Geuze introduced an even safer critical density criterion because he supposed that the volume decrease at the start of a triaxial test would lead to high excess pore pressures under undrained conditions. Geuze conducted ordinary drained triaxial tests with constant ($\sigma_V' + \sigma_H'$) and measured the maximum (negative) volumetric strain, which he plotted against the initial porosity of the sample. He found an upper and lower limit to the critical density, as shown in Figure 4, and stated that only the lower limit can provide a save criterion.

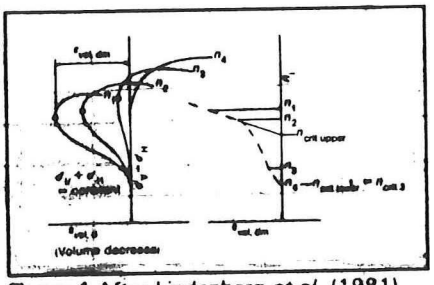

Figure 4 After Lindenberg *et al.* (1981)

Definition of dry critical void ratio:

Geuze's definition of critical density, which will be referred to as "critical void ratio" from this point on, has been used in the classical Dutch approach to liquefaction potential modelling as the *dry critical void ratio*. This dry critical void ratio is determined by conducting a series of ordinary drained triaxial tests - usually 3 to 6 - with samples of different initial void ratios. In order to eliminate any volume deformation other than caused by dilatancy or contractancy (see Volume 2: Chapter 1), the average normal stress $\frac{1}{3}(\sigma_V' + 2\sigma_H')$ is kept constant. This, in fact, means that during the tests the stress path $\sigma_H' = -\frac{1}{2}\sigma_V'$ is run through.

Definition of wet critical void ratio:

As well as there is a critical void ratio for samples subjected to drained triaxial testing, there is one for samples subjected to undrained triaxial testing. This critical void ratio was referred to as the *wet critical void ratio* by Begemann *et al.* (1977) and Lindenberg *et al.* (1981). It is defined as the void ratio of the sample which just not liquefies under undrained loading, but hardens and further behaves as predicted by the steady-state theory (see Figure 5).

It appears that the wet critical void ratio is somewhat higher than the dry critical void ratio. This difference lies in the fact that, in order to liquefy, pore pressures must develop in the sample. Pore pressures develop due to a volume decrease tendency, for which a void ratio just above the no-volume-change-at-all limit (dry critical void ratio) is required.

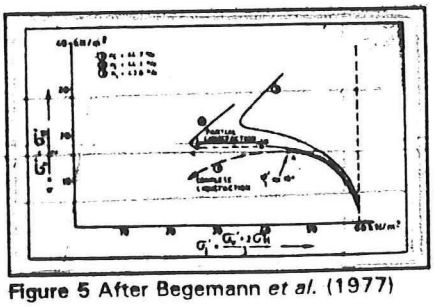

Figure 5 After Begemann *et al.* (1977)

The undrained triaxial tests are supposed to describe the in-situ behaviour of the soil best, but Lindenberg *et al.* (1981) stated in their paper that the wet critical void ratio, obtained from such a test, is an inaccurate criterion as a basis for liquefaction potential prediction. The statement was mainly based on intuitional motives. It was pointed out that there are some problems and difficulties with undrained testing which make the results less reliable. Disadvantages of undrained tests that were pointed out were the risk of performing tests on insufficiently saturated samples and the problem of membrane penetration during testing (see also Lade *et al.* (1977)), both leading to lower excess pore pressures, and hence a higher prediction of the wet critical void ratio.

§ 1.3.3 Liquefaction Potential Modelling

Lindenberg *et al.* (1981) tried to avoid the problems and difficulties with undrained triaxial testing by calculating the stress path development during undrained testing, based on the results of drained tests. Calculation appeared possible and conducted more reliable results. For this reason the results of drained triaxial tests are used to predict undrained behaviour.

First, the strain measured during the drained triaxial tests is corrected for membrane penetration (see Stoutjesdijk *et al.* (1994c)). The correction depends on the relative density of the sample and the particle size. The relative density is determined from the in-situ void ratio and the maximum and minimum obtainable void ratios.

Second, relationships between relative shear stress and normalized shear strain (dilatancy curve) and between isotropic stress and volume strain (decompression curve) are derived from the corrected drained triaxial test results (see Stoutjesdijk *et al.* (1994c)). These two curves together are used to predict the undrained behaviour.

§ 1.3.4 Elastoplastic Modelling of the Soil Behaviour

The stress-strain behaviour of the soil is described by means of an *elastoplastic* model, as explained by Stoutjesdijk *et al.* (1994c). In this model $d\epsilon_z$ is presumed equal to zero. See for a definition sketch Figure 7. The isotropic stress, σ'_{vol}, is derived as:

$$d\epsilon_z = \frac{1}{E} \cdot (d\sigma'_z - \nu^* \cdot (d\sigma'_x + d\sigma'_y)) = 0$$

$$d\sigma'_z = \nu^* (d\sigma'_x + d\sigma'_y) \quad : \quad \sigma'_z = \nu^* (\sigma'_x + \sigma'_y)$$

$$\sigma'_{vol} = \frac{1}{3} \cdot (\sigma'_x + \sigma'_y + \sigma'_z) = \frac{1}{3} \cdot (1 + \nu^*) \cdot (\sigma'_x + \sigma'_y)$$

where ν^* represents a not purely elastic Poisson's ratio[12].

[12] The ratio of the magnitude of the induced diametral strain to the imposed longitudinal strain.

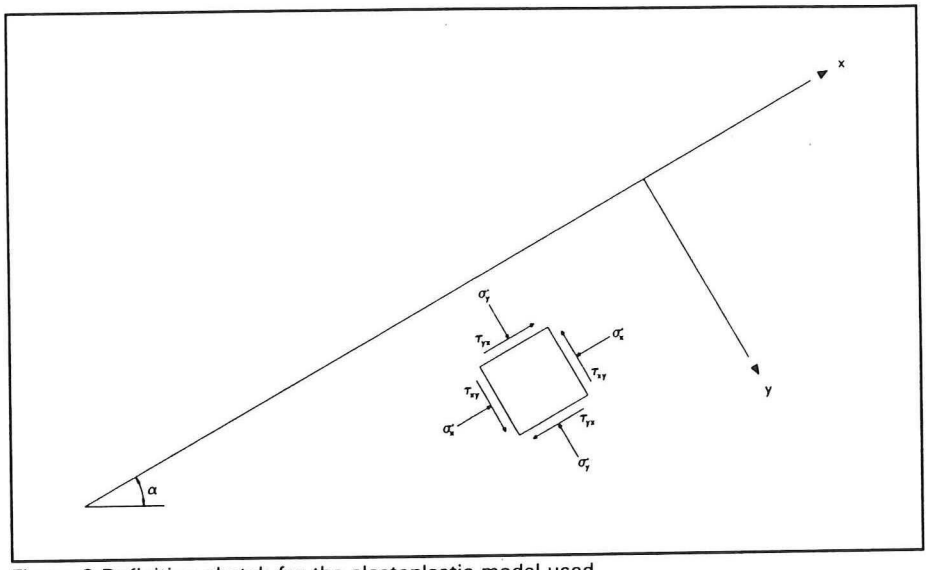

Figure 6 Definition sketch for the elastoplastic model used

The constitutive relations for elastic deformations that are used are:

$$d\gamma_{xy}^{e} = \frac{1}{G} \cdot d\tau_{xy}$$

$$d\epsilon_{x}^{e} = \frac{1}{E} \cdot (d\sigma_{x}' - \nu \cdot (d\sigma_{y}' + d\sigma_{z}'))$$

$$d\epsilon_{y}^{e} = \frac{1}{E} \cdot (d\sigma_{y}' - \nu \cdot (d\sigma_{x}' + d\sigma_{z}'))$$

where:

$$E = 3 \cdot (1 - 2\nu) \cdot K_{s}$$

$$G = \frac{E}{2 \cdot (1 + \nu)} = \frac{3 \cdot (1 - 2\nu)}{2 \cdot (1 + \nu)} \cdot K_{s}$$

K_s represents the bulk modulus of the soil. The constitutive relations for plastic deformations that are used are:

$$d\epsilon_{vol}^{p} = d\epsilon_{x}^{p} + d\epsilon_{y}^{p} = \frac{\partial}{\partial s} (\epsilon_{vol,\, d})\, ds$$

$$d\gamma^{p} = \sqrt{(d\gamma_{xy}^{p})^2 + (d\epsilon_{y}^{p} - d\epsilon_{x}^{p})^2} = \frac{\partial}{\partial s} \left[\frac{1}{G^{*}} \cdot \frac{s}{1 - (\frac{s}{s_{max}})^2} \cdot \left(\frac{\sigma_{vol}}{\sigma_{vol,\, 0}} \right)^{\nu} \right] ds$$

where s represents the relative shear stress and G^{*} represents a dimensionless plastic shear modulus.

Algebraically the stress-strain relations can be formulated in terms of small variations in the following form:

$$\begin{bmatrix} d\gamma_{xy} \\ d\epsilon_y \\ d\epsilon_x \end{bmatrix} = \begin{bmatrix} c_1 & c_2 & c_3 \\ c_4 & c_5 & c_6 \\ c_7 & c_8 & c_9 \end{bmatrix} \cdot \begin{bmatrix} d\tau_{xy} \\ d\sigma_y \\ d\sigma_x \end{bmatrix}$$

Herein the coefficient matrix C is called the 'flexibility matrix'. It contains the superposed elastic and plastic strains. For calculation routines of the coefficients $c_1..c_9$, reference is made to Stoutjesdijk *et al.* (1994c), pp. 66-71.

§ 1.3.5 The Stability Criterion

When stability is evaluated, small changes in shear stress are presumed. In an undrained situation the change in volume is equal to zero, and shear deformations can occur only. In case of a one-dimensional problem (infinite slope) it is presumed that $d\epsilon_x = 0$. Therefore $d\epsilon_y$ must be zero too. From the remaining system of equations the following stability criterion can be derived:

$$d\gamma_{xy} = \frac{1}{\lambda} \cdot d\tau_{xy}$$

The eigenvalue λ of the matrix C is used as the criterion for stability. It represents a complex of stresses, stress-strain relations and equilibrium conditions and has a unique value in each situation. If λ is smaller than zero, this indicates instability: the soil has liquefaction potential.

The stability evaluation procedure has been implemented in a computer program (SLIQ2D). To run this program, at least the following parameters must be established:

1] geometry of the sloping sand body,
2] in-situ void ratio,
3] minimum and maximum void ratios (from laboratory tests), and
4] drained triaxial test results. Further an estimation must be made of general parameters.

§ 1.4 The University of Karlsruhe Approach

§ 1.4.1 Introduction

In this paragraph the approach, which has been developed at the University of Karlsruhe in Germany, will be clarified. This approach comprises two major features: The description of soil behaviour by means of a so-called *hypoplastic constitutive law* and the formulation of a stability criterion for slopes, based on the ideas of Hill.

A noteworthy thesis that has been written on the subject is Raju's "Verflüssigung lockerer granularer Körper - Phänomene, Ursachen, Vermeidung" (1994). Problems with the stability of banks in the *Lausitzer Braunkohlerevier*, in the former German Democratic Republic, gave cause for the study, mainly. The work presented by Raju comprises not only the coupling of a hypoplastic model and Hill's stability criterion, but also the verification of stability predictions by means of laboratory tests. The essence of hypoplastic soil behaviour modelling and the idea behind Hill's stability criterion will be discussed in more detail in the next few paragraphs.

§ 1.4.2 Hypoplastic Modelling of the Soil Behaviour

Hypoplasticity as opposed to elastoplasticity

The conventional way to describe the mechanical behaviour of plastic deformable materials, such as soils, is the theory of elastoplasticity, like used in the aforementioned Dutch approach to liquefaction potential modelling. This theory is dependent on the development of stress paths during homogeneous deformation of the material and uses failure lines or surfaces as criteria for failure, unlike the theory of hypoplasticity.

The stress path dependency of the elastoplastic theory may be considered a major shortcoming in elastoplastic failure modelling. Large deformation is, inevitably, inhomogeneous. During the course of large deformations inhomogeneity, such as shear banding, bulging, internal buckling, etc. set on. Hence, useful stress-strain relations around the point of failure, needed as input for elastoplastic models, can hardly be extracted accurately from triaxial tests.

According to Kolymbas *et al.* (1995), hypoplastic models do not discriminate between elastic and plastic stains, but attempt to describe soil deformation on the basis of soil characteristics, only, by describing the evolution of the stress rate as a function of the stain rate. Hypoplastic models are assumed to describe soil behaviour not only well until failure, but also thereafter. Hence, both small deformations, as well as large deformations, may be predicted.

Another reason why hypoplastic models may be assumed to be superior to other models, especially when loosely packed granular materials are considered, is the fact that the contribution of the changing void ratio and stress-level to the stress development, pycnotropy and barotropy, respectively, are incorporated (Wu (1994)).

The formulation of the hypoplastic constitutive law

According to Kolymbas *et al.* (1995), he was the first to publish a hypoplastic constitutive law, in the year of 1977. The hypoplastic model consisted of one single tensorial equation, with a limited number of constants, which sought to describe the mechanical soil behaviour, without recourse to yield surfaces, etc.

Since its first publication, some improvements have been suggested. Wu accounted for non-feasible stress states, like tensile stresses[13], in 1992. He also introduced *pycnotropy* into the hypoplastic model. Pycnotropy accounts for the fact that granulates have the exclusive property that their void ratio does not depend uniquely on pressure, i.e. on the isotropic stress. Deformation parameters like stiffness, friction angle and dilatancy angle of loose granulates, depend on the void ratio. Thus, the outcomes of deformation experiments are not unique, but depend on the initial void ratio of the specimen.

---

13 *The capability of cohesive soils to support tensile stresses can be described by hypoplasticity if an appropriately internal stress is introduced, as will be shown in future publications* (Kolymbas (1995)).

In 1994, Wu further introduced *barotropy* into the hypoplastic model. Barotropy accounts for the fact that the stress level has an important effect on the material response (friction angle), in contrast with the general assumption in soil mechanics, that normalized stress-strain curves coincide for various stress levels e.g., in a triaxial test.

See for derivation and calculation of the parameters Raju (1994), pp. 10-12. Raju's result is a hypoplastic model, which may be integrated numerically, that describes the soil behaviour from four basic soil parameters, only. These are the strength of the granular material, the friction angle, the void ratio in the residual state (according to Raju approximately equal to the void ratio corresponding to the lowest possible density) and the void ratio after cyclic compaction (according to Raju approximately equal to the void ratio corresponding to the highest possible density), respectively. Three additional pycnotropy and barotropy constants must be determined from Oedometer and Triaxial tests.

§ 1.4.3 The Stability Criterion Suggested by Hill

Introduction to the 2nd order theory of stability:

Raju (1994) states that static liquefaction is not just a problem of equilibrium, or 1st order problem. Moreover, it is a stability problem of a system in equilibrium, or 2nd order problem. A simplified stability problem, of systems that are all in equilibrium initially, is indicated in Figure 7.

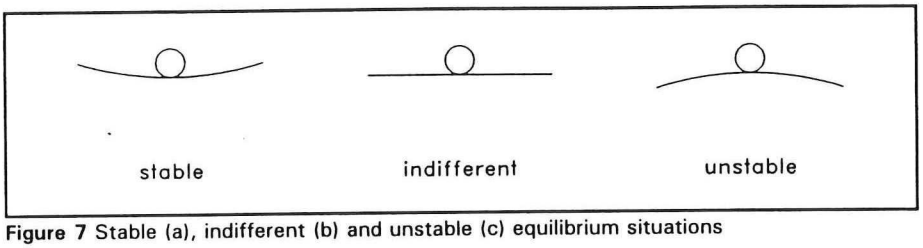

Figure 7 Stable (a), indifferent (b) and unstable (c) equilibrium situations

When the bullet is subjected to a small disturbance, it will return to its initial position of equilibrium without setting any energy free, in case a. The system is called *stable*. In case b the bullet will display, generally, large displacement, but again it will not set any energy free. In this case the system is called *indifferent*. In case c, the bullet will also display large displacement. However, the bullet will now convert potential energy into kinematic energy, unlike in case b, causing a growing displacement. The system is now called *unstable*.

From the above, it can be stated that a situation of equilibrium is stable when an infinitely small disturbance leads to an infinitely small displacement. Based on this statement, Hill suggested a stability criterion, saying that the nett work must be equal to zero (indifferent) or greater than zero, in order to not have a stable system. He defined nett work as the increase in internal energy minus the work employed by external forces.

Hill's suggestion may be clarified by considering a simple mass-spring system. When the mass is thought to be brought off balance, the work employed by the external force (gravity) is equal to the weight of the mass, integrated over the displacement. Because the weight of mass is a constant, we also say the work employed by the external force is equal to the gravity force times the displacement. The work employed by the spring is equal to the spring force, integrated over

the displacement. However, the spring force increases (normally) linear with the displacement. The resulting work employed by the spring is therefore bigger than the work employed by the gravity force and we speak of a second order problem of equilibrium. In this case the system is always stable.

Mathematical formulation of the stability criterion for slopes after Hill:

The use of Hill's criterion in the stability modelling of saturated slopes of loosely packed granular material under static loading, was suggested by Gudehus in 1993. For the mathematical formulation of the nett work the following expression is derived in Raju (1994):

$$\Delta^2 E = \int_V \dot{T}_g \frac{\partial v}{\partial x} dV > 0$$

where the $\dot{T}_g$ is known as the first Piola-Kirchhoff stress matrix (the stress state is related to the original geometry), acting on an arbitrary volume V, which is subjected to a displacement field characterized by $\delta u = v\delta t$. The nett work is calculated and evaluated according to a procedure displayed in Enclosure I on page 41. The preparations for stability analyses come down to the determination of the geometry (see ? for a schematic presentation) and in-situ void ratio (to test the stability criterion), the determination of the material parameters in a laboratory and calibration of the hypoplastic model.

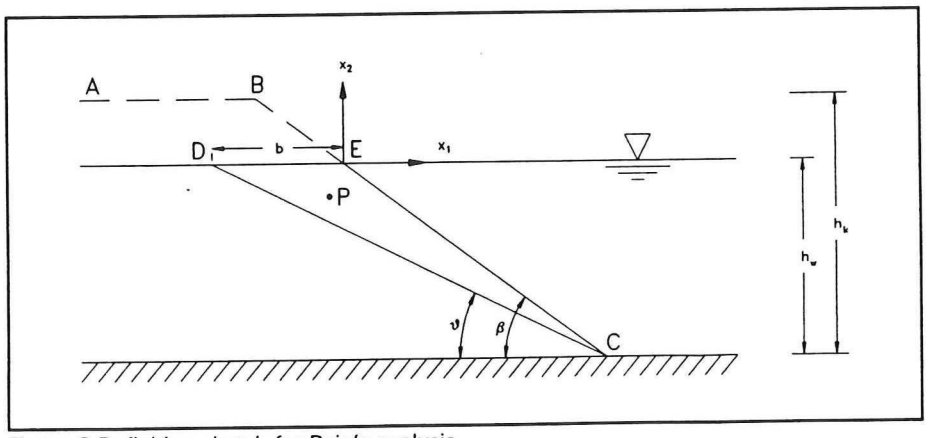

Figure 8 Definition sketch for Raju's analysis

The calculations of the nett work are repeated for all values of the angle ϑ, between 0 and slope angle β, to cover the whole geometry. For a more detailed description, reference is made to the work of Raju (1994), pp. 27-30.

Conclusions of Raju's parameter analyses and experiments:

After an extensive series of calculations, Raju finds that the nett work is positive for all possible angles, ϑ, corresponding with a stable slope, above a certain *kritische Porenzahl*, which is purely based on Hill's stability criterion. For $h_k = 45\ m$, $h_w = 40\ m$ and $\beta = 30°$, e_{kr} appears to be equal to a value of 0,68. For the same geometry, higher in-situ values of the void ratio indicate that the soil has liquefaction potential (on the basis of this analysis).

Raju's critical void ratio should not be confused with the critical void ratio, used in the other approaches to liquefaction potential modelling, which is based on the volume change tendency of soils, when subjected to shear stress. Sensitivity analyses further lead to the following conclusions:

1] e_{kr} decreases little with increasing stress level (overburden), indicating a higher susceptibility to liquefaction,
2] e_{kr} increases with increasing friction angle, which indicates a lower susceptibility to liquefaction, and
3] the stability decreases with increasing mobilized shear stress.

Experiments, conducted by Raju, confirm the existence of e_{kr}. The general conclusions on the susceptibility to liquefaction of slopes, expressed in terms of material properties, drawn on the basis of theoretical modelling and laboratory experiments are:

1] small particles cause low permeabilities, allowing high excess pore pressure to develop, which may lead to liquefaction,
2] (loosely packed) uniform particles exhibit highly contractant behaviour, which increases the susceptibility to liquefaction,
3] round particles cause lower friction angles and hence to a higher susceptibility to liquefaction, and
4] in-situ void ratios higher than e_{kr} indicate immediate liquefaction danger.

§ 1.4.4 Wet Critical Void Ratio Estimation with a Hypoplastic Model

Another possible advantage of a hypoplastic model lies in the prediction of the behaviour of soil in a triaxial test. Kolymbas *et al.* (1995) give an example of the such a model, for ordinary triaxial tests, with constant confining pressure, and explain how to calibrate it. The predicted behaviour seems to comply reasonably well with actual test results.

It may be possible to simulate wet critical void ratio tests with a single tensorial equation, as well, if small adjustments are made in the boundary conditions. Constant confining pressure implies that $\dot{\sigma}_3 = 0$. Suppose $\dot{\sigma}_3$ is set to $-\dot{\sigma}_1$, which would make the Mohr circles concentric along the stress path. The major advantage would be the fact that with one calibration, a series of tests, with different initial void ratios, may be conducted, to establish the point of collapse or theoretical liquefaction.

2 Modelling the Flow Slide Propagation

§ 2.1 Introduction

Once it has been determined that a slope has liquefaction potential, the next question will be how the liquefaction process will propagate in the soil. From experimental observations, see Kroezen (1982) and Silvis (1988), it is known that the liquefaction process has a retrogressive nature, meaning that the liquefied portion of the slope grows into the sand body.

If liquefaction cannot be indicated as the reason for the occurrence of a flow slide, alternative explanations must be sought. Torrey *et al.* (1988) suggest that the development of active banks in dilatant sands may result in flow slides. The development of active banks display a retrogressive nature as well.

It is not fully clear when or why the flow slide propagation comes to a halt. There might be a discontinuity in the soil profile, i.e. a lower void ratio or higher permeability. Discarding these irregularities and considering the soil a homogeneous and isotropic medium, several attempts have been made to describe the retrogressive nature of flow sliding.

In the next few paragraphs methods based on the research of pore pressures near moving underwater slopes and cutting forces in saturated sand, amongst others, will be presented briefly.

§ 2.2 Inverse Cutting Force Approach

§ 2.2.1 Basis of Inverse Cutting Force Approach

Meijer *et al.* (1976) and Van Os *et al.* (1987) conducted fundamental research within the framework of the Dutch dredging 'speurwerk'. They show that the assumption of linear elastic soil behaviour is not justified when rapid deformation is considered and recognize the role of dilatancy in the resistance of soil against deformation. That is, when densely packed sand is considered.

Further, their analyses are based on the observations from a moving coordinate system where the fixed coordinate x is transformed into $\xi = x - vt$, v being the travelling speed of the moving coordinate system.

Van Os *et al.* (1987) considered the failure of densely packed sand, when forced to deform by a cutting blade, as a continuous creation of *discrete sliding surfaces*, all of the same shape, where the porosity suddenly increases from n to $n + \Delta n$. This proposition was supported by experimental evidence. As an approximation, the process of failure was schematized as a thin sliding zone, moving through the soil with a speed equal to v.

§ 2.2.2 Inverting the Results of Research on Cutting Forces in Densely Packed Sand

Verruijt (1992) introduced the idea that the failure of loosely packed saturated sand may be described in a way similar to the force controlled failure of densely packed sand, as suggested by Van Os *et al.* (1987). Now, the sudden change in porosity is assumed to be negative, which means an decrease in void ratio. More specifically, it is assumed that there is a thin zone, of thickness d, at the slope surface, in which the porosity is Δn lower than in the natural state.

Verruijt follows Van Os *et al.* (1987) in rewriting the *storage equation*[14] assuming the soil particles and the pore fluid incompressible, the external fluid supply equal to zero, expressing the volumetric strain rate $\delta e/\delta t$ in terms the change in porosity, substituting Darcy's law and introducing the moving coordinate system. The final result is:

$$\frac{k}{\gamma} \nabla^2 p = - \frac{\nu}{1 - n} \frac{\partial n}{\partial \xi}$$

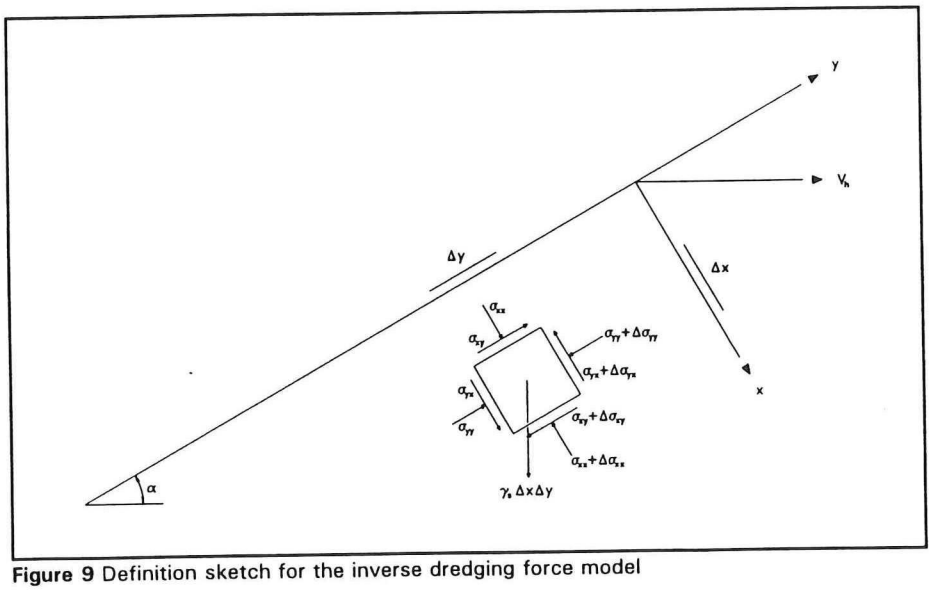

Figure 9 Definition sketch for the inverse dredging force model

A definition sketch of the failing slope is given in Figure 9. Decomposing the total stresses, employing Terzaghi's principle of effective stress, and writing the hydrostatic pressure component in the following form:

$$p = A + \gamma_w x \cos \alpha - \gamma_w y \sin \alpha$$

---

14 The *storage equation* is known from the theory of consolidation and was originally developed by Biot in 1941. It reads:

$$\frac{\partial e}{\partial t} = - n \beta \frac{\partial p}{\partial t} - \nabla \cdot q + g$$

See also Barends (1992).

the equations of equilibrium can be written in terms of effective stress, as follows:

$$\frac{\partial \sigma'_{xx}}{\partial x} - (\gamma_s - \gamma_w) \cos \alpha + \frac{\partial p}{\partial x} = 0$$

$$\frac{\partial \sigma'_{xy}}{\partial x} + (\gamma_s - \gamma_w) \sin \alpha = 0$$

when the slope is assumed to be infinitely long and all derivatives in y-direction are assumed to be equal to zero. Integration and substitution of σ' for σ_{xx}' and $-\tau$ for σ_{xy}' yields:

$$\sigma' + p = (\gamma_s - \gamma_w)\, x \cos \alpha$$

$$\tau = (\gamma_s - \gamma_w)\, x \sin \alpha$$

Solving the rewritten storage equation in one dimension for Δp yields:

$$\Delta p = \gamma_w\, d\, \frac{v}{k}\, \frac{\Delta n}{1-n}$$

Collection of the expressions for stresses and pore pressure in Coulomb's relation $\tau = \sigma' \tan \phi$ and some rewriting eventually yields an expression for the relative propagation velocity, v/k, of the failure surface[15]:

$$\frac{v}{k} = \frac{1-n}{\Delta n}\, \frac{\gamma_s - \gamma_w}{\gamma_w} \sin \alpha \cos \alpha \left(1 - \frac{\tan \alpha}{\tan \phi}\right)$$

The expression found by Verruijt shows that a positive propagation velocity is possible only if $\tan \alpha < \tan \phi$ and $\Delta h > 0$. Thus, he concludes, a slope flatter that the natural slope may display flow slide failure.

There is reason to doubt the validity of the expression derived by Verruijt, however. It predicts an unexpected maximum propagation velocity, midway between level ground and a critical slope with inclination (ϕ)[16] (see also Enclosure II). Figure 10 on page 24 was composed assuming the values of $\gamma_s = 20\ kN/m^3$, $\gamma_w = 10\ kN/m^3$, angle of internal friction $\phi = 30°$, porosity $n = 45\%$ and porosity jump $\Delta n = 5\%$:

§ 2.3 Mississippi Flow Slide Hypothesis

Along the southern part of the Mississippi River (below Baton Rouge), many flow slides have taken place, during the course of history. These flow slide failures have been thought to be caused by static liquefaction, during high discharges of the river. However, from extensive field investigations by Torrey *et al.* (1988) it was concluded that, although lenses with supercritical void ratios existed, the extent of such layers was small, compared to the volume of the displaced material in major bank failures. Also, it as emphasized that the average void ratio of the material concerned

---

15 Note that Van Os *et al.* (1987) used another coordinate system than proposed by Verruijt. This may be taken into account by transforming the increment forward, x, at the failure surface into $d \sin\alpha$.

16 For not densely packed soils, the inclination cannot be greater than imposed by the angle of internal friction, ϕ. Therefore, the expression can only be valid between 0 and ϕ.

was between the upper and lower critical void ratios (see Geuze (1948)), which made the material not particularly susceptible to flow slide failure.

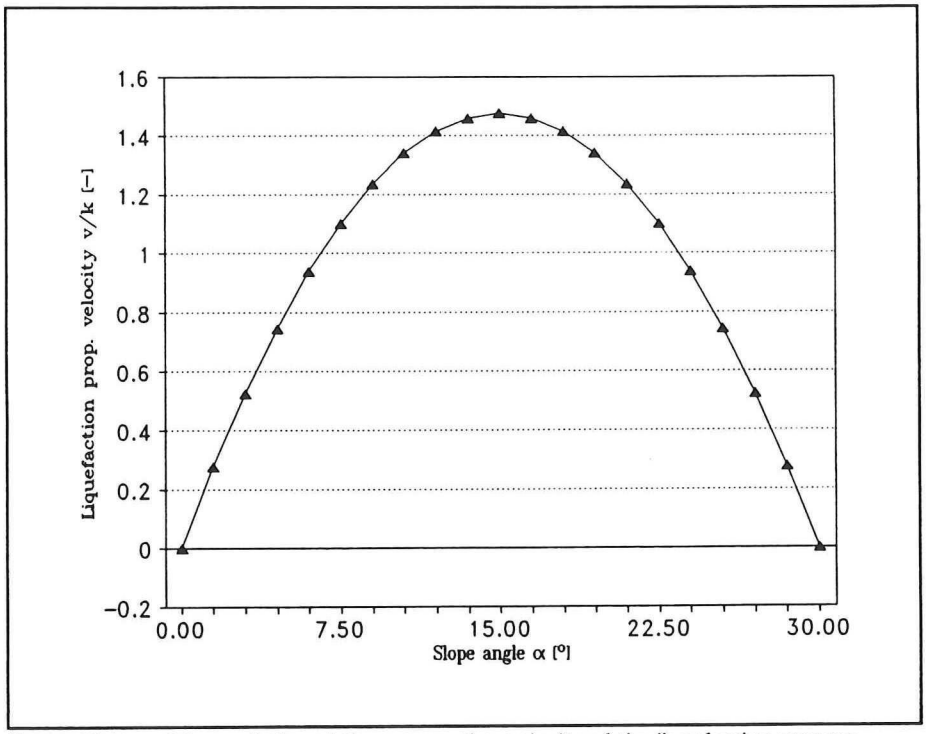

Figure 10 Verruijt's prediction of the propagation velocity of the liquefaction process

Therefore, an alternative failure mechanism was sought. Torrey *et al.* (1988) suggested that a plausible hypothesis could be found in the work of Padfield (1978). The hypothesis comes down to the statement that the dilative behaviour of the material is suspected to be responsible for the flow slide failures, instead of the contractant behaviour.

In fact, two theories have been coupled. As a point of departure the theory of active banks of Meijer *et al.* (1976) is taken. From this theory, the horizontal retrogression velocity, Z, of the initial oversteepened face, caused by severe scour at the toe of the slope during high discharges, is calculated:

$$Z = \frac{k\,\gamma'}{\nu'\,\gamma_w}\left[\frac{\sin(\alpha - \phi)}{\sin\phi}\right]$$

Herein are: k the permeability, γ' the effective unit weight, γ_w the unit weight of water, β the slope angle and ϕ the angle of internal friction. With estimated values of the void ratios in the undisturbed bed of 0.67 and at the free surface 0.75, the volumetric strain, ν', is assumed 0.048.

The vertical velocity, V, at which the base of the viscous carpet of grains, which is formed at the toe of the active bank, is calculated from the fall velocity of a single grain at infinite dilution, W_∞, and the particle volume concentrations in the dispersion, C_0, and the deposit, C_l:

$$V = \frac{C_0\,W_d}{\Delta C} \quad , \quad \Delta C = C_1 - C_0$$

The resulting prediction of the tangent of the run-out angle of the active bank is calculated as the vertical propagation velocity in proportion to the horizontal retrogression velocity, calculating the fall velocity of a grain, W_d, at concentration C_0, as $W_\infty (1-C_0)^n$, with $n = 4$:

$$\tan\alpha = \frac{V}{Z} = \frac{C_0 W_\infty (1 - C_0)^n}{Z \Delta C}$$

Unfortunately, the resulting slope angle appears very sensitive to variations in C_0, while the value of C_0 must remain a guess, in absence of experimental evidence. It has been tried to avoid this difficulty by estimating the horizontal travelling distance of the grains falling of the oversteepened face. From this analyses the encountered low run-out angles can be calculated.

Another noteworthy finding of Torrey *et al.* (1988) is that, from the relation found for the prediction of the horizontal travelling distance of the upper most grains in the fluidized carpet, it appears that the production of the active bank is an important parameter. The formation of the fluidized carpet is implicit in this relation.

The horizontal travelling distance of the grains varies linearly with the height of the active bank. In small scale tests, the horizontal travelling distance, in proportion to the production of the active bank, is such that the run-out angle is closer 30° than to the flat slope angles as were observed by Torrey *et al.* (1988). From this, they conclude that small scale tests are inappropriate to model flow behaviour.

3 Lateral Soil Displacement Modelling

§ 3.1 Introduction

Beside studies that concentrate on the prediction of liquefaction potential and the propagation of flow slide mechanisms into a slope, a small number of studies have been directed toward the prediction of the displacement of soil as a result of flow slides. Information of this type may be useful when a prediction of the extent of a possible failure is requested. All relations presented here are purely empirical and based on regression analyses of field data.

§ 3.2 Calculations of the *Rückgriffweite*

On the basis of observations on 37 liquefaction induced flow slide failures, which occurred in the *Lausitzer Braunkohlerevier* (mine tailings dams) in Germany, Vogt *et al.* (1991) suggested an empirical expression to predict retrogression of the top of a slope, as a result of the failure. In their analysis, they distinguish the following factors of influence (soil properties and soil model parameters are recognized but not used in this analysis):

- Circumstantial factors of influence:
  - the nature and intensity of the initiation of liquefaction
  - the direction of the (groundwater) flow (p = parallel, s = perpendicularly)
  - the liquefied soil flow condition (u = undisturbed, b = disturbed)
- Geometric and geohydrological factors of influence:
  - the slope angle, β, and slope height H_k
  - the height of the phreatic surface, H_{wk}, within the slope

From regression analyses, they found that the cave-in distance, x_r, is (mainly) a function of the initiation, slope angle, height of the slope and height of the phreatic surface. They derived the following expression:

$$x_r = \delta H_k \left[a \exp\left(-b \left(\frac{H_{wk}}{H_k} - 1.0 \right)^2 \right) - \frac{1}{2 \tan\beta} \right]$$

Under normal initiation conditions, δ equals 1.0. Under severe initiation, like fast changes in groundwater level or dynamic initiations, δ may vary between 1.2 and 1.8. The other variables should be picked from the table on page 28, depending on the flow direction and flow condition. The correlation coefficient, r, for the data interpreted and the number of flow slides related to the flow direction and flow condition, f, are presented as well.

Direction/condition	a	b	r	f
p/u	26.910	3.823	-0.872	11
p/b	13.977	3.838	-0.957	15
s/u	9.694	3.831	-0.931	5
s/b	5.759	4.340	-0.864	6

They also give an expression for the critical ratio between the height of the phreatic surface and the slope height, based on previous research by Förster:

$$\eta = 0.8 \left(\frac{H_{wk}}{H_k}\right)^{*} = 0.8\ 0.403\ I_D^{0.195} \left(\frac{1}{\tan\beta}\right)^{0.439}$$

It is emphasized that I_D is the relative density, based on porosity, instead of void ratio!

§ 3.3 Empirical Prediction of Liquefaction-Induced Lateral Spread

Another empirical model, which predicts the amount of horizontal ground displacement, is presented by Bartlett *et al.* (1995). Disadvantage of this method, with respect to this graduate study, is the fact that it is based in the induction of liquefaction by earthquake loading. Probably, the horizontal ground displacement as a result of static liquefaction-induced slope failure, will be considerably less.

The empirical model presented, was developed from multiple linear regression analyses of U.S. and Japanese case histories of lateral soil displacement (spread). Bartlett *et al.* (1995) observed two typed of lateral spreads. First, lateral spread towards a free face (e.g. incised river channel or abrupt subaqueous topographical depression). Second, lateral spread down gentle ground slopes, where a free face was absent.

The free-face component of the model reads:

$$\log(D_H) = -16.366 + 1.178\ M - 0.927\ \log R - 0.013\ R + 0.657\ \log W + 0.348\ \log T_{15} + 4.527\ \log(100-F_{15}) - 0.922\ D50_{15}$$

The ground slope component of the model reads:

$$\log(D_H) = -15.787 + 1.178\ M - 0.927\ \log R - 0.013\ R + 0.429\ \log S + 0.348\ \log T_{15} + 4.527\ \log(100-F_{15}) - 0.922\ D50_{15}$$

In the regression formulae, M represents the moment of magnitude of the earthquake, R the horizontal distance to the nearest seismic energy source or fault rupture in kilometres, W the free-face ratio 100 H/L (H = height of the free face; L = horizontal distance from the channel), S the ground slope in percent, T_{15} the thickness of the liquefied layer in meters (15 = SPT $(N_1)_{60}$ value), F_{15} the average fines content and $D50_{15}$ the mean grain size. A step-by-step explanation of the application of the lateral spread model is given by Bartlett *et al.* (1995).

Conclusions & Outlook

Perhaps, the most conspicuous conclusion that must be drawn from this literature review, is the fact that, during the cause of liquefaction and flow slide research history, far more effort has been put into the clarification of the potential of liquefaction of soils than into the description of flow slides.

This may be inspired by the idea of that prevention is to be preferred over curing. Besides, one may reason that the knowledge of the potential hazards, caused by flow slides, is only useful for risk evaluations. Probabilistics have barely been introduced into the modelling of liquefaction and flow slides.

A more fundamental reason lies in the fact that the process of retrogressively moving liquefaction fronts is too complex to model satisfactory, as yet, and requires more knowledge of the behaviour of soils, heavy viscous fluids and its relation to the known soil parameters, than available today. Hence, available models are very empirical in nature, and not very powerful.

Within the modelling of liquefaction potential, wide differences of opinion are present. The followers of the steady-state approach consider the question of whether liquefaction will occur a mater of equilibrium, whereas others find it a stability problem (definition of Hill). These differences may rest on the differences in aims of the researchers.

The steady-state theory offers a more simple approach than deformation-based theories (stability approach). It may be useful for practical application. On the other hand, the stability approach, together with a sophisticated soil behaviour model, offers good opportunities to describe the potential for liquefaction from a more scientific perspective. However, the latter requires extensive soil investigations and expensive parameter determination techniques, but can be very attractive for computer implication. The decision of the employment of one of both approaches may be based on risk and turnover.

Little research has been conducted to explain and predict the propagation of flow slide mechanisms (i.e. liquefaction and active banks) and the extent of soil displacement as a result of possible flow slides. This is the result of the fact that this type of information is of less use to engineering and consultancy practice and (even) more arbitrary than information on the susceptibility to flow slide failure.

In accordance with the original plan, with a lack of substantial field data however, this graduate study proceeds with a directive for engineering practice and a case history study of flow slides in sand borrow pits in The Netherlands.

References

BARENDS F.B.J. (1992), *Theory of Consolidation*. Lecture notes. Delft: Delft University of Technology, Faculty of Civil Engineering.

BARTLETT S.F. AND T.L. YOUD (1995), *Empirical prediction of liquefaction-induced lateral spread*. Journal of the Geotechnical Engineering Division, Proceedings of the American Society of Civil Engineers, Vol. 121, No. 4, pp. 316-329.

BEGEMANN H.K.S.PH., H.L. KONING AND J. LINDENBERG (1977), *Critical density of sand*. Proceedings 9th International Conference on Soil Mechanics I, Tokyo, Japan, pp. 43-46.

BEZUIJEN A. AND D.R. MASTBERGEN (1988), *On the construction of sand fill dams - Part 2: Soil mechanics aspects*. Modelling Soil-Water-Structure Interactions, pp. 363-371. Rotterdam: Balkema.

CASTRO G. AND S.J. POULOS (1977), *Factors affecting liquefaction and cyclic mobility*. Journal of the Geotechnical Engineering Division, Proceedings of the American Society of Civil Engineers, Vol. 103, No. 6, pp. 501-516.

CASTRO G. (1975), *Liquefaction and cyclic mobility of saturated sands*. Journal of the Geotechnical Engineering Division, Proceedings of the American Society of Civil Engineers, Vol. 101, No. 6, pp. 551-569.

CASTRO G., J.L. ENOS, J.W. FRANCE AND S.J. POULOS (1982), *Liquefaction induced by cyclic loading*. Report to National Science Foundation, Washington, DC, No. NSF/CEE-82018.

CHARLIE W.A., C.E. SCOTT, L.W. BUTLER AND D.O. DOEHRING (1995), *Estimating liquefaction potential of sand using the piezovane*. Géotechnique **45**(1), pp. 55-67.

CUR (1991), *Kunstmatig in water opgebouwde zandlichamen (No. 152)*. Gouda: CUR.

DREGER B.A. (1995), *Verification of predictions of dynamic response in fluid-saturated porous media using shock tube tests*. Master Thesis. Graduate School of The Ohio State University.

EDGERS L. AND K. KARLSRUD (1982), *Soil flows generated by submarine slides - case studies and consequences*. Proceedings International Conference on the Behaviour of Offshore Structures III, Cambridge, Mass., USA, pp. 425-437.

ELLING M.G.M., B.A. ANDEWEG, J.C. DE JONG AND C.E. SWANKHUISEN (1992), *De techniek van het schriftelijk rapporteren*. 6th edition. Lecture notes. Delft: University of Technology, Faculty of Philosophy and Tech-Social Sciences.

FEAR C.E. AND E.C. MCROBERTS (1995), *Reconsideration of initiation of liquefaction in sandy soils*. Journal of the Geotechnical Engineering Division, Proceedings of the American Society of Civil Engineers, Vol. 121, No. 3, pp. 249-261.

FIEGEL G.L. AND B.L. KUTTER (1994), *Liquefaction-induced lateral spreading of mildly sloping ground*. Journal of the Geotechnical Engineering Division, Proceedings of the American Society of Civil Engineers, Vol. 120, No. 12, pp. 2236-2243.

GEUZE E.C.W.A. (1948), *Critical density of some Dutch sands*. Proceedings 2nd International Conference on Soil Mechanics **3**, Rotterdam, The Netherlands, pp. 125-130.

HEEZEN F.T. AND A.C.M. VAN DER STAP (1988), *An engineering approach to under water dumped sandbodies*. Modelling Soil-Water-Structure Interactions, pp. 373-384. Rotterdam: Balkema.

JEYAPALAN J.K., J.M. DUNCAN AND H.B. SEED (1983), *Analyses of flow failures of mine tailings dams*. Journal of the Geotechnical Engineering Division, Proceedings of the American Society of Civil Engineers, Vol. 109, No. 2, pp. 150-171.

JEYAPALAN J.K., J.M. DUNCAN AND H.B. SEED (1983), *Investigation of flow failures of tailings dams*. Journal of the Geotechnical Engineering Division, Proceedings of the American Society of Civil Engineers, Vol. 109, No. 2, pp. 172-189.

JUANG C.H., X.H. HUANG, R.D. HOLTZ AND J.W. CHEN (1996), *Determining relative density of sands from CPT using fuzzy sets*. Journal of the Geotechnical Engineering Division, Proceedings of the American Society of Civil Engineers, Vol. 122, No. 1, pp. 1-6.

KAGAWA T. AND L.M. KRAFT (1981), *Modelling the liquefaction process*. Journal of the Geotechnical Engineering Division, Proceedings of the American Society of Civil Engineers, Vol. 107, No. 12, pp. 1593-1607.

KOLYMBAS D., I. HERLE AND P.A. VON WOLFFERSDORFF (1995), *Hypoplastic constitutive equation with internal variables*. International Journal for Numerical and Analytical Methods in Geomechanics, Vol. 19, pp. 415-436.

KRAMER S.L. AND H.B. SEED (1988), *Initiation of soil liquefaction under static loading conditions*. Journal of the Geotechnical Engineering Division, Proceedings of the American Society of Civil Engineers, Vol. 114, No. 4, pp. 412-430.

KROEZEN M., F. VELLINGA, J. LINDENBERG AND A.M. BURGER (1982), *Geotechnical and hydraulic aspects with regard to seabed and slope stability*. Proceedings 2nd Canadian Conference on Marine Geotechnical Engineering, Halifax, Nova Scotia, Canada.

LADE P.V. AND S.B. HERNANDEZ (1977), *Membrane penetration effects in undrained tests*. Journal of the Geotechnical Engineering Division, Proceedings of the American Society of Civil Engineers, Vol. 103, No. 2, pp. 109-125.

LADE P.V. (1978), *Prediction of undrained behaviour of sand*. Journal of the Geotechnical Engineering Division, Proceedings of the American Society of Civil Engineers, Vol. 104, No. 6, pp. 721-735.

LADE P.V. (1992), *Static instability and liquefaction of loose fine sandy slopes*. Journal of the Geotechnical Engineering Division, Proceedings of the American Society of Civil Engineers, Vol. 118, No. 1, pp. 51-71.

LINDENBERG J. AND H.L. KONING (1981), *Critical density of sand*. Géotechnique **31**(2), pp. 231-245.

LINDENBERG J.L. (1985), *Inventarisatie adviespraktijk zettingsvloeiingen*. Delft: Delft Geotechnics.

LINDENBERG J.L. (1986A), *Oevervallen in Zeeland*. I²-Bouwkunde en Civiele Techniek, No. 11, pp. 11-15.

LINDENBERG J.L. (1986B), *Zettingsvloeiingen in het buitenland*. I²-Bouwkunde en Civiele Techniek, No. 12, pp. 34-37.

MASTBERGEN D.R., J.C. WINTERWERP J.C. AND A. BEZUIJEN (1988), *On the construction of sand fill dams - Part 1: Hydraulic aspects*. Modelling Soil-Water-Structure Interactions, pp. 353-362. Rotterdam: Balkema.

MEIJER K.L. AND A.G. VAN OS (1976), *Pore pressures near moving underwater slope*. Journal of the Geotechnical Engineering Division, Proceedings of the American Society of Civil Engineers, Vol. 102, No. 4, pp. 361-372.

MORRIS D.V. 1983, *A note on earthquake-induced liquefaction*. Géotechnique, **33**(4), pp. 451-454.

OS A.G. VAN AND W. VAN LEUSSEN (1987), *Basic research on cutting forces in saturated sand*. Journal of the Geotechnical Engineering Division, Proceedings of the American Society of Civil Engineers, Vol. 113, No. 12, pp. 1501-1515.

PADFIELD C.J. (1978), *The stability of river banks and flood embankments*. Final Technical Report. US Army European Research Office, london, England.

POULOS S.J. (1981), *The steady state of deformation*. Journal of the Geotechnical Engineering Division, Proceedings of the American Society of Civil Engineers, Vol. 107, No. 5, 553-562.

POULOS S.J., G. CASTRO AND J.W. FRANCE (1985), *Liquefaction evaluation procedure*. Journal of the Geotechnical Engineering Division, Proceedings of the American Society of Civil Engineers, Vol. 111, No. 6, pp. 773-792.

PRISCO C. DI, R. MATIOTTI AND NOVA R. (1995), *Theoretical investigation of the undrained stability of shallow submerged slopes*. Géotechnique **45**(3), pp. 479-496.

RAJU V.R. (1994), *Spontane Verflüssigung lockerer granularer Körper - Phänomene, Ursachen, Vermeidung*. Veröffentlichungen des Institutes für Bodenmechanik und Felsmechanik der Universität Fridericiana in Karlsruhe, Heft 134.

REYNOLDS O. (1885), *The dilating of media composed of rigid particles in contact*. Phil. Trans. R. Soc. 20, S5, No. 127, pp. 469-481.

RHEE C. VAN AND A. BEZUIJEN (1992), *Influence of seepage on stability of sandy slope*. Journal of the Geotechnical Engineering Division, Proceedings of the American Society of Civil Engineers, Vol. 118, No. 8, pp. 1236-1240.

SCHRIECK G.L.M. VAN DER (1996), *Baggertechniek deel V t/m VIII*. Delft: Delft University of Technology, Faculty of Civil Engineering.

SEED H.B. (1979), *Soil liquefaction and cyclic mobility evaluation for level ground during earthquakes*. Journal of the Geotechnical Engineering Division, Proceedings of the American Society of Civil Engineers, Vol. 105, No. 2, pp. 201-255.

SEED H.B., K. TOKIMATSU, L.F. HARDER AND R.M. CHUNG (1985), *Influence of SPT procedures in soil liquefaction resistance evaluations*. Journal of the Geotechnical Engineering Division, Proceedings of the American Society of Civil Engineers, Vol. 111, No. 12, pp. 1425-1445.

SILVIS F. (1986), *Doorgronden wij zettingsvloeiingen?* KIvI-lecture. The Hague: Royal Institute of Civil Engineers.

SILVIS F., J. LINDENBERG AND J. VAN HETEREN (1988), *A numerical model to describe the initiation of flow slides in under water sand slopes*. Modelling Soil-Water-Structure Interactions, pp. 385-392. Rotterdam: Balkema.

SLADEN J.A., R.D. D'HOLLANDER AND J. KRAHN (1985), *The liquefaction of sands, a collapse surface approach*. Canadian Geotechnical Journal, No. 22, pp. 564-578.

SLADEN J.A., R.D. D'HOLLANDER, J. KRAHN AND D.E. MITCHELL (1985), *Back analysis of the Nerlerk berm liquefaction slides*. Canadian Geotechnical Journal, No. 22, pp. 579-588.

STOUTJESDIJK T.P., J. HEEMSTRA, C.J. SWART AND M.B. DE GROOT (1995), *Bodemloze put bestaat niet*. Land+Water, No. 10, 1995.

STOUTJESDIJK T.P., M.B. DE GROOT AND J. LINDENBERG (1994A), *Oever-, dijk- en plaatvallen (concept)*.

STOUTJESDIJK T.P., M.B. DE GROOT AND J. LINDENBERG (1994B), *Engineering approach to coastal flow slides*. Proceedings Coastal Engineering Congress III, Tokyo, Japan, pp. 3350-3359.

STOUTJESDIJK T.P. AND M.B. DE GROOT (1994C), *Handboek zettingsvloeiing*. Delft: Ministry of Public Works, DWW.

TERZAGHI K. (1925), *Erdbaumechanik auf bodenphysikalischer Grundlage*. Wien: Franz Deuticke.

TERZAGHI K. (1956), *Varieties of submarine slope failures*. Proceedings 8th Texas Conference on Soil Mechanics and Foundation Engineering, Austin, Texas, USA.

TEUNISSEN J.A.M. AND S.E.J. SPIERENBURG (1995), *Stability of infinite slopes*. Géotechnique **45**(2), pp. 321-323.

THORBORG B. (1986), *A one-dimensional parametric model of liquefaction of slopes*. Master thesis. Delft: University of Technology, Faculty of Civil Engineering.

TORREY III V.H., J.B. DUNBAR AND R.W. PETERSON (1988), *Retrogressive failures in sand deposits of the Mississippi River (Report 1: Field investigations, laboratory studies and analysis of the hypothesized failure mechanism)*. Vicksburg, MS: Waterways Experiment Station, Geotechnical Laboratory, Corps of Engineers.

VAID Y.P. AND J. THOMAS (1995), *Liquefaction and postliquefaction behaviour of sand*. Journal of the Geotechnical Engineering Division, Proceedings of the American Society of Civil Engineers, Vol. 121, No. 2, pp. 163-173.

VERRUIJT A. (1990), *Grondmechanica*. 3rd edition. Lecture notes. Delft: VSSD, Delft Publishing Company.

VERRUIJT A. (1992), *Offshore Soil Mechanics*. 5th edition. Lecture notes. Delft: University of Technology, Faculty of Civil Engineering.

VOGT A. AND W. FÖRSTER (1991), *Abschätzung der Rückgriffweite von Setzungsfließrutschungen*. Neue Bergbautechnik, 21. Jg., Heft 10/11.

WILDEROM M.H. (1979), *Resultaten van het vooroeveronderzoek langs de Zeeuwse stromen*. Vlissingen: Ministry of Public Works, Research Departement Vlissingen.

WINTERWERP J.C., M.B. DE GROOT, D.R. MASTBERGEN AND H. VERWOERT (1990), *Hyperconcentrated sand-water mixture flows over flat bed*. Journal of the Geotechnical Engineering Division, Proceedings of the American Society of Civil Engineers, Vol. 116, No. 1, pp. 36-54.

WINTERWERP J.C., W.T. BAKKER, D.R. MASTBERGEN AND H. VAN ROSSUM (1992), *Hyperconcentrated sand-water mixture flows over erodible bed*. Journal of the Geotechnical Engineering Division, Proceedings of the American Society of Civil Engineers, Vol. 118, No. 11, pp. 1508-1523.

WOOD D.M. (1990), *Soil behaviour and critical state soil mechanics*. Cambridge: Cambridge University Press.

WU W. AND E. BAUER (1994), *A simple hypoplastic constitutive model for sand*. International Journal for Numerical and Analytical Methods in Geomechanics, Vol. 18, pp. 833-862.

YOSHIMI Y., K. TOKIMATSU AND J. OHARA (1994), *In situ liquefaction resistance of clean sands over a wide density range*. Géotechnique **44**(3), pp. 479-494.

ZENG X. AND K. ARULANANDAN (1995), *Modelling lateral sliding of slope due to liquefaction of sand layer*. Journal of the Geotechnical Engineering Division, Proceedings of the American Society of Civil Engineers, Vol. 121, No. 11, 814-816.

Index

List of Figures

Enclosure I: Course of the Stability Analysis of Raju (1994)

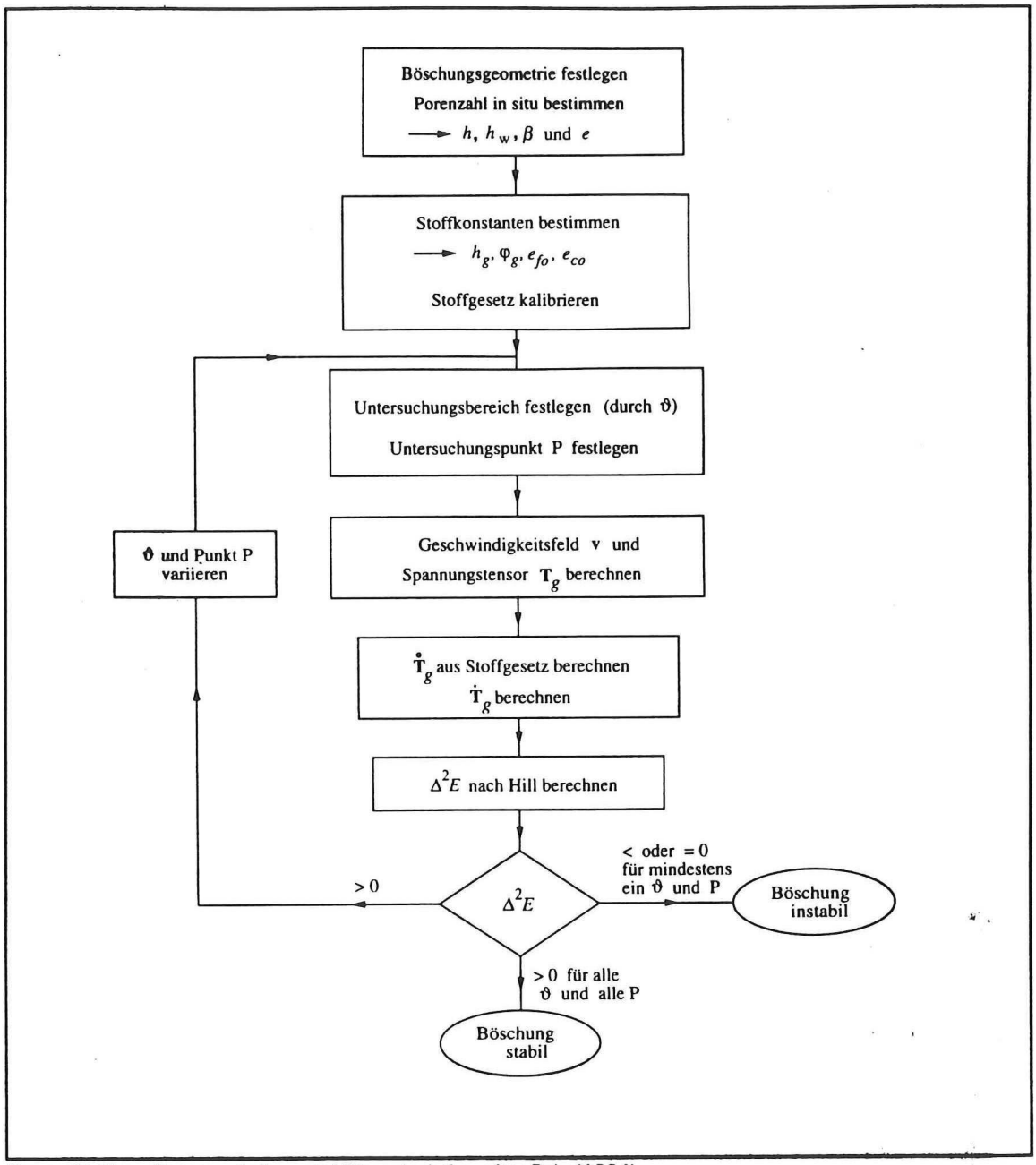

Figure 11 Flow diagram of slope stability calculation after Raju (1994)

Enclosure II: Discussion on Inverse Dredging Force Approach

As mentioned in chapter 2, there is reason to doubt the model, based on the inverse interpretation of dredging forces, because of the unexpected outcome: the liquefaction propagation velocity increases for slopes with an angle smaller than half the angle of internal friction. Thereafter, it predicts the liquefaction propagation velocity to decrease.

A substantial explanation of this phenomenon cannot be given at this point. However, it is felt that it may not be allowed to exchange σ_{xy}' for a negative value of τ. In this case, the liquefaction propagation velocity would increase for increasing slope angle, for the complete range between level ground and the angle of internal friction:

$$\frac{v}{k} = \frac{1-n}{\Delta n} \frac{\gamma_s - \gamma_w}{\gamma_w} \sin \alpha \cos \alpha \left(1 + \frac{\tan \alpha}{\tan \phi}\right)$$

The following graph was composed assuming γ_s = 20 kN/m^3, γ_w = 10 kN/m^3, angle of internal friction ϕ = 30°, porosity n = 45% and porosity jump Δn = 5%:

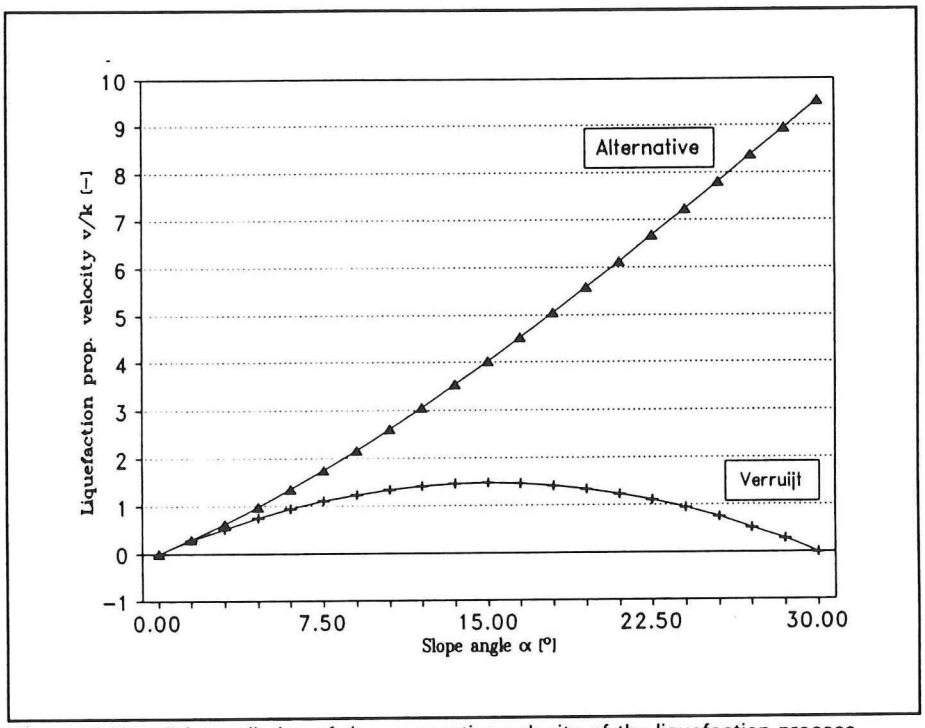

Figure 12 Verruijt's prediction of the propagation velocity of the liquefaction process

Volume 2:

Directive for Engineering Practice

Flow Slide Failure

of

Excavated Subaqueous Slopes

master thesis prepared by:

Tim Helbo

February - August 1996

Preface

Although flow slides have been studied intensively for a long time, the fundamental mechanisms leading to this kind of soil (structure) failure are still, at least partly, a mystery.

In September, 1995, Fugro Ingenieursbureau b.v. in Leidschendam suggested to study subaqueous slope failures resulting in a flow slide, within the framework of my graduate study program. I accepted in December, 1995, and started my research, conducted in partial fulfilment of the requirements for the degree Master of Science in the Delft University of Technology, on February 1st, 1996.

The report lying before you contains the results of a recommendation study to improve engineering and consultancy practice by furthering the understanding of the fundamental material properties and associated mechanisms, suspected to lead to flow slide failure. Apart from this Directive for Engineering Practice, a Literature Review (Volume 1) and Case History Study / Appendix (Volume 3) have been prepared, as part of the graduate study program.

I wish to extend my sincere thanks to J.L. Lindenberg[1], J.W. Heijting[2], J.D. van Rheenen[3], I. Herle[4], V.H. Torrey[5], J. Brouwer[6] and J. de Koning for their effort to help me further knowledge of theory and practice related to flow slide problems.

This graduate study program has been supervised by a graduate committee. The following advisors were seated in this committee:

A. Verruijt	Delft University of Technology
K. d'Angremond	Delft University of Technology
G.L.M. van der Schrieck	Delft University of Technology
M.Th.J.H. Smits	Fugro Ingenieursbureau b.v.

I wish to thank my graduate committee for its assistance.

Leidschendam, 12 September 1996,
Tim Helbo.

---

1 Ministry of Transport and Public Works (RWS), Department of Road and Hydraulic Engineering (DWW)

2 Heijting Aannemersbedrijf en Handelsonderneming bv

3 Province of Gelderland

4 Institut Für Bodenmechanik und Felsmechanik (IBF), Universität (TH) Fridericiana Karlsruhe, Germany

5 US Army Waterways Experiment Station, Vicksburg, MS, USA

6 Delft University of Technology, Faculty of Mechanical and Marine Engineering

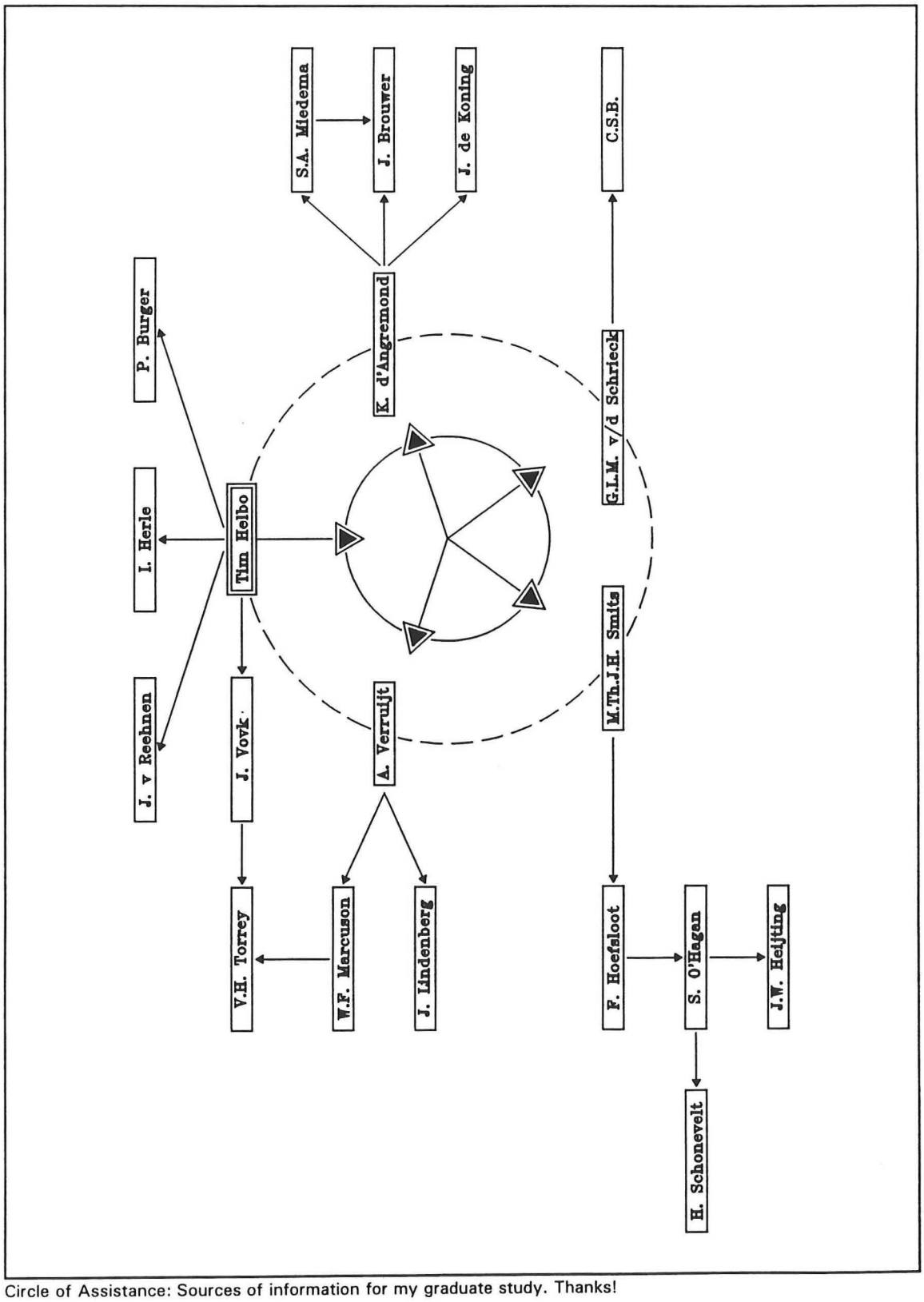

Circle of Assistance: Sources of information for my graduate study. Thanks!

Summary

Several recent flow slide failures in sand borrow pits, together with uncertainties in engineering and consultancy practice with regard to the fundamental mechanisms causing this type of failure, gave cause for this study. The main aim of this study was formulated as: "How, from an engineering point of view, can we understand and predict flow failure of excavated (or being excavated) slopes, better?".

Generally, the term "flow slide", in Dutch often disputably indicated with "*zettingsvloeiing*", is used to refer to the consequences of failure rather than to the fundamental mechanisms, causing failure. In fact, the resulting failure profile, i.e. flat subaqueous slopes and caved-in embankments, may be established by different fundamental mechanisms:

First, 'static liquefaction' of part of a subaqueous slope, subjected to a monotonically increasing shear stress level, may cause a spontaneous collapse of the grain skeleton. A large part of the slope liquefies and flows in a manner resembling a heavy viscous fluid. This type of flow slide failure should be referred to as 'settlement flow' or in Dutch as '*zettingsvloeiing*', only, relating it to its fundamental mechanism. Static liquefaction is a result of shear-induced undrained negative volume strain (contractancy) of fine loosely packed saturated granular material. The decrease in void ratio induces excess pore pressures which reduce the effective stress level.

Second, a flow slide failure profile may be the result of an alternative mechanism, which plays an important role in the mining of sand. It is known as 'active bank development' or in Dutch as '*bressen*'. Active banks are initiated, purposely, in fine sands to set on the flow of sand towards the suction pipe entrance. In fine granular material, sustaining active banks may develop, which virtually propagate away from the suction pipe entrance at angles, which are not restricted to the angle of natural repose. The resulting slope angle is likely to depend on the equilibrium flow of the density current towards the suction pipe entrance.

The potential for static liquefaction may be evaluated on the basis of two criteria: 1] The in-situ void ratio must be below the critical void ratio of the sand considered, taking the dependency of the critical void ratio on the confining pressure into account, (thus no negative volume strain will be the result of shear induced plastic deformation); 2] The in-situ shear stress level must be lower than the residual shear resistance of the soil (thus no plastic deformation can occur to begin with). On the basis of both criteria, the potential for static liquefaction may be excluded. However, the latter criterion is less useful as in-situ shear stress levels are hard to determine and, locally, the residual shear resistance may be exceeded during sand mining. The susceptibility is greatly influenced by the permeability of the soil and sharpness of the particles.

The soils at four case history sites were evaluated on their potential for static liquefaction, as far as possible. It was concluded that non of the soil masses were potentially susceptible on the basis of these analyses, but also that more specific data are needed to make the evaluation method more reliable. To be able to exclude the potential for settlement flow, it is necessary to establish the critical void ratio (in relation to confining pressure), maximum and minimum void ratios of the sand considered and an indication of the in-situ void ratio (based on the interpretation cone resistances and/or undisturbed sample testing). On the basis of static liquefaction potential analysis, used in the current study, flow slide failure which occurred in case histories could not be explained.

On the other hand, if the potential for settlement flow has been excluded, flow slide failure may still occur as a result of the development of active banks. Advice towards the prevention of flow slide failure as a result of active bank development should be pointed at restrictions to the mining activities. A useful advice may be to excavate an embankment, which must be protected against flow slide failure, by non-hydraulic means, before allowing hydraulic sand mining in the area.

Combination of the main conclusions, that were drawn from the case history and a literature review, has lead to the thought that purely liquefaction-induced flow slide failure is not as common as we may think. In fact, flow slide failures resulting of static liquefaction are thought to be a rarity, let alone those induced by human activities. An explanation for flow slides should thus be sought in alternative explanations, as was attempted in this study.

Contents

Scope of Flow Slide Study

Introduction

Flow slides occur around the globe in deltic areas, along rivers and during dredging activities, like sand fill construction or sand mining. Many of these flow slide failures, which may involve the movement of millions of cubic meters of soil, pass and have passed unnoticed by mankind because they take place under water, according to Terzaghi (1956).

However, if flow slide failures cause changes in the morphology of rivers and coastlines, they do become known. Sometimes even uncomfortably, when they bring damage to our flood protection works, newly reclaimed land or other structures. The province of Zeeland in The Netherlands has a rich history in - sometimes destructive - flow slides, as mentioned by Lindenberg (1986a).

In the next few paragraphs, the general idea of what a flow slide is will be discussed, followed by the problem definition and formulation of the main aims of this flow slide study as well as the set-up of this Volume 2: Directive for Engineering Practice.

The Cause of Flow Slides

Generally spoken, it is assumed that the cause of flow slide failures lies in the liquefaction of (part of) a sloping body. However, this explanation can be made plausible only when loose to very loose fine sand layers are encountered in the subsoil, over substantial depths. This is likely to be the case in areas where young marine sands have been deposited relatively fast and along (former) river beds where erosion and sedimentation of sand are continuously taking place.

Sometimes, flow slide failures are encountered in areas where the above does not hold, or at least does not give a credible explanation. Therefore, there is a tendency toward developing alternative explanations for the exact mechanisms, leading to flow slide failure. One of those alternative mechanisms may be the development of active banks, after initial oversteepening at the toe of a slope.

Because the actual mechanism, leading to flow slide failure, is not fully understood, the term "flow slide" is used to refer to the consequences of the failure, rather than to the cause of it. The distinctive features of flow slide failures are large soil displacements, very flat resulting subaqueous slope angles and embankments which have caved in. The fact that the term "flow slide" always has been related to the consequences of the failure, has lead the attention away from the actual causing phenomena. Thus, the misleading thought that liquefaction can be the only mechanism to be held responsible, could strike root.

Problem Definition and Formulation of Main Aims

Unexpected failure of subaqueous excavated slopes in the form of flow slides is considered in this graduate study. Excavated slopes are not the same as slopes constructed by means of hydraulic fill. Several recent flow slide failures in sand borrow pits, together with qualms in engineering practice about not knowing exactly what fundamental mechanism causes flow slide failure, gave cause for this study.

The knowledge that flow slide failure may be caused by either static liquefaction of (part of) a sloping body (also called spontaneous collapse)[7], or by the development of active banks, is taken as a point of departure. Liquefaction due to dynamic loading will be left out of consideration. Special attention will be paid to the geological circumstances of The Netherlands.

Herewith, the central problem of this flow slide study becomes: "How, from an engineering point of view, can we understand and predict flow slide failure of excavated (or being excavated) slopes, better?". To be able to answer the question at issue, we need to understand the fundamental mechanisms, leading to flow slide failure. Then, the soil properties may be related to the mechanisms and specific circumstances may be taken into account.

The main aim of this graduate study is to obtain insight in different mechanisms, possibly triggering flow slide failure and causing its retrogressive nature. Since the extent of a flow slide can be very large, and seems hard to predict, the prediction of the potential for failure will be the pith of the study, not the consequences of failure (Volume 1: Literature Review). The possible ways to model failure potential are investigated and their prediction values are evaluated on the basis of case histories (Volume 3: Case History Study / Appendix). With the insights obtained, an effort has been made to formulate a practical guideline for flow slide analyses, which should lead to improvements in engineering practice (this Volume 2: Directive for Engineering Practice).

Set-up of this Volume 2: Directive for Engineering Practice

As stated in the above, one of the main aims of this graduate study was to formulate a practical guideline for engineering and consultancy practice. This is how the report lying before you should be looked upon. Chapter 1 serves as an introduction to soil properties and phenomena, related to flow slide failure. The main aim of this chapter is to offer the reader some basic knowledge and to avoid semantics in the following chapters.

Chapter 2 describes the recommended static liquefaction potential analysis for engineering practice. It may serve as a directive in future analyses of the stability of subaqueous (to be) excavated slopes, as well in slope design as in failure reconstruction. Chapter 3 comprises a qualitative discussion on construction aspects and the dangers of the development of active banks. This chapter is meant to familiarize the reader with the possible contribution of active banks to flow slide failure. Conclusions and recommendations are summarized thereafter.

---

7 Static liquefaction occurs as a result of contraction of the soil under a monotonically increasing shear stress level (see Chapter 1)

1 Clarification of Flow-Slide Related Parameters and Mechanisms

§ 1.1 Definition of the Packing of Sands

For many reasons it is necessary to define a relationship between the volume occupied by pores and the volume occupied by particles. As will be discussed in this chapter, many such relationships have been proposed.

Void Ratio: The term "void ratio" (e) is used in most Anglo-Saxon literature. It has been defined as the ratio of the volume taken by the pores over the volume taken by the solids:

$$e = \frac{V_{pores}}{V_{solids}} \quad [-]$$

In this report, all theory and experiments will be explained in terms of void ratio.

Porosity: The term "porosity" (n) is mostly employed in Germany and surrounding countries. Also, most of the Dutch engineers are taught geomechanics in terms of porosity. It has been defined as the ratio of the volume taken by the pores over the volume taken by the pores and solids together. It may be expressed as follows:

$$n = \left[\frac{V_{pores}}{V_{solids} + V_{pores}}\right] \quad [-]$$

Often n is expressed in percent. In this report, some theory and experiments will be explained in terms of porosity, in addition to the explanation in terms of void ratio.

Density: The term "density" (γ) is often employed in road construction environments. It is defined as the unit (m^3) weight (kg or kN) of the soil. Depending on whether or not the pores are (partially) filled with water, "density" is preceded by the adjective "wet" or "dry". It may be obvious that "density" does not make an unequivocal parameter to express the pore volume ratio, unless also the rate of saturation is considered. The term "density" will not be used in this report except when speaking of "relative density" (see page 5).

Figure 1 on page 4 serves to explain the difference between void ratio and porosity once more. Also from this graph, one may easily derive that void ratio and porosity may be expressed in terms of the other as follows:

$$e = \left[\frac{n}{1 - n}\right] \quad [-] \qquad , \qquad n = \left[\frac{e}{1 + e}\right] \quad [-]$$

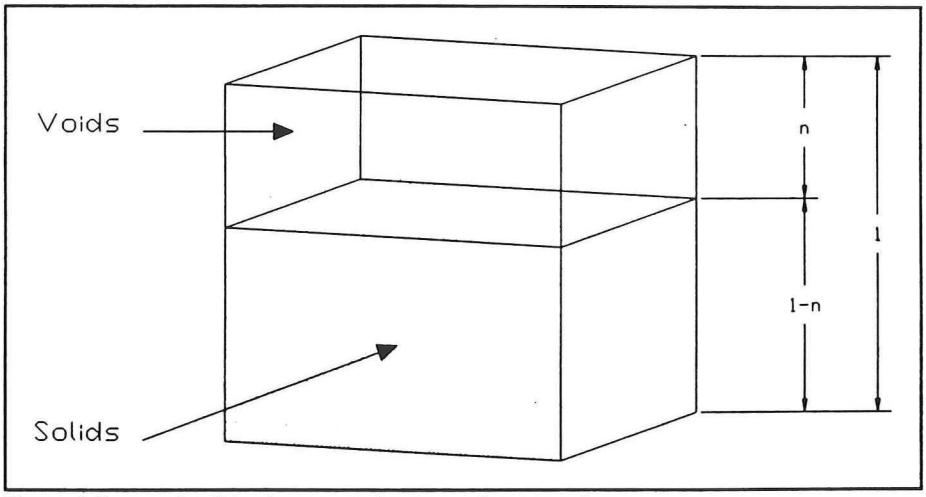

Figure 1 Pore and solid volumes relative to a reference volume

§ 1.2 In-Situ Void Ratio

The in-situ void ratio obviously expresses the packing of the sand in undisturbed circumstances. The in-situ void ratio is an important parameter in any evaluation of static liquefaction potential. It is, however, very difficult to estimate the in-situ void ratio of a particular soil body for a number of reasons.

First, most in-situ void ratio determination methods[8] involve disturbances of the original packing. Especially in liquefaction analyses, where loosely packed sands are involved, this may lead to inaccurate results. Second, any sampling method obviously leads to very local estimations of the in-situ void ratio.

Pushed fixed piston sampling with thin-walled tubes leads to acceptable results in most cases, when carried out with particular care. A description is given by Poulos *et al.* (1985). Other in-situ density measurement methods, which may be considered, are sampling of frozen soil and nuclear measurement methods.

§ 1.3 Maximum and Minimum Void Ratio

Knowledge of the maximum and minimum void ratios is very important for different reasons. First, the range between maximum and minimum void ratio appears in the definition of relative density (see page 5). Second, the range between maximum and minimum void ratio may give an indication of the (wet) critical void ratio and the possible fall in void ratio, when soil is loosely packed.

The maximum and minimum void ratios of a particular sand may be influenced by many factors, of which grading is the most important one. When the voids between the skeleton, formed by a certain fraction, are perfectly filled with another fraction, the skeleton of which is perfectly filled

[8] A description of the most widely used methods of in-situ void ratio determination is given by Veldhuis (1992).

with again another fraction, the minimum void ratio may be obtained. On the other hand, if a sand is more narrowly graded, the maximum void ratio may be obtained.

Not only the grading has a great influence on the maximum and minimum void ratios, also the sharpness of the particles has. The sharper the particles, the higher the maximum obtainable void ratio may be, due to a high internal friction as a result of a larger contact area. The area of contact also grows with the decreasing size of the particles. Therefore, the smaller the particles, the greater the opportunity for building a loose arrangement of particles.

The maximum obtainable void ratio of uniform spheres is 0.91 and the minimum obtainable void ratio is 0.35 (see Volume 3, Appendix 5). The most loosely packed state and the second densely packed state are represented graphically in Figure 2 and Figure 3.

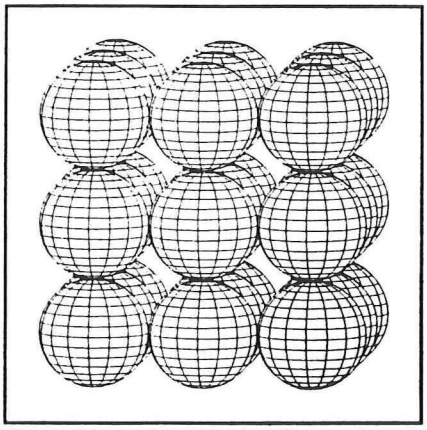

Figure 2 Loosely packed uniform spheres

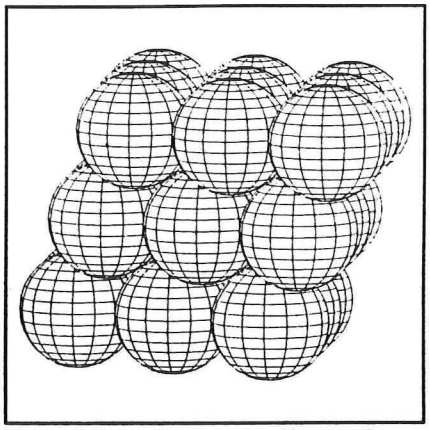

Figure 3 Densely packed uniform spheres

§ 1.4 Relative Density

§ 1.4.1 Description and Use of Relative Density

As stated in the above, various properties of sands influence the maximum and minimum void ratio possibly obtainable. Therefore, the void ratio in-situ, or any other absolute void ratio, cannot be compared with that of other sands when deformation problems are studied. For this reason, an absolute void ratio value may be made relative to the range of possible densities.

This relative number is known as "relative density". It is obvious that a relative density is bound to a state in which a is sand considered. Relative density may be associated with the in-situ void ratio, critical void ratio or any other void ratio. It has been defined as:

$$Dr_{state} = 100\% \left[\frac{e_{max} - e_{state}}{e_{max} - e_{min}} \right] \quad [\%]$$

§ 1.4.2 Difference between Void Ratio and Porosity Based Relative Density

It is important to remember that relative density has been defined in terms of void ratio. It is, however, possible to express relative density in terms of porosity too. Once relative densities have been calculated, it is not obvious on the basis of what parameter the calculations were made. Comparing relative densities, calculated from porosities and void ratios, leads to erroneous results, which may be more than 30% off. The error grows with increasing state porosity and decreasing minimum porosity. The difference is expressed in the following formula (see also Figure 4, which is based on sands investigated by SCW (1979)):

$$Dr_{state,\ void\ ratio} = c_{n\to e}\ Dr_{state,\ porosity} \quad , \quad c_{n\to e} = \frac{1 - n_{min}}{1 - n_{state}}$$

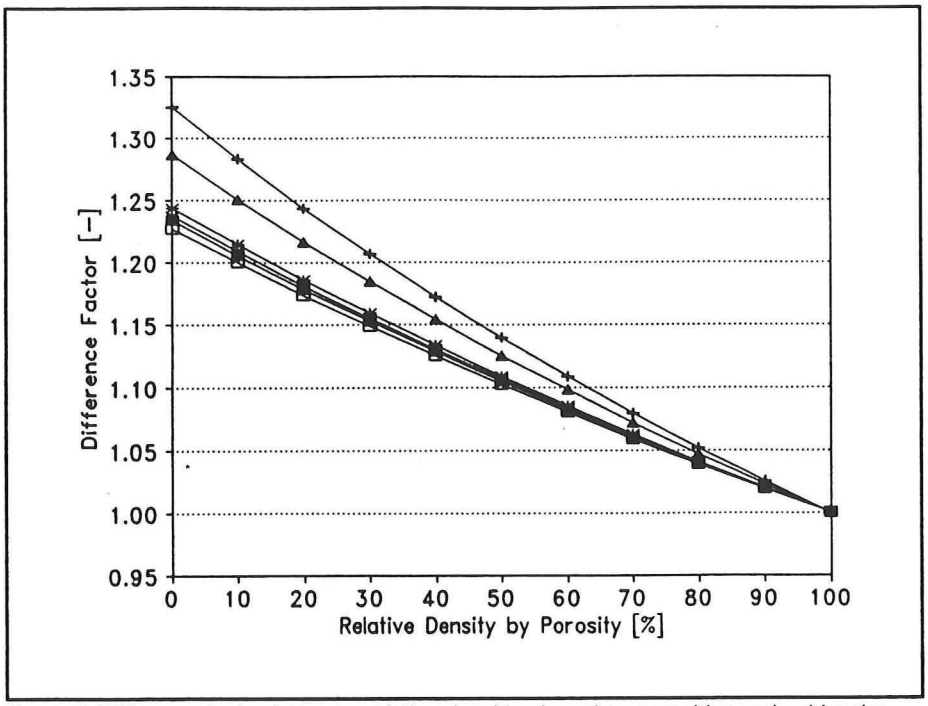

Figure 4 Difference factor between relative densities based on porosities and void ratios

§ 1.4.3 Estimation of Relative Density from Cone Penetration Tests

Several investigators have tried to estimate the relative density from cone penetration tests. They found that the relative density depends on cone resistance as well as on the effective stress. In this report the formula of Jamiolkowski *et al.* (1988), which is identical to that of Baldi *et al.* (1986), is used. With the cone resistance, q_c, in *Mpa* and the mean effective stress σ'_m in kN/m^2, they estimate the relative density with:

$$Dr_{in-situ} = 100\% \left[\frac{1}{2{,}93} \ln \frac{1000\ q_c}{205\ \sigma'^{0.51}_m} \right]$$

Jamiolkowski's formula does not account for the compressibility of sands. Therefore, an extension to the existing theory has been developed by Juang *et al.* (1996). Their approach uses

a weighted scheme that relates the compressibility, measured by friction ratio and expressed as a *fuzzy number*, to the existing base relations. The effect of compressibility is not suspected to play a major role in the determination of sands in The Netherlands. The base relation used by Juang *et al.* (1996) reads:

$$D_r^2 = \left(\frac{1}{Q_f}\right)\left[\frac{(q_c / P_a)}{(\sigma'_v / P_a)^{0.5}}\right]$$

where P_a = atmospheric pressure ($\pm$ 100 kPa) and Q_f = an empirical constant, varying with different compressibilities: 332, 305 and 278 for low, medium and high compressibility, respectively. With the use of the fuzzy numbers, a weighted average of the relative density, based on the friction ratio, is established using these values. The case history studies have shown that the prediction of the relative density is somewhat higher than Jamiolkowski's.

Other estimating formulae are available. The difference, however, is not very big. The formula used in this report has shown to give the lowest predictions, which is useful when approaching the stability limit from below, as is the case in the flow slide analysis presented in Chapter 2.

§ 1.5 Critical Void Ratio

§ 1.5.1 Dry Critical Void Ratio

In essence, the "dry critical void ratio" is that void ratio at which, at the instant of pure shear loading under drained conditions, no volume change occurs. The adjective "dry" refers to the drained loading conditions. The "dry critical void ratio" may be determined by conducting a series of triaxial tests at constant mean effective stress, while varying the initial void ratio. From extrapolation of the initial void ratio and related maximum volumetric strain, the dry critical void ratio may be estimated (Lindenberg *et al.* (1981)).

The dry critical void ratio is an important parameter for flow slide analysis when evaluating liquefaction potential. It is assumed that no excess pore pressure can develop when no (negative) volume change occurs at the instant of loading. For static liquefaction potential analyses, the dry critical void ratio seems to offer a safe upper limit to the in-situ void ratio (see Chapter 2).

§ 1.5.2 Wet Critical Void Ratio

The definition of the "wet critical void ratio" is different from that of the dry critical void ratio. The wet critical void ratio is that void ratio at which, during undrained force-controlled pure shear loading at constant mean effective stress, a sample liquefies. In this context, liquefaction is defined after Seed (1976): a sample has liquefied when the increment in deviator stress becomes equal to zero, or: at liquefaction the pore pressure equals the confining pressure (almost).

In other words: at the point on the stress path in the state diagram (q - p) where the vertical stress level (σ'_1) becomes equal to the confining pressure (σ'_3), theoretically liquefaction has occurred. Passing this point, *hardening* of the sample may be experienced, which means that the soil no longer contracts and the shear resistance picks up (limited liquefaction).

On the other hand, the sample may still be contractant (see page 8) after the point of theoretical liquefaction and the process of *softening* may continue, resulting in total collapse. Whether liquefaction occurs depends also on the level of confining pressure. Higher confining pressures may cause liquefaction of samples that would not have liquefied at lower confining pressures.

The wet critical void ratio may be determined by conducting a series of undrained triaxial tests at constant mean effective stress, while varying the (initial) void ratio. However, according to Lindenberg *et al.* (1981) it is very difficult to obtain accurate results. From Lindenberg's tests it was concluded that the wet critical void ratio exceeds the dry critical void ratio by 0.5 to 7%. The wet critical void ratio will always be higher than the dry critical void ratio, as excess pore pressure must be able to develop to let a sample liquefy. In other words: the sample must be contractant (see page 8).

§ 1.5.3 Other Appellations of the Critical Void Ratio

In their papers, Begemann *et al.* (1977) and Lindenberg *et al.* (1981) use the term "wet/dry critical density" to indicate the critical void ratios as discussed in the above. However, they express their critical void ratios in terms of porosity. Thus one may also be tempted to speak of "wet/dry critical porosity". To avoid semantics, it seems advisable to restrict ourselves to one term, only. In this report "wet/dry critical void ratio" will be used.

Further confusion may be induced by the fact that the term "critical void ratio" is also used to indicate the void ratio in the steady state of deformation (see for a definition Poulos (1981)). This is the result of the fact that the steady state of deformation may also be called the "critical state" in the analysis of sand behaviour (Sladen *et al.* (1985a)). Although the values do not differ a lot in practice, their definition is fundamentally different. Also in this case, it seems advisable to restrict ourselves to one term, only. In this report "steady-state void ratio" will be employed.

§ 1.6 Dilatant and Contractant Deformation Behaviour

In the late 19th century, Reynolds (1885) proved the existence of *dilatancy*: a (positive) change in volume due to shear stress. When a shear stress is applied to a mass of sand, it will tend to increase in volume, normally. Hence the void ratio of the sand will increase. This is indeed the fact when the initial void ratio of the sand is below the dry critical void ratio, as discussed in the above.

However, if the initial void ratio of the mass of sand is above the dry critical void ratio, it will decrease in volume, when it is subjected to shear loading. This opposite deformation reaction of the soil is known as *contractancy*. This idea was originally used by Terzaghi (1925) to explain the principle of static liquefaction.

§ 1.7 Static Liquefaction

Although flow slides had been a known phenomenon in the history of soil mechanics, it was not until the 1920s that the forming of quicksand was suggested by Terzaghi (1925) as a possible cause to this type of slope failure. He stated that saturated and loosely packed sand, subjected to shear stress, would tend to decrease in volume (contractancy), creating a gradient in pore pressure. If the permeability of the sand was low enough, he said, dissipation of excess pore pressure would

be hindered. With the increase in pore pressure, the effective stress would decrease[9] and ultimately become equal to zero (softening). At this point, the sand would loose its shear resistance completely and liquefy. Later, the forming of quicksand as described by Terzaghi, was called "liquefaction".

In 1947, Bernatzik demonstrated the existence of liquefaction on a laboratory scale, as mentioned by Raju (1994). Bernatzik had sand settled very carefully in a container filled with water. On the loosely packed saturated sand, he carefully placed a weight, which sank into the sand after a mild hit on the container wall. The same effect can be observed when pushing a rod into the sand.

A more contemporary description of the same phenomenon, relating it to flow slide failure, is given by Sladen *et al.* (1985a). They state that a considerable amount of controversy surrounding the liquefaction phenomenon has been attributed to semantics, and suggest to use the following definition[10] of liquefaction:

> "LIQUEFACTION IS A PHENOMENON WHEREIN A MASS OF SOIL LOSES A LARGE PERCENTAGE OF ITS SHEAR RESISTANCE, WHEN SUBJECTED TO MONOTONIC, CYCLIC OR SHOCK LOADING, AND FLOWS IN A MANNER RESEMBLING A LIQUID UNTIL THE SHEAR STRESSES ACTING ON THE MASS ARE AS LOW AS THE REDUCED SHEAR RESISTANCE.".

In nature, there are different causes to shear stresses that may lead to a volume decrease tendency. They may be of a different nature: static, quasi static (shock) or dynamic. In this graduate study, only liquefaction as a result of static liquefaction is considered. With static, as opposed to dynamic, a monotonous increasing level of shear stress is meant. This is the case when a subaqueous slope with an increasing slope angle or slope hight is considered. Both the increasing slope gradient and the increasing hight of the slope may be caused by erosion at the toe.

§ 1.8 Active Bank Development (*Bressen*)

As stated in the introduction to this graduate study, static liquefaction may not be the only mechanism that can lead to flow slide failure. It is recalled that the term "flow slide" is related to the consequences of the failure, rather than to the fundamental mechanisms. In other words: a flow slide is not, by definition, caused by static liquefaction of (part of) a subaqueous slope.

The distinct difference between the two fundamental mechanisms, that hold the potential to cause flow slide failure, is indicated, ironically, by the fact that the second mechanism, for which the term "active bank development" was adopted, is based on the dilative deformation behaviour of sand under shear loading.

The idea of active bank development originates from the dredging industry. Until the late 1960s, it was assumed that plain suction dredging resulted in a conical pit. The sand was thought to run down a slope at the angle of natural repose under water. It was assumed that the disintegration and sand flow towards the suction pipe entrance were controlled by the process of suction itself.

---

[9] According to Terzaghi's principle of effective stress, the (constant) total stress level is equal to the sum of the effective stress and pore pressure.

[10] Sladen *et al.* (1985) took this definition from Morris (1983). Essentially this definition was offered by Castro (1982) except that the adjective "undrained", with which those workers qualified "loading", was omitted.

De Koning (1970) first suggested that the disintegration of sand and the flow of sand towards the suction pipe entrance were autonomous processes, which occurred, once initiated, independently from the actual suction. His explanation of what happened was based on a series of echo soundings of the development of the bathometry below a suction dredger.

De Koning stated that initially oversteepened slopes, caused by the penetration of the suction pipe, take their temporary stability from cohesive forces. These forces were assumed to be induced by the fact that the grains must be released from their (dilative) packing. Hence the void ratio must increase, which induces negative pore pressure. Only when enough pore water has penetrated the pores, and the negative pore pressure has been reduced, a slide may occur.

The released material was assumed to be transported to the suction pipe entrance in a density current (see next paragraph). With the transportation of the released material away from the toe of the slip surface, a new oversteepened slope is generated, and another slide may develop. The successive slides were referred to as "active bank" (Dutch: *bres*).

Today, we must admit that the exact phenomena, which play a part in the complex soil disintegration process, are still not fully understood. However, general agreement has been reached on the fact that the soil disintegration is an autonomous process, the development of which depends on the local soil parameters and profile, and that an active bank is a retrogressing oversteepened slope failure[11] (see Figure 5).

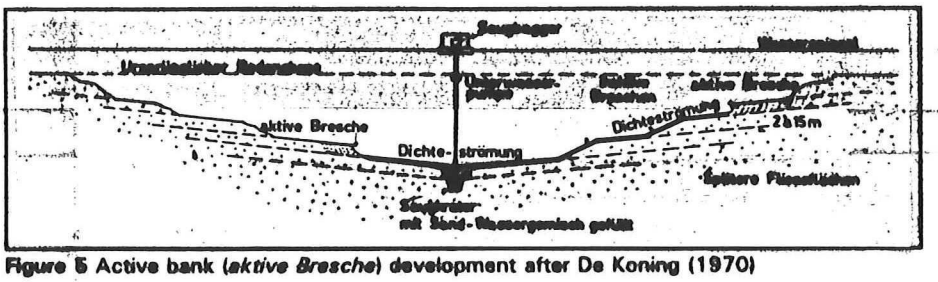

Figure 5 Active bank (*aktive Bresche*) development after De Koning (1970)

§ 1.9 Density Currents

Density currents are currents induced by the difference in density (unit weight) between two fluids. This may be the difference between salt and fresh water or between water and a mixture of sand and water. The subaqueous flow of mixtures of water with a very high concentration of sediments, are significant to this graduate study.

Two types of sand-water-mixture density currents should be distinguished. First, one that is initiated by the continuous softening, resulting in liquefaction of (part of) a slope. As mentioned above, the liquefied soil flows in a manner resembling a fluid until the shear stresses acting on the mass are as low as the reduced shear resistance. The density of this current is so high that settlement of individual particles is hindered (nearly) completely[12].

---

[11] More fundamental research in the field of dredging technology within the framework of "Combinatie Speurwerk Baggertechniek (CSB)" has been released, recently.

[12] Try to mix some sand with just enough water to make the mixture a fluid, when shacking it. Observe that the fluid is more stable when poring it than a mixture of the same sand with an over-measure of water.

Second, in all plain suction dredging theory, it is assumed that the disintegrated soil is transported to the suction pipe entrance in a density current. This flow is generated at the toe of an active bank and flows under influence of gravity to the bottom of the pit. The formation of the density flow depends chiefly on the production of the active bank. A little further from the formation of the current, an equilibrium will be established between gravity forces and shear resistances. By means of sedimentation, the concentration (and hence the density) and sedimentation angle, which influence the gravity forces, may fluctuate.

2 Recommended Static Liquefaction Potential Analysis

§ 2.1 Introduction

Currently, two types of stability analyses of subaqueous slopes are common in engineering practice. These are the reconstruction of failures that actually have occurred and the prediction of stability for slopes to be excavated in future. The complete stability analysis comprises, amongst others, micro stability analyses (pore pressure gradient out of the slope surface), macro stability analyses (slip surface), flow slide analysis and wave attack analysis (see Figure 6).

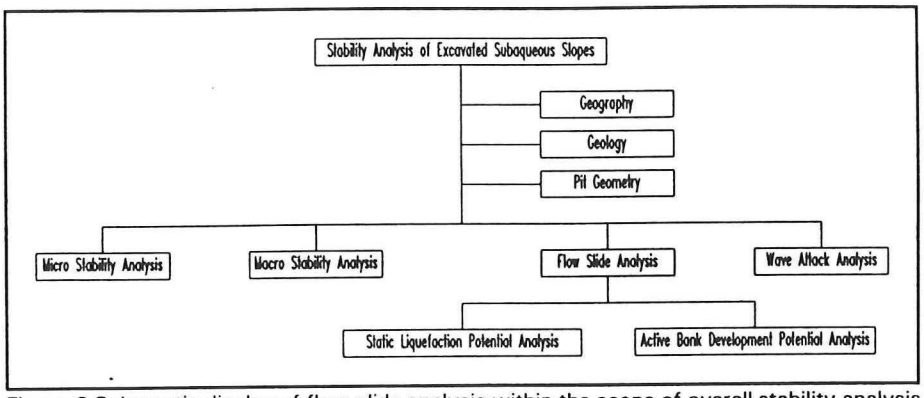

Figure 6 Schematic display of flow slide analysis within the scope of overall stability analysis

In this chapter and the following, a method of stability analysis will be suggested to predict the stability of slopes with respect to flow slide failure. This method consists of two parts: an improved static liquefaction potential analysis (this chapter) and an alternative failure mechanism consideration (Chapter 3). The considerations in these chapters may also lead to a better understanding of the failures that have occurred in the past. The improved static liquefaction potential analysis has been based mainly on literature review, and was used to reevaluate four case histories. These case history studies are included in Volume 3.

§ 2.2 General Considerations

Whether or not flow slide failure due to static liquefaction occurs, is a matter of many different factors. The potential for flow failure due to static liquefaction failure could be looked upon as a chain of factors. Only if all factors are in favour, one can expect flow failure to occur.

In engineering and consultancy practice, it is impossible to develop design tools that cover all links in the static liquefaction failure chain, as yet. Many factors of in influence may be evaluated individually, resulting in a likelihood prediction of the occurrence of static liquefaction. Some of the factors may be predicted with reasonable probability.

Two decisive ('hard') criteria have been established, on the basis of which the failure chain may be broken, and the occurrence of flow slide failure, as a result of static liquefaction, may be excluded. Evaluation of these criteria is difficult, however, which makes them more evident in a theoretical perspective than in practice. The first, and most important criterion, on the basis of which static liquefaction can be excluded, is the void ratio criterion:

> The in-situ void ratio, in combination with the local level of confining stress, must be below the critical void ratio at all depths.

The second criterion, which is only normative in the case that the in-situ void ratio is not definitely below the critical void ratio, so that the soil is potentially liquefiable, is the reduced shear strength criterion:

> The maximum in-situ shear stress must be below the undrained reduced shear resistance of the soil.

The strategy of static liquefaction potential analysis, as will be described in the following paragraphs, will be to evaluate several important factors ('soft' criteria) to point out the most susceptible layer in the soil profile and to generate an idea of the over-all susceptibility of the soil for static liquefaction induced flow slide failure. Thereafter, the most critical zones will be analyzed in more detail, and an attempt will be made to develop a tool to assess the potential for static liquefaction, in different situations with different sources of information ('hard' criteria).

§ 2.2.1 Field Investigations

The ideal analysis starts with the interpretation of several indicative cone penetration tests and a soil boring. From the cone resistance and the friction ratio, the location of different layers can be established. Low cone resistances ($\leq$ 5 *MPa*, depending on depth) in sand layers (friction coefficient $\leq$ 1.0) are suspicious. The soil boring may help to identify the texture of the possibly susceptible layers (critical zones). If the material is homogeneous and consists of clean fine sand, this adds to the suspicion. Field investigations may at be the start of any substantial analysis, they should go with a study of the geological formations in the local subsoil.

§ 2.2.2 Geography and Geology

According to SCW (1979), the geohydrological and mechanical properties of a granular mass are determined chiefly by: a) the granular material; b) the grain shape and surface roughness; and c) the shape and location of the particle size distribution curve (i.e. average grain size and grading). The properties of sand are furthermore determined by the geological history of the sand: the manner of deposition and all the natural influences, to which it has subsequently been subjected (rain, tides, surcharge, jolts and vibrations, etc.).

The geological composition of the soil profile itself, which depends on the geographical position of the case site, can never give a decisive answer to the question whether or not the soil considered is susceptible to static liquefaction. However, it may give a good indication.

Roughly, the geological history over the last two and a half million years, in which the sand layers from which usually sand is borrowed were formed, consists of two main periods: the pleistocene

and the holocene. During the pleistocene period, large fluctuations in temperature, resulting in successive ice ages alternated with periods of transgression, governed the formation of soils in The Netherlands. The holocene period, which started about ten thousand years ago, is characterized by a more moderate climatologic regime.

Almost all flow slides, assumed to have been caused by static liquefaction, took place in holocene sand deposits (see Lindenberg (1985)). This has lead to the general conclusion that the failure mechanism considered cannot occur in other sand formations (i.e. pleistocene deposits). To be able to understand why this criterion for static liquefaction potential judgement is not without any foundation, it is necessary to study a bit of geology.

Loosely packed sand is in an unstable equilibrium situation. This means that the soil will seize every opportunity to compact. This process may take place very slowly, in which case the circumstances may be considered drained. The main formations deposited during the pleistocene period are likely to have little potential for static liquefaction, because they have been deposited by meltwater in rough river regimes. This relatively fast deposition allows little sorting of fractions and erosion of the particles. Hence these formations largely consist of coarse to very course graded (sub-)angular sands and gravel.

Among the most influential loading conditions, we must consider to be the freezing and defrosting of the subsoil, the drive of the ice formations during the ice ages, also causing high horizontal stress levels[13] (overconsolidation), and the large fluctuations in groundwater-level during transgression periods. All these factors have helped potentially unstable soil masses to compact and become dilative under shear loading. Of course, some of the aspects mentioned have negative effects too. The angularity of the particles increases the shear resistance of the soil which makes it more difficult to compact.

With the aid of cone penetration tests, the exact location of the formations in the subsoil may be identified. To verify the geological origin of the sand from the critical zones, and to standardize the naming of the sand, classification of the sand considered may be useful. SCW (1975) has suggested a very thorough method of classification, which has been used to classify the sand from the most critical zones of the case history sites (see Appendix 1 of Volume 3).

The classification method is based on the analysis of sieve data, and includes information on the M_{63} (d_{50} of the sand fraction), the percentage of fines, the gravel content and the grading. On the basis of classifications of different characteristic sands, found in The Netherlands, SCW has defined areas of characteristic classifications within their sand classification triangle (see Volume 3: Appendix 1). Fine little loamy poorly graded sand, which is possibly an estuarine deposit, should be considered the most susceptible soil type.

[13] This results in lower initial shear stress levels, which is in favour of the residual shear strength of the soil (see second criterion). On the other hand, high confining pressures cause a decrease in critical void ratio.

§ 2.2.3 Slope Geometry and Formation

Analysis of the slope geometry may not bring information of the actual static liquefaction potential of the soil, but the (design) steepness of the slopes, and knowledge of the proposed dredging procedures, may give an idea of the shear stress levels that will be reached in the slope. With this information, the second criterion (undrained reduced shear strength) may be evaluated.

Another point is the potential (economic) losses that are involved, should a flow slide take place. Economic losses may involve damages to infrastructure or flood protection works. If no potential (economic) losses are to be expected, extensive static liquefaction analysis may not be necessary. In such a case, it might be enough to start the dredging (tactically) away form the slope and monitor the development of the bathometry. Evaluation of the results of the soundings may give information on the susceptibility to flow slides of the local soil profile.

On the other hand, if a flow slide would lead to (economic) losses, it is advisable to conduct extensive in-situ testing and static liquefaction potential analyses. Because if a soil is suspected to be susceptible to static liquefaction, a potential time bomb is waiting to blow away any structure. It is recalled that an in-situ void ratio above the critical void ratio is not a natural state for any soil.

§ 2.3 Static Liquefaction Potential Analysis

In the next few paragraphs, the two most important criteria, on the basis of which the potential for static liquefaction may be excluded, are discussed. An activity scheme, that may be useful to follow the steps below, is presented in Figure 7 on page 17.

§ 2.3.1 Critical Void Ratio Criterion

No soil formation can liquefy under static loading if not both the in-situ void ratio and horizontal stress level are well above the associated critical void ratio of that particular soil type at the confining pressure, corresponding the considered depth (see Castro *et al.* (1977) and Torrey *et al.* (1988)). To exclude the potential for static liquefaction, it must be proven that no significant part of the slope to be evaluated has such a high in-situ void ratio.

Here is where the difficulties start. It may not be too difficult to understand the criterion, but how to prove it is false? The easiest answer would be to measure the in-situ void ratio and stress levels through the whole area of concern, take undisturbed samples to the laboratory, determine the wet critical void ratios at the corresponding confining pressures and compare the results.

However, both in-situ void ratio measurements and wet critical void ratio determinations are not easy to conduct (and hence they are expensive), let alone the determination of the in-situ stress levels. Besides, the accuracy of the tests are disputable. For these reasons it seems better to resort to a modified criterion, which is true only if the criterion mentioned above is true. This would be the case if we took not the wet critical void ratio as a reference, but the somewhat lower, dry critical void ratio. Hence, this criterion is somewhat on the safe side:

$$\frac{e_{crit,\,dry}}{e_{in-situ}} \geq 1$$

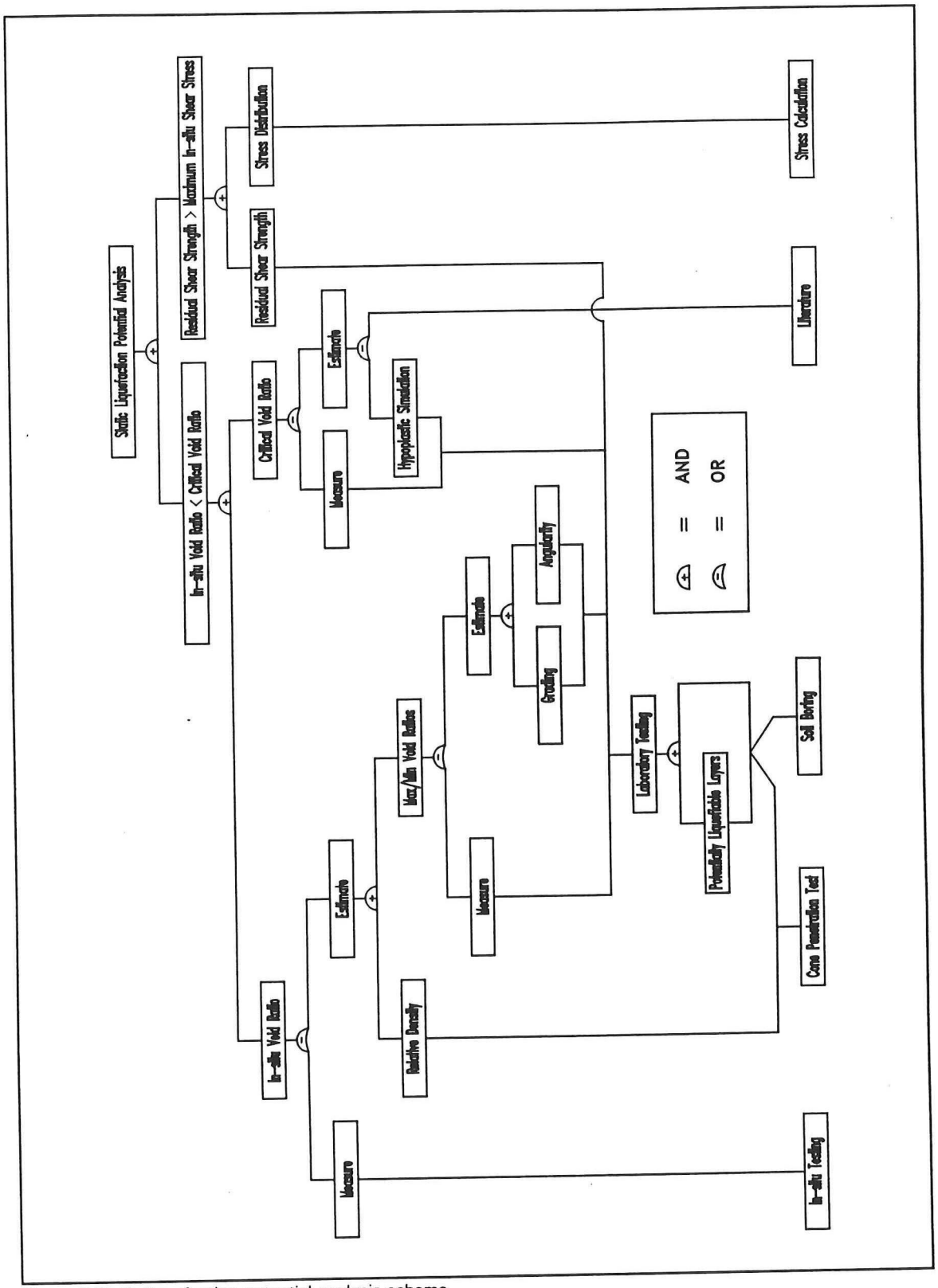

Figure 7 Static liquefaction potential analysis scheme

Here, normally consolidated soil profiles are assumed. If the geological survey casts suspicion on the fact that high initial stress levels are present, extra caution is needed. Also, it should be noted that critical void ratio tests involve the reconstitution of the soil, before testing. This means that the influence of anisotropy is discarded. It might be worth to test an undisturbed sample from the most critical zone on its deformation behaviour under shear loading. However, the least disturbance may cause such a fall in void ratio, that the specimen does not exhibit continuous softening, resulting in liquefaction, any more.

Remains the difficulty of determining the void ratio in-situ. If in-situ measurements are not available, an estimation must be made. This may be done via relations between the cone resistance values and the void-ratio-based relative density of granular soils, together with the maximum and minimum void ratios obtainable for the soil considered. Of all relative density prediction methods, the formula of Jamiolkowski *et al.* (1988) seems to give the lowest values. The expression is given on page 5. However, the compressibility of the sand is not accounted for, by Jamiolkowski. For Dutch soils, this is not considered to be a significant shortcoming, because in general, Dutch sands consist mainly of quartz, which has a medium to low compressibility. Jamiolkowski's formula is based on medium compressible sands, see Juang *et al.* (1996). Therefore, it underestimates the relative density in-situ, somewhat, which is favourable.

Lower cone resistances and higher mean effective stress levels lead to lower predictions of the relative density: $\sigma'_m = \frac{1}{3}(\sigma'_v + 2\sigma'_h)$. In normally consolidated soils, σ'_h may be estimated with the aid of: $K_0\,\sigma'_v$, where K_0 equals approximately $1 - \sin\phi \approx 0.5$ (high estimation). The value of σ'_v may be calculated using $(\gamma_s - \gamma_w) \approx 20\ kN/m^3$ for sandy layers and $(\gamma_s - \gamma_w) \approx 15\ kN/m^3$ for clayey layers (high estimations). The unit weight of the pore water may be estimated to be $\gamma_w \approx 10\ kN/m^3$.

To verify the sensitivity of the relative density estimation with Jamiolkowski's formula, a prediction has been made for case history I, assuming $(\gamma_s - \gamma_w) \approx 10\ kN/m^3$ for sandy layers and for clayey layers: $(\gamma_s - \gamma_w) \approx 5\ kN/m^3$. The results are presented in Figure 8 on page 19 through Figure 10 on page 20. It may be concluded that the higher values of $(\gamma_s - \gamma_w)$ lead to an underestimation of the relative density, but the influence is only a few percent. The difference increases with depth.

To calculate the in-situ void ratio from the estimated relative density, the maximum and minimum void ratios of the sand from the most critical zones must be determined. If not available, which is mostly the case, the maximum and minimum void ratios must be estimated. Youd (1973) investigated the factors influencing the maximum and minimum void ratios. He concluded that these depend on the grading, $C_u = d_{60} / d_{10}$, and the angularity of the material. The maximum and minimum void ratios both increase with more uniform and more angular material (see Figure 11 on page 21 and Lambe *et al.* (1979)).

Having established values for the relative density and maximum and minimum void ratios, we may estimate the in-situ void ratio. The static liquefaction potential criterion thus turns into:

$$\frac{e_{crit,\ dry}}{e_{in\text{-}situ,\ estimated}} \geq 1$$

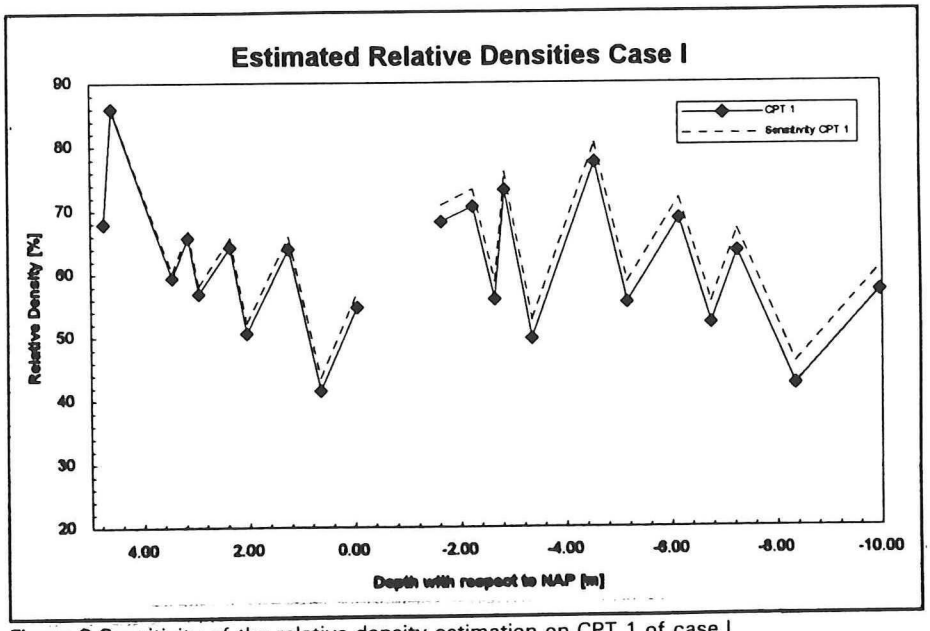

Figure 8 Sensitivity of the relative density estimation on CPT 1 of case I

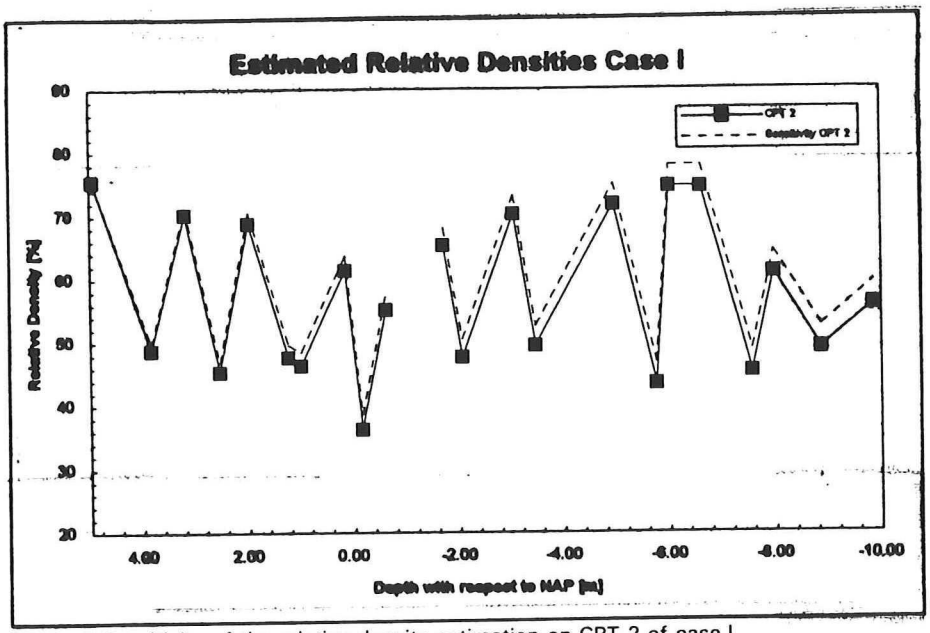

Figure 9 Sensitivity of the relative density estimation on CPT 2 of case I

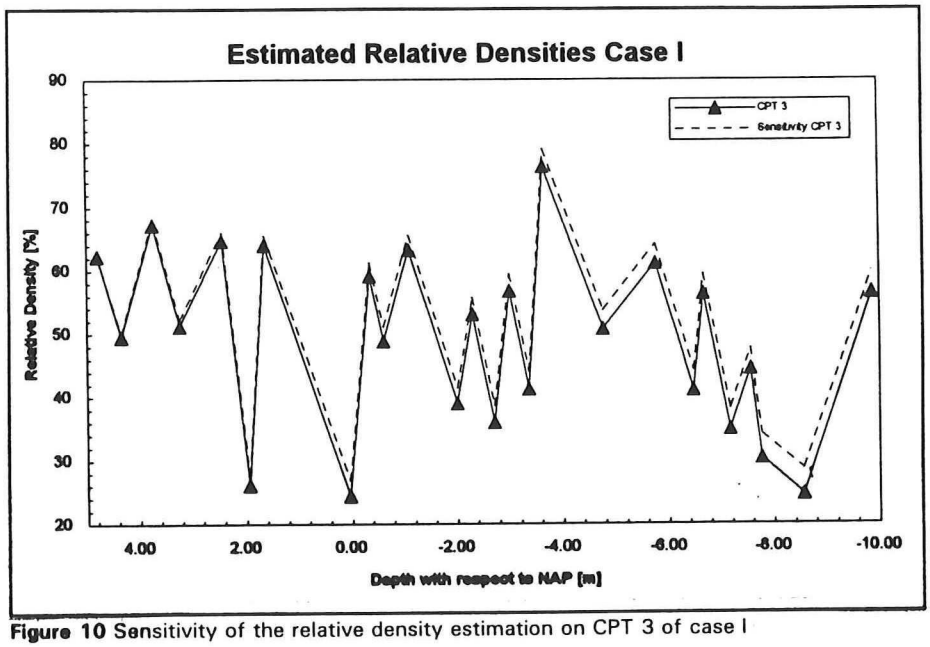

Figure 10 Sensitivity of the relative density estimation on CPT 3 of case I

Alternatively, the void ratio criterion may now be written in terms of relative density, when the critical void ratio is made relative to the maximum and minimum void ratios. Note that densities act inversely proportional in relation to void ratios.

$$\frac{Dr_{in\text{-}situ,\ estimated}}{Dr_{crit,\ dry}} \geq 1$$

What happens if no critical void ratio test results are available? If fact, now there are two possible options. First, it is possible to simulate critical void ratio tests with a hypoplastic single tensorial equation model (see e.g. Kolymbas *et al.* (1994)) or elastoplastic deformation models (see e.g. Stoutjesdijk *et al.* (1994)). To be able to run these models, ordinary triaxial test and several other standard laboratory test results are needed.

Second, it is possible to resort to previously conducted critical void ratio tests, which have been described in literature. However, any estimation from literature will lead to very poor results, as the critical void ratio should be considered a specific material constant, which may vary with the mean particle size, the grading and angularity of the particles (possibly among other factors of influence). No direct relation has been established, as yet, between the (wet) critical void and C_u, the angularity, maximum and minimum void ratios, or any other (combination of) material properties. Other case histories have shown that there is no evident (quantitative) relation between the relative density and the critical void ratio, other than that densely packed sand (Dr $\geq$ 67) will not liquefy.

A direct relation between the relative density and the critical void ratio is not imaginarily, however, as the minimum and maximum void ratios are expected to be material constants. If the relative density at the critical void ratio could be established, it would be a useful criterion for the in-situ relative density. Extensive laboratory research would be necessary to be able to derive such a relationship.

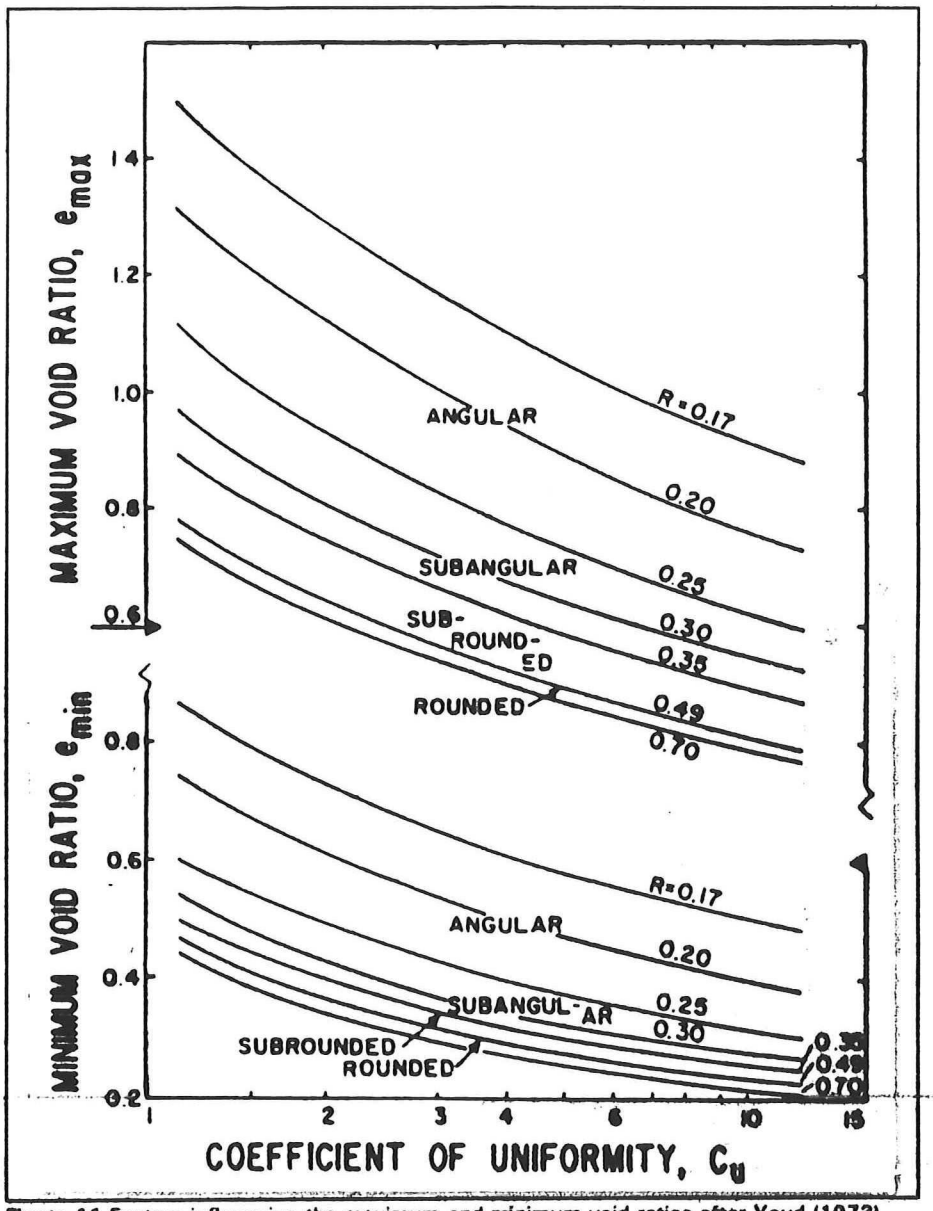

Figure 11 Factors influencing the maximum and minimum void ratios after Youd (1973)

For want of results of critical void ratio tests, the values found by Lindenberg *et al.* (1981) have been adopted to work out the case histories. Again it is stressed that estimation of the critical void ratio from literature is by no means an accurate way to predict static liquefaction potential. This may be evidenced by the fact that the material from the most critical zone of case history IV does not seem to have a critical void ratio at all, as is suggested by the in-situ void ratio estimation chart (see Volume 3, Appendix 1)

Concluding, at least the results of a cone penetration test must be available, together with sieve analyses of the material from the most critical zone and critical void ratio test results, to be able to do any substantial static liquefaction potential analysis. Preferably, an estimation of the in-situ void ratio and maximum and minimum void ratio determinations should be available too.

§ 2.3.2 Shear Resistance Criterion

If a soil mass could not be proven to be non-susceptible to static liquefaction on the basis of the first 'hard' criterion (critical void ratio criterion), a flow slide may be triggered at any time. However, not if the undrained reduced shear strength of the soil is not exceeded by the in-situ shear stress level. The undrained reduced shear strength criterion reads:

$$\frac{\tau_{reduced,\ undrained}}{\tau_{in\text{-}situ,\ max}} \geq 1$$

The reduced shear strength is composed of the shear resistance in the steady state of deformation and the initial shear stress level in-situ (see Kramer *et al.* (1987)). Thus, it may be concluded that high initial shear stress levels have an unfavourable effect on the static liquefaction potential. One should thus be cautious with respect to large stress combinations in the subsoil. In The Netherlands, this pre-compression may be present at the boundary of the former ice mantle (The soil at these locations, however, are not likely to be contractant, however. Thus the critical void ratio criterion is normative).

This phenomenon may be understood when one realizes that, to start plastic deformation, the peak shear strength of the soil must be exceeded, which is just beyond the shear resistance in the steady state of deformation, for loosely packed soils (see Kramer *et al.* (1987). In the case of loosely packed sands, the peak resistance is governed by the intergrain sliding friction. Therefore also, little angular material is more susceptible to static liquefaction than more angular material.

A procedure to estimate the reduced shear strength of the material in-situ has been proposed by Poulos *et al.* (1985). The maximum in-situ shear stress level may be determined from stress calculations, using the design pit geometry and stress history. During the construction phase however, slope angles may be steeper (within the design profile), temporarily. At this time, the undrained reduced shear strength may be exceeded, causing liquefaction anyway. For this reason, evaluation of the shear resistance criterion, alone, is not sufficient.

§ 2.4 Resume of Recommended Step Analyses

In the previous paragraphs, the evaluation of factors of influence on the prediction of has been discussed. So-called 'soft' criteria, like the thickness of layers in the soil profile and the geological history of the soil, may help to judge in a specific situation. However, on the basis of these 'soft' criteria, the occurrence of liquefaction, possibly leading to flow slide failure, cannot be excluded.

On the other hand we have seen that there are in fact two criteria on the basis of which the occurrence of liquefaction induced flow slide failure may be excluded. The evaluation of these 'hard' criteria demands the establishment of the critical void ratio and reduced shear resistance, respectively, of the material in-situ. Also, it has been argued that the only acceptable 'hard' criterion is that of the evaluation of the critical void ratio.

Below, a summary has been given of activities that could be carried out within the framework of static liquefaction potential analysis. It comprises the evaluation of 'soft' and 'hard' criteria as well as office, field and laboratory data. On the basis of this step analysis flow slide failure cannot be excluded entirely, as flow slide failure may be induced by other mechanisms than liquefaction alone (see Chapter 3).

1. **Conduct one or more (indicative) cone penetration tests at the site of concern.**

2. **Evaluate, on the basis of the geography of the site the following geological data:**

   a. expected geological formations,
   b. probable means of deposit and grain characteristics,
   c. loading history.

3. **Interpret the cone penetration tests and evaluate:**

   a. the exact soil profile (stratigraphy and inhomogeneity),
   b. the location and thickness of possibly loosely packed sand layers and, in combination with the geological data, establish the *most critical zone(s)*,
   c. the normative cone resistance and friction ratio profiles,
   d. the depths at which (special) samples must be taken, in such a way that:

      I. of every significant layer the unit weight may be estimated,
      II. from the most critical zone(s) every 1 meter, depending on the layer thickness, a sample is taken (at least three in total per most critical zone),

4. **Conduct one or more a soil borings and:**

   a. take undisturbed samples, as cautiously as possible, form the significant layer(s) for in situ void ratio determination in the laboratory,
   b. retrieve enough material from the selected depths in the most critical zone(s) for laboratory tests (critical, maximum & minimum void ratio).

5. **Conduct laboratory tests and determine:**

   a. the oven dry weight of the samples from each significant layer,
   b. the maximum & minimum void ratios,
   c. the dry critical void ratio at (three) different levels of confining pressure, under which one close to the expected in-situ horizontal stress to establish the dependency of the critical void ratio on the confining pressure, and if required (optional):
   d. extensive classification (including particle size distribution curves) of the material from the most critical zone(s), according to the SCW (1975) proposition,
   e. Volders & Verhoeven sharpness index,
   f. reduced shear resistance of the soil in the most critical zone(s).

6. **Estimate the relative density of the soil in-situ on the basis of the cone resistance and the friction ratio, from the normative cone penetration test profile, with for example Jamiolkowski's relation or Juang's fuzzy numbers.**

7. Estimate the in-situ void ratio profile with depth from the maximum and minimum void ratios and the interpreted relative density. If these values are lower than those of the in-situ weighed samples, they may need to be adjusted to the in-situ measurements, or other means of in-situ void ratio determination must be applied.

8. Plot the critical void ratios versus the confining pressure used in the critical void ratio tests and plot, in the same graph, the estimated in-situ void ratios versus the presumed normally consolidated in-situ stress level, for each most critical zone. The latter line must be well above the first, for all samples, to classify the soil "susceptible to flow slide failure due to liquefaction".

9. Evaluate the reduced shear strength criterion on the basis of the design of the pit (optional).

The resulting prediction of the tangent of the run-out angle of the active bank is calculated as the vertical propagation velocity in proportion to the horizontal retrogression velocity, calculating the fall velocity of a grain, W_d, at concentration C_0, as $W_\infty (1-C_0)^n$, with $n = 4$:

$$\tan\alpha = \frac{V}{Z} = \frac{C_0 W_\infty (1 - C_0)^n}{Z \Delta C}$$

Unfortunately, the resulting slope angle appears very sensitive to variations in C_0, while the value of C_0 must remain a guess, in absence of experimental evidence. It has been tried to avoid this difficulty by estimating the horizontal travelling distance of the grains falling of the oversteepened face. From this analyses the encountered low run-out angles can be calculated.

Another noteworthy finding of Torrey *et al.* (1988) is that, from the relation found for the prediction of the horizontal travelling distance of the upper most grains in the fluidized carpet, it appears that the production of the active bank is an important parameter. The formation of the fluidized carpet is implicit in this relation.

The horizontal travelling distance of the grains varies linearly with the height of the active bank. In small scale tests, the horizontal travelling distance, in proportion to the production of the active bank, is such that the run-out angle is closer 30° than to the flat slope angles as were observed by Torrey *et al.* (1988). From this, they conclude that small scale tests are inappropriate to model flow behaviour.

§ 3.2 Basic Mechanisms Related to Active Bank Development

Active banks may develop in clean non-cohesive low permeable granular materials, that are densely packed, and stretch over reasonable depths, only. An active bank is always initiated by an unstable oversteepened face, which may have been formed by severe local scour in the outer bend of rivers (see Torrey (1988)) or dredging activities (De Koning (1970, 1981) and also Brouwer *et al.* (1989, 1992, 1995)).

De Koning (1970) first stated that active banks should be seen as successive slides, which are delayed by virtual cohesion. The cohesive forces, that give the sand mass a temporary shear resistance, and even the potential to resist tensile stresses, are induced by negative pore pressures as a result of dilatancy. The rate of increase in pore volume depends on the groundwater flow towards a critical slip surface. Once enough water has flowed towards the pores, and the virtual cohesion has diminished in such a way that the shear resistance is lower than the gravity induced shear stress level, a slice slips from the oversteepened face, leaving again an oversteepened face in which the same process continues.

Meijer *et al.* (1976) and Van Os *et al.* (1987) also formulated the process of successive sliding, using a moving coordinate system. Hence, a force controlled continuous failure mechanism is simulated, not a spontaneous and autonomous one.

Torrey (1988) considers an active bank as an oversteepened face, of which the granular material rains off, particle-wise, and is transported away from the toe of the active bank in a density current, successively. Again, negative pore pressures, caused by dilatancy, initially prevent the individual particles to come off. The rate of retrogression depends on the permeability and the necessary volume strain (Δn effect) to loosen the particles. This is in complete agreement with the basic mechanisms considered by De Koning, Brouwer, Meijer & Van Os.

An important feature of active bank development is a density current that may or may not develop at the toe of the active bank. Whether a sustaining active bank develops, depends on whether the material coming off the face of the bank is transported away from the toe. If it settles near the toe, the height of the active bank will diminish and the mechanism will come to a halt. Whether a density current develops from the toe of the active bank, heavily depends on the production (and hence on the height of the face and the packing and grading of the material).

§ 3.3 Hypothesized Development of Active Banks

All mechanisms mentioned above are thought to play a vital role in the development of sustaining active banks, as we will see. Now, lets hypothesize, following De Koning (1981), on what may actually happen when a suction pipe is lowered into a sand formation, in order to mine sand in a sand borrow pit. Suppose we separate the life-cycle of an active bank into four stages:

1 the penetration of the suction pipe,
2 the successive sliding of the initial suction hole walls,
3 the development of a sustaining active bank,
4 the active bank propagation comes to a halt.

STAGE 1: A sand formation is penetrated with a suction pipe, say vertically for the sake of simplicity. As the suction pipe is lowered onto the pit floor, water is pumped up through it. Near the pit floor, a very strong current develops between the pit floor and the suction pipe entrance, which causes the pit floor to erode. A small conical initial suction hole develops due to scour (see Brouwer (1992)). The suction pipe never touches the pit floor, which makes the pit floor appear to be 'as soft as butter'.

Theoretically, very careful suction and low penetration rates would result in conically formed suction pits, with slopes at the angle of natural repose, in any cohesionless sand formation. However, the production would be very low for more fine sand, because of its low permeability.

Relatively fast penetration, in relation to the permeability of the sand, causes a cylindrical initial suction hole, the walls of which remain stable, temporary, as a result of the delating behaviour of the sand mass at plastic deformation. The size of the hole depends on the scouring properties of the mixture flow between the suction pipe and the soil mass (see Brouwer (1992)). A schematic view is given in Figure 15 on page 47 in Enclosure I.

STAGE 2: As the initial hole becomes deeper, through continuous penetration of the suction pipe, the shear stresses in the suction hole walls increase. Depending on the geometry and soil properties, part of the initial hole collapses as a result of geomechanical instability. The slice liquefies instantly, filling the initial hole with a mixture of sand and water. Temporarily, other slices are less critical, as the mixture is heavier than water. The number and extent of the slides depend on the aggressiveness in the suction operation (penetration speed and suction).

The slip surface of the collapsed part of the wall is not stable itself because the liquefied material is dredged before it gets the opportunity to resettle. This leads to a pattern of successive slides. The lower end of the slip surface tends to be less steep. Therefore, the height of the successive slides is expected to decrease. The resulting slope may be in the order of the angle of natural repose under water (α_r). A schematic view is given in Figure 16 on page 47 through Figure 18 on page 48 of Enclosure I.

STAGE 3: When the successive slides, which are decreasing in height, occur further from the suction pipe, the disintegration of the sand at the previous slip surface may become more important than the geomechanical instabilities. The individual particles come raining off the previous slip surface and the oversteepened face retrogresses. It is supposed that if the retrogression of the face, which depends on the permeability properties of the soil mass and the scouring properties of the disintegrated sand, exceeds the development of new potential slip surfaces, no new geomechanical instabilities will occur and a sustaining active bank may develop (see Figure 19 on page 49 of Enclosure I).

Whether or not a sustaining active bank may develop, depends on the grading (uniformity, permeability & dilatancy), fine content (cohesion & permeability) and angularity (raining & scour). Supposedly, fine (low permeability & hindered settlement) clean (little cohesive) well packed uniform (large dilatancy effect & little natural cohesion) angular (high shear resistance & heavy scour when raining) sands are among the most likely sands to develop active banks.

If the retrogression velocity of the oversteepened face should not exceed the propagation of the development of critical slip surfaces at any time, no sustaining active bank can develop and the resulting slope angle will be approximately that of natural repose under water. Maybe, this usually happens in suction operations, when coarse sand or gravel is dredged from sand borrow pits.

STAGE 4: An active bank may cease to exist as a result of one of three main processes. First, as stated in the above, transportation of all disintegrated sand away from the toe of the bank is necessary for an active bank to be able to sustain. The development of a density current towards the suction pipe entrance is vital to the continuation of the active bank. As soon as material settles near the toe of the retrogressing face, its height will diminish and eventually the disintegration process will stop, resulting in an angle of natural repose. Obviously, fine material may form a density current more easily than coarse material. However, not only the particle size is considered to be important, but also the production of the active bank. A high bank production will keep the disintegrated material in suspension.

Second, even if a density current develops, the propagation of an active bank may come to a halt as a result of local disturbances. Inhomogeneity, in any form, are considered to be the reason for these disturbances, always causing a sudden overproduction. A clay layer, for example, may mark the end of an active bank: the active bank will propagate underneath it until the layer fails, blocking the density current from the active bank, if not all clay is transported away by the density current. Also, differences in packing may cause sudden overproduction. The resulting slope profile of an active bank, which stopped as a result of a local disturbance, will display an equilibrium slope angle, at which the density current flowed towards the suction pipe, with an angle of natural repose under water, at the location of the fatal disturbance.

Third, an active bank may cease to exist because its production exceeds the pump capacity of the suction dredger (see Brouwer (1992)). If not all material, which is transported from the active bank to the suction pipe entrance in a density current, is pumped up by the dredger, it will inevitably settle near the suction pipe. This sedimentation process will cause an upward pressure gradient in the density current, resulting in a lower flow velocity and hence in a sedimentation process, moving toward the active bank. Resedimentation of the disintegrated sand will diminish the height of the active bank, and eventually cause the active bank to silt in (see Figure 19 on page 49 of Enclosure I). The resulting slope angle may have any value between 0 (horizontal) and the angle of natural repose.

Overproduction is (mainly) caused by the three dimensional nature of an active bank. According to Brouwer *et al.* (1992, 1995) active banks develop in sectors around the suction pipe as a result of inhomogeneity. With increasing radius, the effective area of the active bank increases. Hence the production of the sector increases too (see for an example plan view of a sand borrow pit Figure 20 on page 49 in Enclosure I).

§ 3.4 Hypothesized Active Bank Induced Flow Slide Failure Mechanism

Obviously, in coarse material, a sustaining active bank nor a density current will ever develop. Take for example gravel: on a very small scale successive slides may be observed, but immediate settlement prevents active bank development. Therefore, a conically formed suction pit will be the result of gravel suction. However, with increasing fineness (relative to the scale of the processes and forces), other mechanisms, like active bank development, may set on.

As long as the capacity of the pump of the suction dredger exceeds the total production of the active bank, the active bank may continue to exist. It will probably move away form the suction pipe at an angle which is equal to an equilibrium angle of the density current (gravity against friction for stationary flow)[14]. On the other hand, if the density current may flow from the active bank towards and beyond the suction pipe, resedimentation may not occur (at the same rate) as before. This also results in the fact that the active bank is more likely to sustain.

An active bank may simply continue under a layer of overburden material (loam or clay). As soon as the hole underneath the undermined clay is big enough and the shear stresses in the overburden layer exceed its shear resistance, it will slide. By blocking the density current, the slide will stop the active bank. The resulting subaqueous slope angle will be equal to the equilibrium slope angle, at which the density current flowed towards the suction pipe entrance.

Herewith, the formation of the damage profile of a flow slide failure, as defined in the Introduction to this study, has been explained. This makes active bank development a plausible mechanism leading to what is often called "flow slide failure".

§ 3.5 Recommendations to Suction Operations

If the potential for static liquefaction has been excluded, it would be useful to engineering consultancy practice to be able to predict the potential for active bank induced flow slide failure. Unfortunately, at this stage, it is impossible to do so in a quantitative way. The potential for flow failure may be expressed in terms of likelihood, considering the soil profile, soil properties and construction method. As the prediction of the development of active banks remains a difficulty, advise shall be given in terms of pit formation limitations.

Sometimes, it is proposed to start dredging tactically from the middle of the future pit contours. Together with regular survey of the bathometry of the pit, average resulting slope angles may be established, as well as the potential for liquefaction induced failure. However, if static liquefaction has been proven to be out of the question, and th risk of active bank induced flow slide failure is to be reduced to a minimum, it seems advisable to start near the edge of the permitted profile. Possible active banks will then be stopped as a result of overproduction, when careful suction is applied: the disintegrated soil must accumulate near the suction pipe entrance.

Another, even safer possibility, is to excavate the permitted slope profile by other means of dredging, for example with backhoes or special slope suction dredgers. From the initial canal, or any other point within the future pit contours, suction may be commenced without running the risk of active bank induced flow slide failure of the constructed embankment, as long as suction is restricted to a level no deeper the than the depth of the initial canal (see Figure 13 on page 30).

---

[14] De Koning proposes to describe the flow of the density current with the theory of Chézy, which says that for equally formed streams, the flow velocity is proportional to the square root of the hydraulic radius and the slope gradient: $U = C \cdot \sqrt{(R \cdot i)}$. This would mean that with increasing hydraulic radius (thickness of density current), which is the case when moving in the direction of the suction pipe as a result of three dimensional effects, the slope gradient must decrease at constant flow velocity.

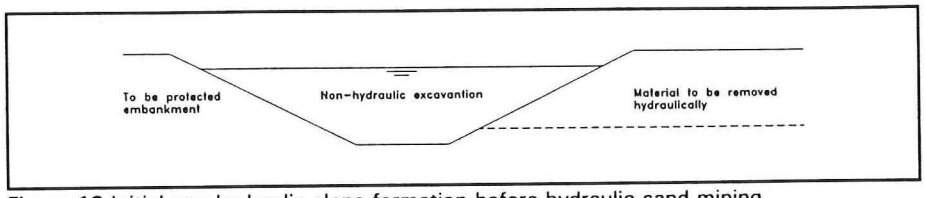

Figure 13 Initial non-hydraulic slope formation before hydraulic sand mining

Finally, it may be possible to increase the stability of the most critical slopes with the aid of groundwater suction around the pit. The imposed gradient in groundwater flow from the pit into the slope may help to increase the micro stability. When the desired subaqueous slope angles have been established, the ground water suction may be released. This method may lower the risk of active bank development, but does not exclude it. Besides, for deep sand borrow pits, this may be an expensive solution.

Conclusions & Outlook

The subject of study has been the failure of subaqueous excavated slopes. This graduate study has been a quest for the mechanism leading to unintended failures, retrogressing into the embankment and resulting in extremely flat subaqueous slopes. It has been a quest through different fields of science: geomechanics, dredging technology, river mechanics, geology, road construction, and hydraulics.

The main conclusion that may be drawn, is that many flow slide failures (presumably) have been wrongly imputed to a spontaneous collapse of loosely packed soils, resulting in liquefaction of a large part of the slope, in the past. Hypothetically, this failure mechanism belongs to the possible causes of flow failure accidents, but in reality its occurrence is not very plausible, in most cases.

To confirm the statement above, an answer has been sought to the question of what may happen instead, if liquefaction cannot be indicated to be the actual cause of flow slide failure. The answer has been found in the process of active bank development, also known as retrogressive (slip) failure. With this mechanism the very flat slopes, after failure, may be explained. However, a dispute remains on the exact origin of the (virtual) run out angle of the active bank. See for a schematic presentation of the scope of slope failures in general, and the position of possible flow slide failures therein, Figure 14 on page 33.

In this chapter, all conclusions that may be drawn from the previous chapters are summarized. This chapter is concluded with recommendations toward engineering consultancy and further study.

Conclusions in general:

1. A flow slide is generally known as a reference to a failure type of subaqueous slopes, which involves large soil displacements, causes the embankments to cave in and results in very flat slope angles after failure.
2. The term "flow slide" itself does not hold an explanation for the actual failure mechanism. It refers to the consequences of the failure rather than the fundamental mechanisms.
3. Flow slides may be caused by different failure mechanisms:

    a. Static Liquefaction of (part of) the subaqueous slope;
    b. Active bank development from the toe of the subaqueous slope.

Conclusions with respect to liquefaction induced flows slide failure:

4. Static liquefaction is the result of continuing softening behaviour of a contractant soil mass, being exposed to a monotonic level of shear stress.

5. The potential for static liquefaction is governed by the potential fall in void ratio, the extent of the contractant body, the level of shear stress, the in-situ stress level, and whether or not the loading conditions may be considered undrained.

a. A void ratio above the dry critical void ratio is, by definition, not a natural state. Therefore, soil that has a void ratio above the dry critical void ratio finds itself in an unstable equilibrium.

b. Soil will always tend to decrease its void ratio, as long as it is above the dry critical void ratio. In this process it is hindered by its internal friction properties.

6. In a significant part of a subaqueous slope, the combination of void ratio and confining stress must be well above critical-void-ratio line, which may be established from critical void ratio tests. Soils that are not definitely supercritical, often dilate after initial contraction and fall back into a hardening regime: no full liquefaction develops.

7. There appears to be a critical shear strength, which must be exceeded before plastic contractant deformation can occur. This critical shear stress is always a little higher than the shear stress needed to break the individual particle contacts. The reduced shear strength, which should be looked upon as to the sum of the initial shear stress level and the constant shear resistance in the steady state of deformation, is a safe limit to the maximum allowable shear stress.

8. The shear loading of the contractant soil may gradually increase with the steepening or lengthening of the slope and, at some point, exceed the peak shear resistance.

9. Well graded soils have low permeabilities but high shear resistances and lower potential falls in void ratio. Soils consisting of angular particles have high shear resistances, caused by larger contact surfaces, but also have higher potential falls in void ratio (difficult to compact). The influences of soil properties are very difficult to quantify, as their part may be dual.

10. The most influential soil properties are directly related to their geological history and means of deposit. In engineering consultancy, geological considerations must play a prominent role.

11. If excess pore pressures develop high enough to liquefy a large part of the slope, the liquefied front is thought to propagate very fast through the soil mass, depending on the (in)compressibility of the pore fluid. Thus, liquefaction induced slides must take place in a relative short period of time.

Conclusions with respect to active bank induced flows slide failure:

12. An active bank may take the form of an oversteepened face, which retrogresses as individual particles rain off. The oversteepened face can exist through virtual cohesion, induced by the dilatant behaviour of the soil, under shear loading.

13. The main soil properties that govern the development of active banks are the d_{50} value and grading, both having their effect on the permeability as well as the packing. Also the angularity of the sand is important.

14. An active bank may be initiated by dredging activities as well as natural processes like scouring, by creating an oversteepened face in dilatant soil.

15. The initiation of active banks, when used for sand mining, is fairly well controllable. However, the process of disintegration of soil thereafter, is not. Until now, no prediction method has been found, based on a scientific explanation of the physical phenomenon of active bank development, on the basis of which safe design slope angles may be established. Some suggest an empirical value of $\approx$ 1:8.

16. Depending on the permeability (packing and grading), lack of inter-granular connections, homogeneity and extent (height) of the soil mass in which an active bank develops, failure occurs at a low rate, relative to the failure rate of a liquefied body. Also, unlike static liquefaction failure, active bank induced failure may seem unstoppable.

17. The subaqueous angle of repose ($\approx$ 1:3 to 1:4), which is mostly applied in the design of sand borrow pits, is not valid in general. Depending on the mining procedures, processes may be set on which may lead to arbitrary flat slope angles.

18. The active bank development is regularly disturbed by inhomogeneity in the soil, which cause discontinuities in the production of the bank. A local slide may cause an active bank to stop. The result may be a slope at the subaqueous angle of repose, locally. The more inhomogeneity, the more likely the eventual slope angle will approach the subaqueous angle of repose.

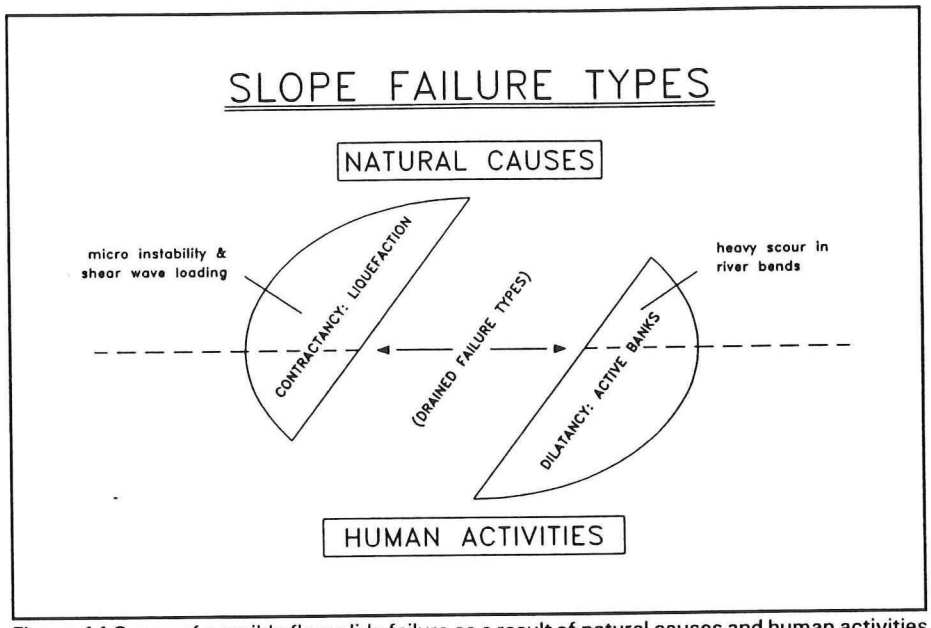

Figure 14 Scope of possible flow slide failure as a result of natural causes and human activities

Recommendations:

1. The potential for static liquefaction is not hypothetical. A static liquefaction analysis is needed in the design of sand borrow pits, especially when trigger mechanisms are likely to lie in wait (e.g. gradients in ground water flow or (traffic) vibrations). This is best done by comparing the measured or estimated in-situ void ratio to the associated critical void ratio of laboratory tested samples, from the most critical layers (taking into account the effect at increasing confining pressure).

2. The dry critical void ratio may serve as a safe and practical upper limit to the maximum allowable void ratio.

3. If structures near the boundary of the sand borrow pit are to be protected against flow slide failure as a result of static liquefaction, a good option is to create a hidden dam of compacted material, before mining. Compaction may be achieved with vibrations by means of deep compaction methods or a series of explosions.

4. If structures near the boundary of the sand borrow pit are to be protected against flow slide failure as a result of the development of active banks, a good option is to excavate a channel near the structure mechanically.

5. The mechanism of active bank development needs to be understood and be mathematically described. Then, it may be possible to be more precise in sand borrow pit design and slope angle prediction as well as in suction directions.

6. An attempt should be made to find a direct relation between the relative density and at the critical void ratio and the critical void ratio, as a function of material properties at a fundamental (individual grains) level, i.e. grading, maximum and minimum void ratio and angularity.

7. Further research in the field of stress path prediction in triaxial tests, with a tensorial equation (hypoplastic modelling), may be useful. It may lead to a way of numerically predicting the (wet) critical void ratio from standard laboratory tests.

8. To employ the thorough classification method, proposed by SCW (1975), the following sieve sizes should be added to the analysis: 710 μm, 180 μm and 90 μm.

References

BALDI G., R. BELLOTTI, V. GHIONNA, M. JAMOILKOWSKI AND E. PASQUALINI (1986), *Interpretation of CPT's and CPTU's. 2nd Part: drained penetration on sands*. Proceedings 4th International Geotechnical Seminar: Field Instrumentation and In Situ Measurements, Singapore: Nanyang Technology University, pp. 143-162.

BEGEMANN H.K.S.PH., H.L. KONING AND J. LINDENBERG (1977), *Critical density of sand*. Proceedings 9th International Conference on Soil Mechanics I, Tokyo, Japan, pp. 43-46.

BROUWER J. (1989), *Deep Dredging, its process and attractive application offshore*. Proceedings XIIth World Dredging Congress, 2-5 May 1989, Orlando, Florida USA, pp. 307-330.

BROUWER J. (1992), *Deep Dredging, some Hydraulic and Production Aspects*. Proceedings Symposium 'Zicht op Baggerprocessen', Delft University of Technology, Delft, The Netherlands.

BROUWER J., F.P. HALLIE AND A.P. LOOFF (1995), *Marine environmental effects of sand extraction at near shore locations*. Proceedings XIVth World Dredging Congress, 14-17 November 1995, Amsterdam, The Netherlands, pp. 605-626.

ELLING M.G.M., B.A. ANDEWEG, J.C. DE JONG AND C.E. SWANKHUISEN (1992), *De techniek van het schriftelijk rapporteren*. 6th edition. Lecture notes. Delft: University of Technology, Faculty of Philosophy and Tech-Social Sciences.

JAMIOLKOWSKI M., V.N. GHIONNA, R. LANCELOTTA AND E. PASQUALINI (1988), *New correlations of penetration tests for design practice*. Penetration Testing 1988, ISOPT-1. Rotterdam: Balkema.

JUANG C.H., X.H. HUANG, R.D. HOLTZ AND J.W. CHEN (1996), *Determining relative density of sands from CPT using fuzzy sets*. Journal of the Geotechnical Engineering Division, Proceedings of the American Society of Civil Engineers, Vol. 122, No. 1, pp. 1-6.

KOLYMBAS D., I. HERLE AND P.A. VON WOLFFERSDORFF (1995), *Hypoplastic constitutive equation with internal variables*. International Journal for Numerical and Analytical Methods in Geomechanics, Vol. 19, pp. 415-436.

KONING J. DE (1970), *Neue Erkenntnisse beim Gewinnen und Transport von Sand im Spülprojekt Venserpolder*. V.D.I. Tagung "Bauen im Ausland", 21.-25. April 1970, Hamburg.

KONING J. DE (1981), *Developments in hydraulic deep dredging*. Proceedings of the IVth Latin American Dredging Congress, 5-10 April 1981, Mexico-City.

LADE P.V. AND S.B. HERNANDEZ (1977), *Membrane penetration effects in undrained tests*. Journal of the Geotechnical Engineering Division, Proceedings of the American Society of Civil Engineers, Vol. 103, No. 2, pp. 109-125.

LADE P.V. (1992), *Static instability and liquefaction of loose fine sandy slopes*. Journal of the Geotechnical Engineering Division, Proceedings of the American Society of Civil Engineers, Vol. 118, No. 1, pp. 51-71.

LAMBE T.W. AND R.V. WHITMAN (1979), *Soil Mechanics, SI Version*. New York: John Wiley & Sons.

LINDENBERG J. AND H.L. KONING (1981), *Critical density of sand*. Géotechnique **31**(2), pp. 231-245.

LINDENBERG J. (1985), *Verslag inventarisatie adviespraktijk zettingsvloeiingen (report CO-416509/1)*. Delft: Delft Soil Mechanics Laboratory.

LINDENBERG J.L. (1986A), *Oevervallen in Zeeland*. I²-Bouwkunde en Civiele Techniek, No. 11, pp. 11-15.

MEIJER K.L. AND A.G. VAN OS (1976), *Pore pressures near moving underwater slope*. Journal of the Geotechnical Engineering Division, Proceedings of the American Society of Civil Engineers, Vol. 102, No. 4, pp. 361-372.

OS A.G. VAN AND W. VAN LEUSSEN (1987), *Basic research on cutting forces in saturated sand*. Journal of the Geotechnical Engineering Division, Proceedings of the American Society of Civil Engineers, Vol. 113, No. 12, pp. 1501-1515.

POULOS S.J. (1981), *The steady state of deformation*. Journal of the Geotechnical Engineering Division, Proceedings of the American Society of Civil Engineers, Vol. 107, No. 5, 553-562.

POULOS S.J., G. CASTRO AND J.W. FRANCE (1985), *Liquefaction evaluation procedure*. Journal of the Geotechnical Engineering Division, Proceedings of the American Society of Civil Engineers, Vol. 111, No. 6, pp. 773-792.

RAJU V.R. (1994), *Spontane Verflüssigung lockerer granularer Körper - Phänomene, Ursachen, Vermeidung*. Veröffentlichungen des Institutes für Bodenmechanik und Felsmechanik der Universität Fridericiana in Karlsruhe, Heft 134.

REYNOLDS O. (1885), *The dilating of media composed of rigid particles in contact*. Phil. Trans. R. Soc. 20, S5, No. 127, pp. 469-481.

SCHRIECK G.L.M. VAN DER (1996), *Baggertechniek deel V t/m VIII*. Lecture Notes. Delft: Delft University of Technology, Faculty of Civil Engineering.

SCW STUDY CENTRE FOR ROAD CONSTRUCTION (1975), *Classificatie van Zand*, Arnhem, The Netherlands.

SCW STUDY CENTRE FOR ROAD CONSTRUCTION (1979), *Various Properties of Natural Sands for Netherlands Highway Engineering*, Arnhem, The Netherlands.

SEED H.B. (1976), *Evaluation of soil liquefaction effects on level round during earthquakes*. Liquefaction problems in geotechnical engineering. New York: American Society of Civil Engineers.

SLADEN J.A., R.D. D'HOLLANDER AND J. KRAHN (1985A), *The liquefaction of sands, a collapse surface approach*. Canadian Geotechnical Journal, No. 22, pp. 564-578.

STOUTJESDIJK T.P. AND M.B. DE GROOT (1994C), *Handboek zettingsvloeiing*. Delft: Ministry of Public Works, DWW.

TERZAGHI K. (1925), *Erdbaumechanik auf bodenphysikalischer Grundlage*. Wien: Franz Deuticke.

TERZAGHI K. (1956), *Varieties of submarine slope failures*. Proceedings 8th Texas Conference on Soil Mechanics and Foundation Engineering, Austin, Texas, USA.

TORREY III V.H., J.B. DUNBAR AND R.W. PETERSON (1988), *Retrogressive failures in sand deposits of the Mississippi River (Report 1: Field investigations, laboratory studies and analysis of the hypothesized failure mechanism)*. Vicksburg, MS: Waterways Experiment Station, Geotechnical Laboratory, Corps of Engineers.

VELDHUIS A. (1992), *De uitlevering van zand, bepaling van relatieve dichtheid*. Master Thesis. Delft: Delft University of Technology.

VERRUIJT A. (1990), *Grondmechanica*. 3rd edition. Lecture notes. Delft: VSSD, Delft Publishing Company.

VERRUIJT A. (1992), *Offshore Soil Mechanics*. 5th edition. Lecture notes. Delft: University of Technology, Faculty of Civil Engineering.

WINTERWERP J.C., M.B. DE GROOT, D.R. MASTBERGEN AND H. VERWOERT (1990), *Hyperconcentrated sand-water mixture flows over flat bed*. Journal of the Geotechnical Engineering Division, Proceedings of the American Society of Civil Engineers, Vol. 116, No. 1, pp. 36-54.

WINTERWERP J.C., W.T. BAKKER, D.R. MASTBERGEN AND H. VAN ROSSUM (1992), *Hyperconcentrated sand-water mixture flows over erodible bed*. Journal of the Geotechnical Engineering Division, Proceedings of the American Society of Civil Engineers, Vol. 118, No. 11, pp. 1508-1523.

WOOD D.M. (1990), *Soil behaviour and critical state soil mechanics*. Cambridge: Cambridge University Press.

YOUD T.L. (1973), *Factors controlling maximum and minimum densities of sands*, ASTM Special Technical Publications 523.

Index

Q

R

S

V

List of Figures

English-Dutch Glossary

Active bank	Bres
Confining stress/pressure	Steunspaning/-druk [$\sigma_2 = \sigma_3$]
Density	Dichtheid
Density current	Dichtheidstroom
Deviator stress	Deviatorspanning [q] (hoofdspanning σ_1 - steundruk σ_3)
Fluidization	Fluïdisatie
Liquefaction	Verweking tot visceuze vloeistof (verlies schuifweerstand)
Mean effective stress	Gemmiddelde hoofdspanning [$p = \frac{1}{3}(\sigma_1 + 2\sigma_3)$]
Porosity	Porositeit [n]
Retrogression	Teruggang/achteruitgang
Softening	Verweking (afname schuifweerstand)
Stress path	Spanningspad (in triaxiaalproef)
Hardening	Verharden (toename schuifweerstand)
Void ratio	Poriëngetal (e)

Enclosure I: Active Bank Development Sketches

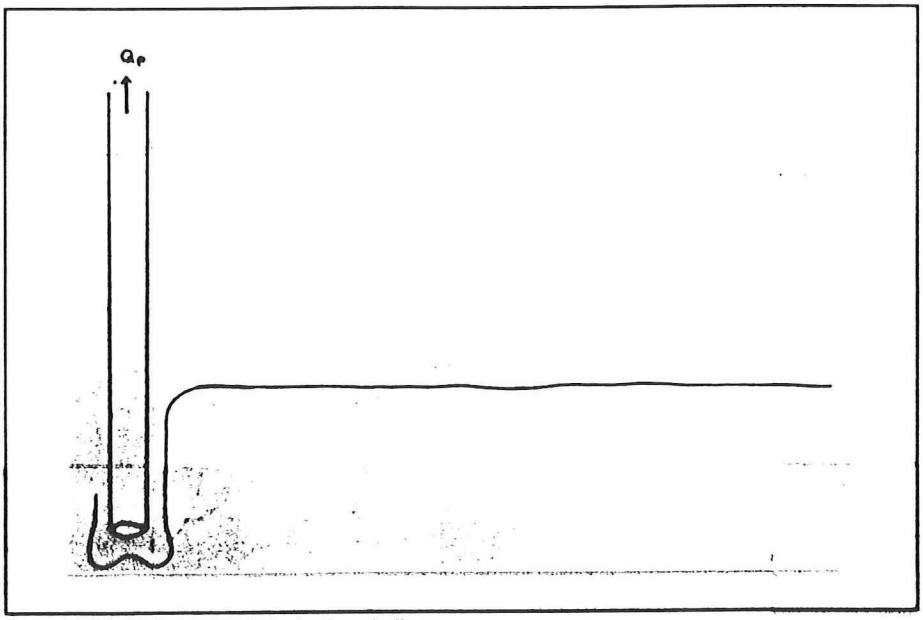

Figure 15 Initial suction hole in the pit floor

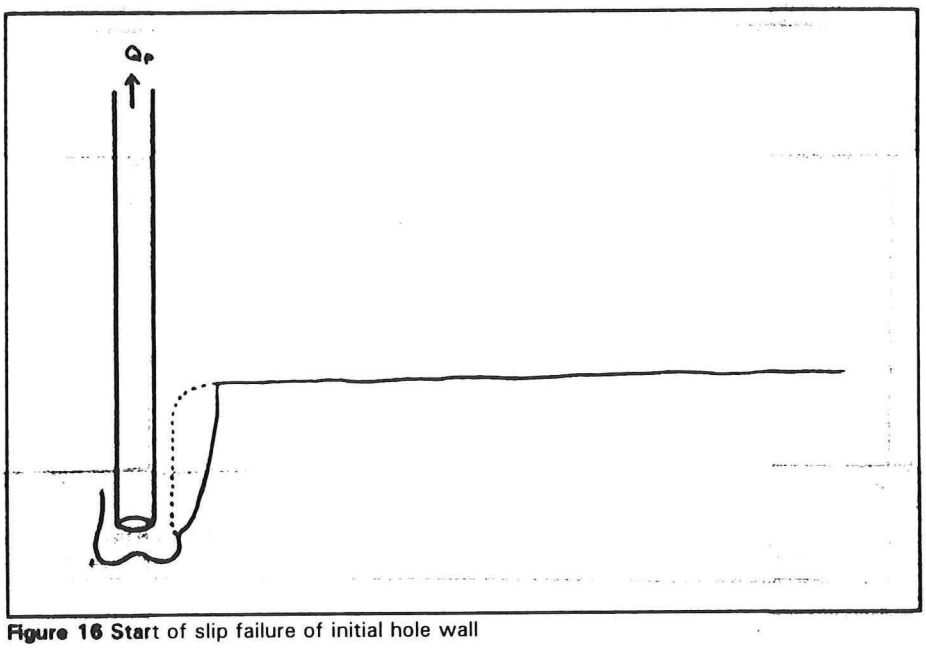

Figure 16 Start of slip failure of initial hole wall

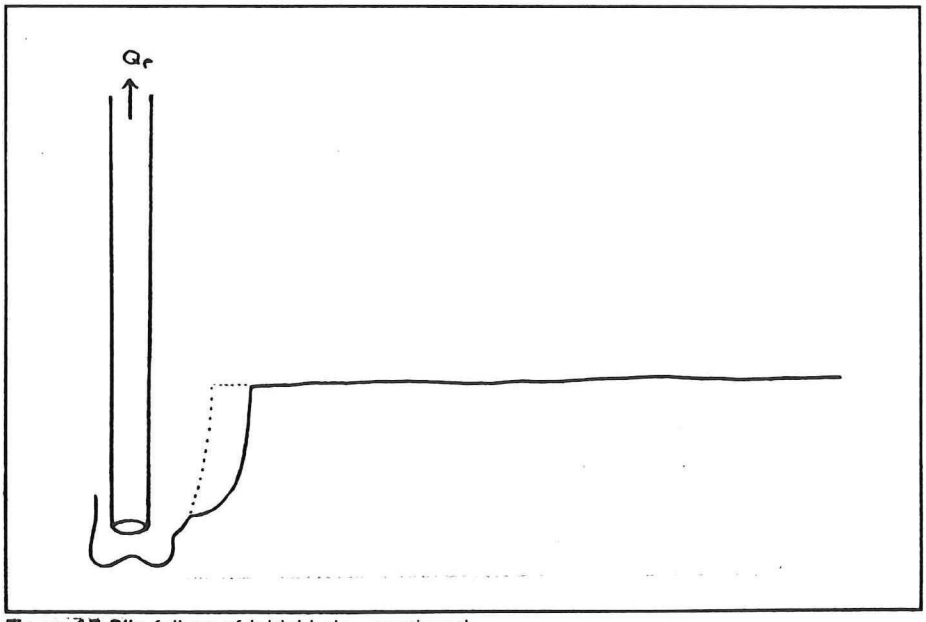

Figure 17 Slip failure of initial hole - continued

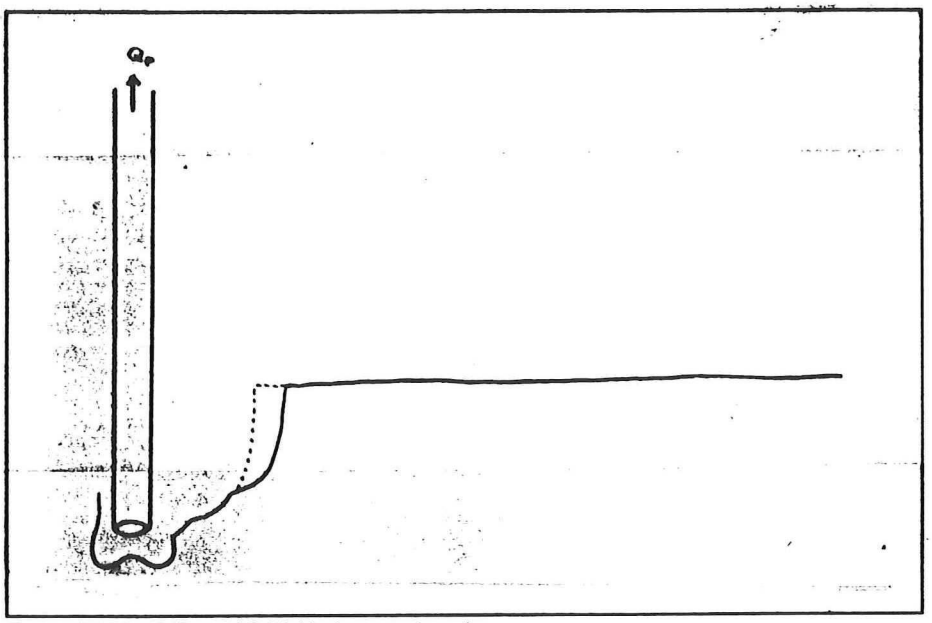

Figure 18 Slip failure of initial hole - continued

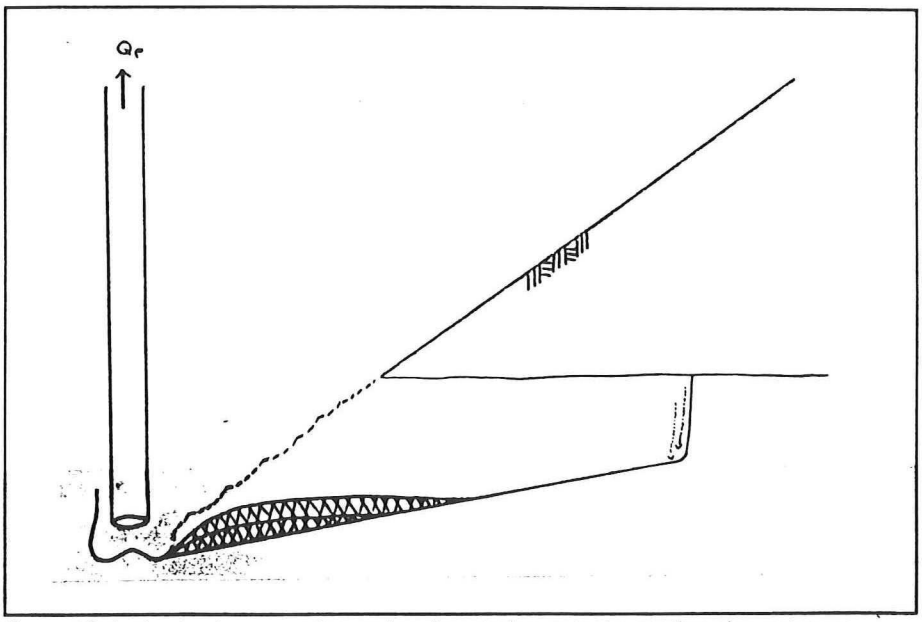

Figure 19 Active bank propagation and sedimentation near the suction pipe entrance

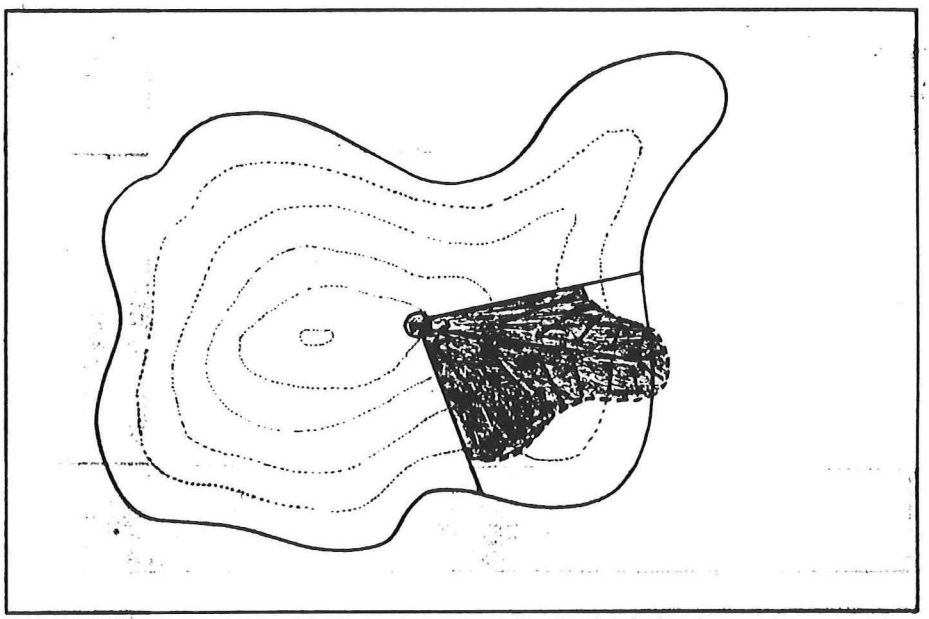

Figure 20 Plan view of the pit bathometry: sectorial active bank development

Volume 3:

Case History Study / Appendix

Flow Slide Failure

of

Excavated Subaqueous Slopes

A study of the prediction of liquefaction potential and the retrogressive nature of flow slide failure prepared by:

Tim Helbo

February - August 1996

Delft University of Technology / Fugro Ingenieursbureau b.v.

"Über die Ursachen und das Wesen der Schwimmsanderscheinung gehen die Meinungen auch heute noch recht weit auseinander"

Karl Terzaghi (1925)

"I urge you to think originally and not be bound by any standing versions of explanations"

Victor H. Torrey III (1996)

Preface

Although flow slides have been studied intensively for a long time, the fundamental mechanisms leading to this kind of soil (structure) failure are still, at least partly, a mystery.

In September, 1995, Fugro Ingenieursbureau b.v. in Leidschendam suggested to study subaqueous slope failures resulting in a flow slide, within the framework of my graduate study program. I accepted in December, 1995, and started my research, conducted in partial fulfilment of the requirements for the degree Master of Science in the Delft University of Technology, on February 1st, 1996.

The report lying before you contains the results of a case history study and trial laboratory tests. Apart from this Case History Study / Appendix, a Literature Review (Volume 1) and Directive for the Analyses of Flow Slide Failure (Volume 2) have been prepared, as part of the graduate study program.

I wish to extend my sincere thanks to J.L. Lindenberg[1], J.W. Heijting[2], J.D. van Rheenen[3], I. Herle[4], V.H. Torrey[5], J. Brouwer[6] and J. de Koning for their effort to help me further knowledge of theory and practice related to flow slide problems.

This graduate study program has been supervised by a graduate committee. The following advisors were seated in this committee:

A. Verruijt	Delft University of Technology
K. d'Angremond	Delft University of Technology
G.L.M. van der Schrieck	Delft University of Technology
M.Th.J.H. Smits	Fugro Ingenieursbureau b.v.

I wish to thank my graduate committee for its assistance.

Leidschendam, 12 September 1996,
Tim Helbo.

---

1 Ministry of Transport and Public Works (RWS), Department of Road and Hydraulic Engineering (DWW)

2 Heijting Aannemersbedrijf en Handelsonderneming bv

3 Province of Gelderland

4 Institut Für Bodenmechanik und Felsmechanik (IBF), Universität (TH) Fridericiana Karlsruhe, Germany

5 US Army Waterways Experiment Station, Vicksburg, MS, USA

6 Delft University of Technology, Faculty of Mechanical and Marine Engineering

Contents

1 Static Liquefaction Potential Analyses on four Case Histories

§ 1.1 Introduction

In chapter 2 of Volume 2 a method of analysis has been introduced, for evaluating flow slide failure(s) (potential) as a result of static liquefaction. In this appendix, four case histories from engineering consultancy practice will be evaluated, accordingly, as far as the limited available data allowed for. The case histories I & II involve actual flow slide failures. Case histories III & IV concern sand borrow pits, of which the designs have previously been evaluated for static liquefaction potential, that are not yet in (full) use.

§ 1.2 Geography & Geology

All case history sites are situated along historical streams. The formations found are likely to have been deposited by these streams. Only case history site II has been covered with ice during the ice ages. The others are situated just below the farthest ice limit. On the basis of their geographical location and knowledge of geological history (Geological Survey of The Netherlands), the following formations are expected:

Site	Pleistocene Deposits	Holocene Deposits
Case history I	o Driven medium to coarse periglacial deposits with gravel. o Fluvio-glacial layer of fine to medium fine sands, locally with gravel. o Post-glacial river valley fill of fine horizontally layered sands (terrace).	o River clay.
Case history II	o Post-glacial river valley fill of fine horizontally layered sands (terrace).	[No holocene deposits]
Case history III	o Driven medium to coarse periglacial deposits sand with gravel. Interlayered with fine sands (River Rhine and River Meuse terrace). o Post-glacial river valley fill of fine horizontally layered sands (terrace).	o Fine to medium holocene sands, interlayered with clayey sand layers.
Case history IV	o Fine and coarse fluvio-periglacial deposits and coversands.	[No holocene deposits]

From the table above, we must conclude that in none of the case histories holocene formations are expected to be present, that could lead to static liquefaction failure, except in case history III. This means we must concentrate on local irregularities in the general geological profile.

§ 1.3 Geometry

It is no use discussing the geometries of the case history sites I and II, in which failure occurred. To the north of the site of case history III lies a canal with heavy navigation. However, there is no large economic hazards in this case. To the south of the site of case history IV lies an important railway connection. Traffic vibrations may trigger liquefaction of susceptible slopes. As the most hazardous slope is the one near the existing railway, the cone penetration tests along this track were studied with extra care.

§ 1.4 Static liquefaction Potential Analysis

§ 1.4.1 Qualitative Interpretation of Cone Penetration Tests and Soil Borings

On the basis of available cone penetration tests (see Figure 5 on page 12 through Figure 18 on page 25), the exact location of the formations are determined. The cone penetration record was scrutinized for low cone resistances in sand layers. Also the possibilities for drainage (impermeable layers) were investigated. Field classifications of the borings were used for a first judgement on static liquefaction potential, from a sand property point of view (grain size, grading, cohesiveness). Altogether, this led to the identification of the most critical zones in the soil profiles (see Figure 1).

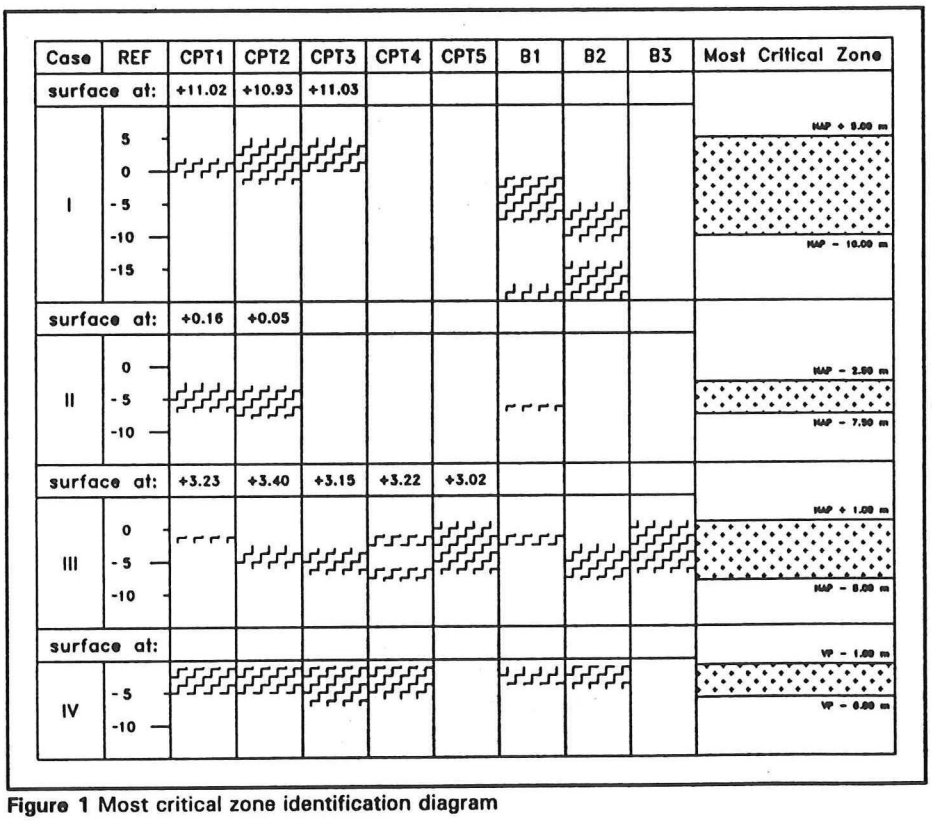

Figure 1 Most critical zone identification diagram

The conclusions, that we may draw from the interpretation of the cone penetration tests and soil borings, are summarized per case history, below:

Case I: Loosely packed layers are suspected between NAP + 5.00 *m* and NAP. This conclusion is based on low cone resistance values (in the order of 5 to 10 *MPa*), although these are not extremely low. Fine sand layers with (supposedly) low permeabilities are present between the depths of NAP - 0.50 *m* and NAP - 8.50 *m*, as well as below NAP - 14.5 *m*. Sensitive layers with thicknesses of more than 5 meter are present. All layers may drain in both upward and downward direction. If liquefaction occurs, it will probably be in the zone ranging from NAP + 5.00 *m* to a depth of NAP - 10.00 *m*. A sample from boring B1 at NAP - 1.00 *m* will be used for further analysis.

Case II: Loosely packed layers are suspected between NAP - 2.50 *m* and NAP - 8.00 *m*. This conclusion is based on low cone resistance values (in the order of 2 to 4 *MPa*), although these are not extremely low. A fine sand layer with (supposedly) low permeability is present at a depth of NAP - 7.0 *m*. No sensitive layers with thicknesses of more than 5 meter are present. The fine sand layer may drain in both upward and downward direction. If liquefaction occurs, it will probably be in the zone between NAP - 2.50 *m* and NAP - 7.50 *m*. A sample from boring B2 at NAP - 6.50 *m* would have been used for further analysis, but no test data were available.

Case III: Loosely packed layers are suspected between NAP + 1.00 *m* and NAP - 8.00 *m*. This conclusion is based on low cone resistance values (in the order of 4 to 10 *MPa*), although these are not extremely low. Fine sand layers with (supposedly) low permeabilities are present between NAP + 1.00 *m* and NAP - 8.00 *m*. Sensitive layers with thicknesses of more than 5 *m* are present, incidentally. Drainage of the fine sand layers is mostly prevented in both upward and downward direction. If liquefaction occurs, it will probably be in the zone ranging from NAP + 1.00 *m* to a depth of NAP - 8.00 *m*. Samples B5/3 at NAP - 5.65 *m* and B6/5 at NAP - 6.38 *m* will be used for further analysis (no sufficient data is available from B6/1).

Case IV: Loosely packed layers are suspected between VP - 1.00 *m* and VP - 7.00 *m*. This conclusion is based on low cone resistance values (in the order of 2 to 4 *MPa*), although these are not extremely low. Silty fine sand layers with (supposedly) low permeabilities are present between VP - 1.20 *m* and VP - 4.70 *m*. No sensitive layers with thicknesses of more than 5 meter are present. All layers may drain in both upward and downward direction. If liquefaction occurs, it will probably be in the zone between VP - 1.00 *m* and VP - 6.00 *m*. A sample from boring B2/1 at VP - 3.00 *m* will be used for further analysis.

§ 1.4.2 Laboratory Classification of Samples from the Most Critical Zones

To get a little more objective insight in the properties of the sands in the critical zones, some standard laboratory tests must be conducted. Not all information necessary was available for all case histories. Therefore, some interpretations of alternative test performances have been used.

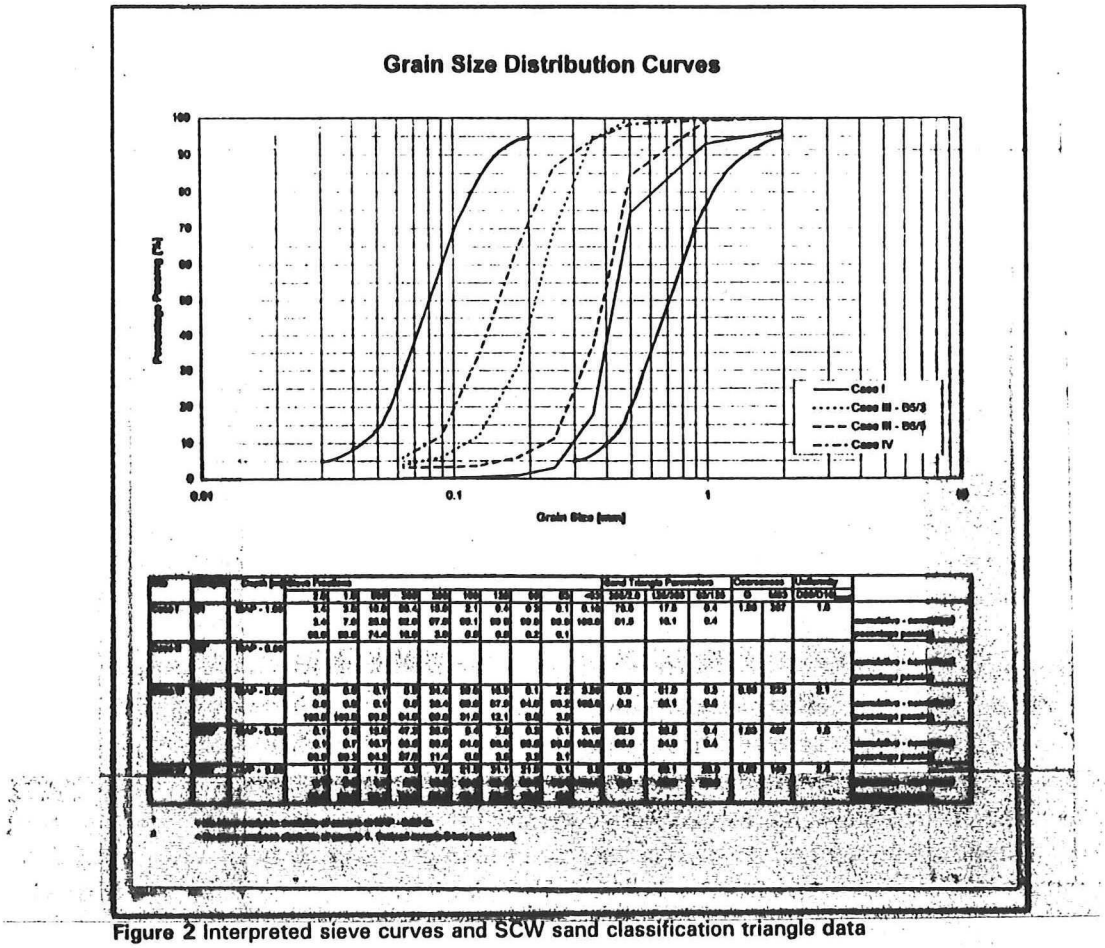

Figure 2 Interpreted sieve curves and SCW sand classification triangle data

The sieve data, of the samples to be investigated, were not fully adaptable to the SCW (1975) classification method, which has been used. The interpreted sieve curves, as well as the sand triangle classification parameters, are shown in Figure 2. Note that of case history II no sieve analyses were available. All other samples are within Ishihara's (1986) limits of most liquefiable soils.

The tested samples are drawn in the SCW sand classification triangle, as shown in Figure 3 on page 5. We must conclude that only the first sample of case history III and the sample of case IV lie in the fine-sand region. All other tested samples are more coarse.

When comparing the location of the tested samples to the general locations of eight characteristic sandy deposits for The Netherlands (see Figure 19 on page 26), the sand from the critical zones of case histories I & III (sample B6/5) seem likely to be coarse river sand deposits. The sand from sample B5/3 of case history III seems likely to be a fine river sand deposit. The sand from case history IV is likely to be a coversand These findings are in accordance with the geological survey.

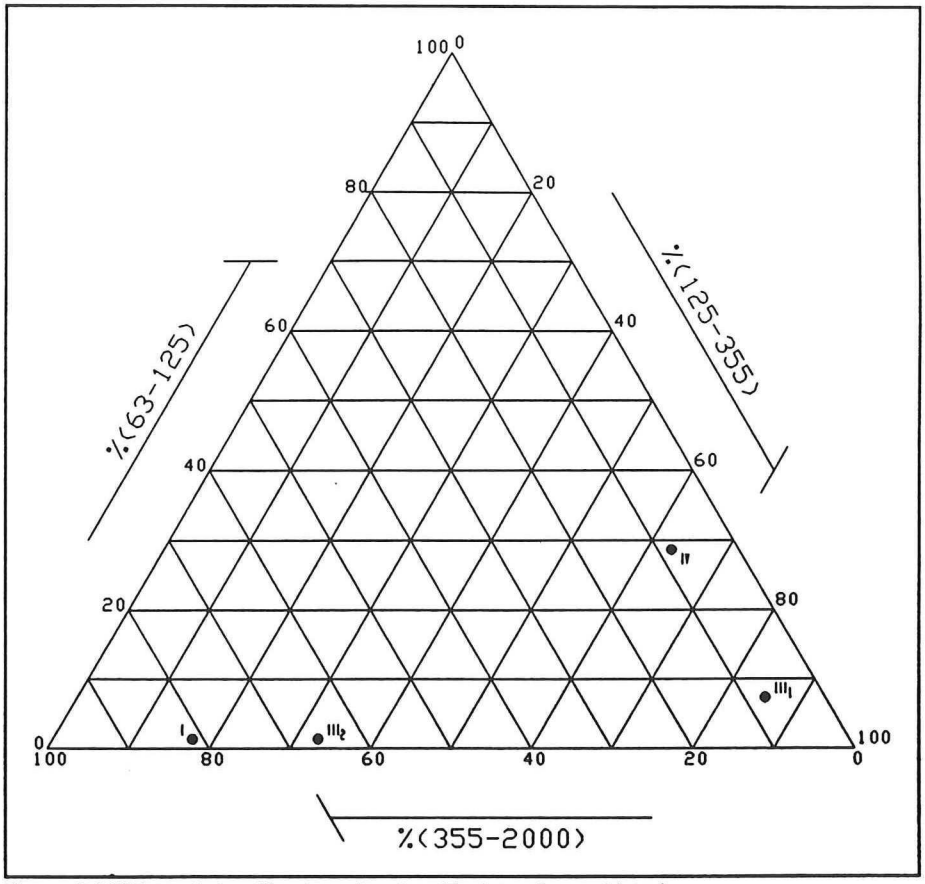

Figure 3 SCW sand classification triangle with data of case histories

The appellations of the sands, according to the SCW classification procedure, are mentioned below. Note, again, that classification of sample B2 of case history II was not possible, as no sieve data were available.

Case I-B1: Very coarse sand, very little loamy, little gravel, poorly graded.
(M_{63} = 387; G = 1.98) (l = 10) (g = 3.4) ($[D_{60}/D_{10}]_{63}$ = 1.6)

Case III-B5/3: Medium fine sand, very loamy, little gravel, moderately graded.
(M_{63} = 223; G = 0.98) (l = 38) (g = 0.0) ($[D_{60}/D_{10}]_{63}$ = 2.1)

Case III-B6/5: Very coarse sand, loamy, little gravel, moderately graded.
(M_{63} = 407; G = 1.83) (l = 31) (g = 0.0) ($[D_{60}/D_{10}]_{63}$ = 1.8)

Case IV-B2/1: Medium fine sand, very loamy, little gravel, well graded.
(M_{63} = 156; G = 0.62) (l = 59) (g = 0.1) ($[D_{60}/D_{10}]_{63}$ = 2.4)

§ 1.4.3 Angularity Determination

Although it is not difficult to determine the Volders & Verhoeven sharpness index, it was not done on any of the samples of any of the case histories. Nor microscopic analyses were performed. In general, the angularity of granular materials are not often investigated because angularity is considered to be very difficult to quantify, objectively and standardized. Also, angularity is not often used in investigations of relationships between other properties of sands, in literature. Nevertheless,

angularity is suspected to have a decisive influence on plastic deformation behaviour (see also the fundamental research of Niekerk (1995)).

For further analysis, we will assume that all sands investigated may be classified as "sub-angular", on the basis of the fact that they are suspected to have been deposited relatively fast. This information is necessary for estimation of the maximum and minimum void ratios.

§ 1.4.4 Estimation of Maximum and Minimum Void Ratios

Also the maximum and minimum void ratio determination is not a difficult laboratory test, although different standardized procedures have been established. The results may differ as much as 5% (see Bowels (1992)), depending on the operating laborant.

Youd (1973) investigated the factors influencing the maximum and minimum void ratios. He established a general diagram in which the relationship between the coefficient of uniformity of the sieve curve, C_u and the angularity (expressed in roundness, R) of the particles, on the one hand, and the maximum and minimum void ratios on the other, are represented. The parameters necessary in the present cases, are given in the following table (the value of C_u of case history II-B2 is estimated to be 1.5, which is fairly uniform):

Site	C_u (from sieve curve)	R (estimated qualitatively)	e_{min} (Youd)	e_{max} (Youd)
Case history I	1.6	sub-angular	0.47	0.87
Case history II	1.5	sub-angular	0.48	0.88
Case history III-B5/3	2.1	sub-angular	0.67	1.05
Case history III-B6/5	1.8	sub-angular	0.52	0.84
Case history IV	2.4	sub-angular	0.39	0.76

The maximum and minimum void ratios, which are added in the table above, have been derived from Youd's diagram (see Figure 4 on page 7).

§ 1.4.5 Critical Void Ratio Determination

Again we are having trouble determining accurate values for specific material properties. This time, however, not completely unexpected, as critical void ratio tests are quite laborious and not usually performed. Drained critical void ratio tests were conducted only on the samples of case history III. According to Lindenberg *et al.* (1981), the wet critical void ratio will be within the range of 0.5 to 7% above the dry critical void ratio.

For all other samples, nothing else was left to do but to estimate the critical void ratio from previously conducted tests on other sands. Here, the findings of Lindenberg *et al.* (1981) are used. They conducted critical void ratio tests at a confining pressure of 50 *kPa*, which corresponds to a depth of 3 - 5 *m* for normally consolidated soils. Obviously, this way an arbitrary value is obtained, without any relation to the sand investigated. Further analyses should be looked upon as educational rather than quantitative. Wet critical void ratios, used as criteria in further analyses, are presented in the table on page 8.

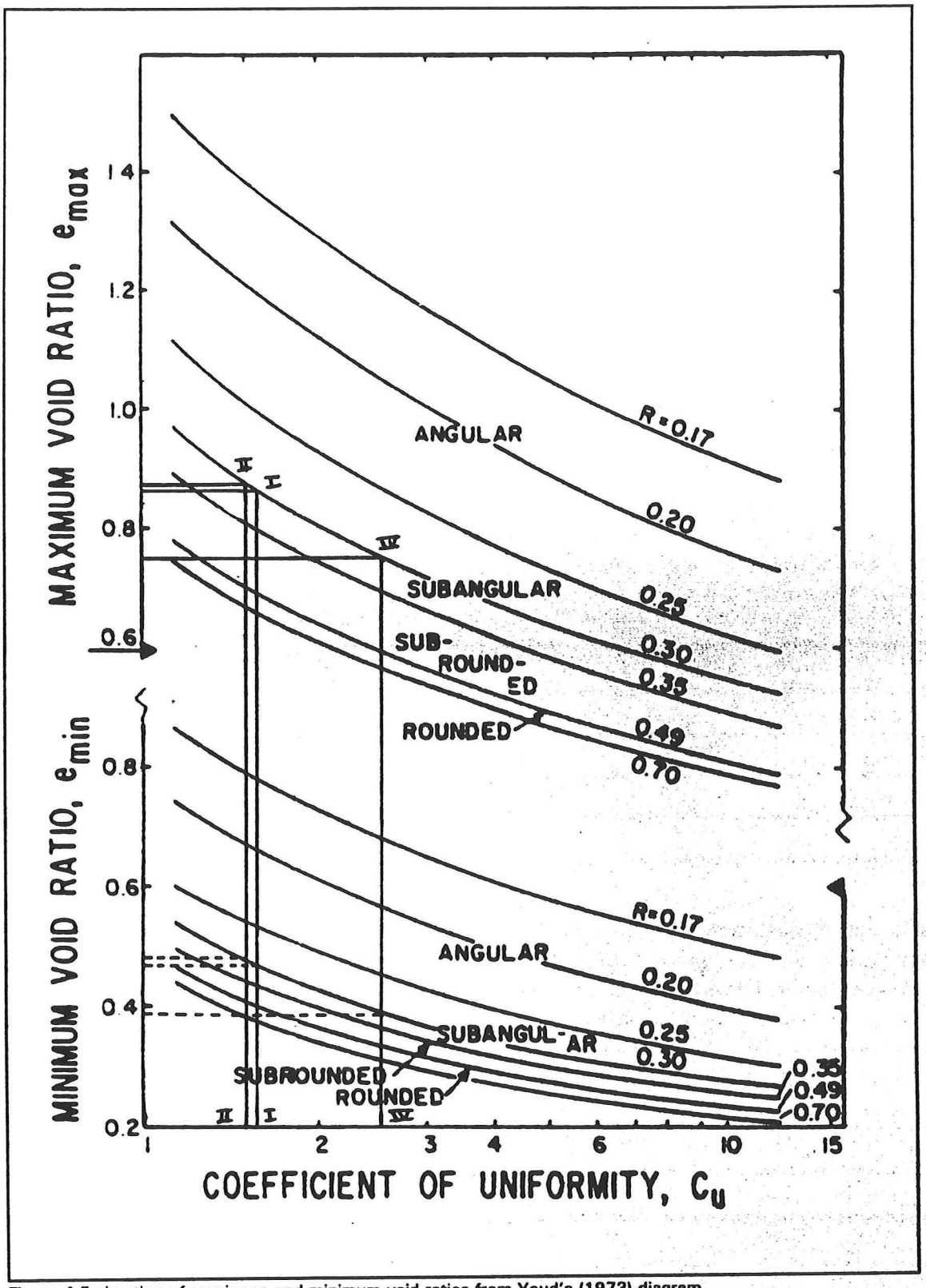

Figure 4 Estimation of maximum and minimum void ratios from Youd's (1973) diagram

Site	$e_{crit,\ dry}$	+0.5% limit	$e_{crit,\ wet}$	+7% limit
Case history I-B1	-	-	0.79	-
Case history II-B2	-	-	0.79	-
Case history III-B5/3	0.98	0.98	-	1.05
Case history III-B5/3	0.74	0.74	-	0.79
Case history IV-B2/1	-	-	0.79	-

§ 1.4.6 Estimation of the In-situ Relative Density from Cone Penetration Tests

Several workers have searched (and found) relations between the relative density, related to the in-situ void ratio, and the cone resistance values. They found a dependency of the relative density on the cone resistance and the vertical effective stress.

To calculate the vertical effective stress, a unit weight of 20 kN/m^3 and 15 kN/m^3 for sand and clay layers, respectively, were assigned on the basis of NEN Codes (1993). Low estimations of the unit weight lead to higher estimations of the average in-situ relative density in the most critical zones. The results are given in the following table:

Site	Estimated Low Relative Density [%]
Case history I	40
Case history II	30
Case history III	40
Case history IV	40

See for the estimation of the development of the in-situ relative densities with depth, calculated by means of Jamiolkowski's formula, on the basis of all cone penetration tests available per case history, Figure 20 on page 27 through Figure 23 on page 28. To verify the estimations, other formulae were employed, all of which predicted relative densities in the same range, but little higher. Also the compressibility of the sands was taken into account, by considering the friction ratio, using fuzzy numbers. This second analysis yielded the following ranges of relative densities for the most unfavourable combinations of σ'_v, q_c and R_f.

Case I	Case II	Case III	Case IV
40% - 50%	33% - 37%	30% - 45%	28% - 37%

§ 1.4.7 In-situ Void Ratio Determination

In none of the case histories, in-situ density measurements were performed. Therefore, it was tried to approximate the in-situ void ratio from the estimated maximum and minimum void ratios and in-situ relative density, based on the definition of the relative density. The results are given in the table below:

Site	Estimated High In-situ Void Ratio [-]
Case history I	0.71
Case history II	0.76
Case history III - B5/3	0.90
Case history III - B6/5	0.71
Case history IV	0.61

A graphical presentation of the procedure is given in Figure 24 on page 29 through Figure 28 on page 31. On the left y-axis, the maximum obtainable void ratio is plotted. On the right y-axis, the minimum obtainable void ratio is plotted. The line connecting both represents the range of obtainable densities between the relative loosest packing (0) and relative densest packing (100), on the x-axis.

The values of the maximum and minimum obtainable void ratio's may differ as much as 5%. These boundary values to the maximum and minimum void ratios, as well as the estimated wet critical void ratios, have been plotted in the charts.

§ 1.5 Static Liquefaction Potential Evaluation

Now that all aspects of the static liquefaction investigation have been completed, we may proceed to the interpretation of the findings. In the following paragraph, an enumeration will be given per case history.

Case history I:

- The zone most critical to static liquefaction is very probably situated in a pleistocene layer. The cone resistances found in the most critical zone, which consisted of medium fine to medium coarse river deposits and not definite potentially susceptible sands, were not extremely low, as should be expected in truly static liquefiable sands, at that depth.
- The sieve curve was interpreted from an alternative sieve analysis. However, the coefficient of uniformity is not likely to be lower than the estimated value of 1.6. Therefore, the values for maximum and minimum void ratios are probably lower than estimated, which, in turn, leads to a lower approximation of the in-situ void ratio.
- The adopted value for the wet critical void ratio was based on findings on other sands. These sands are not very likely to have the same wet critical void ratios as the sand considered. The sands, on which the wet critical void ratio criterion has been based (Lindenberg *et al.* (1981)), are likely to be more uniform and less angular. Possibly, the actual wet critical void ratio of the sand considered is higher, which would make the soil less susceptible to static liquefaction.

o The approximated in-situ void ratio is below the (assumed) wet critical void ratio, but the confining pressure used to establish the critical void ratio was lower than the expected horizontal stress level at the depth from which the sample was taken (± 10 m). However, on the basis of this analysis, static liquefaction seems out of the question. The cause of failure should be sought in other phenomena, like active bank development.

Case history II:

o The zone most critical to static liquefaction is very probably situated in a pleistocene layer. Moreover, the critical zone is very thin. The cone resistances found in the most critical zone, which was not classified, but probably river deposited, were not extremely low, as should be expected in truly static liquefiable sands, at that depth.
o No sieve analyses were performed. However, the coefficient of uniformity in not likely to be lower than the estimated value of 1.5. Therefore, the values for maximum and minimum void ratios are probably lower than estimated, which, in turn, leads to a lower approximation of the in-situ void ratio.
o The adopted value for the wet critical void ratio was based on findings on other sands. These sands are not very likely to have the same wet critical void ratios as the sand considered. The sands, on which the wet critical void ratio criterion has been based (Lindenberg *et al.* (1981)), are likely to be more uniform and less angular. Possibly, the actual wet critical void ratio of the sand considered is higher, which would make the soil less likely to be susceptible to static liquefaction.
o The approximated in-situ void ratio is below the (assumed) wet critical void ratio. On the basis of this analysis, static liquefaction seems out of the question. The cause of failure should be sought in other phenomena, like active bank development (see also the failure profile presented in Figure 29 on page 32).

Case history III:

o The zone most critical to static liquefaction is probably situated in a holocene sand layer. The cone resistances found in the most critical zone, which consisted of medium fine to medium coarse not definite potentially susceptible sands, were not extremely low, as should be expected in truly static liquefiable sands, at that depth. Sample B5/3 seems the most critical one, judging by classification and dry critical void ratio test result. Note that the actual dry critical void ratio was not determined. The laboratory tests indicated the dry critical void ratio to be higher than 0.74.
o The adopted value for the wet critical void ratio has been based on the findings of Lindenberg *et al.* (1981), who found that the wet critical void ratio is between 0.5 and 7% above the dry critical void ratio. Possibly, the actual wet critical void ratio of the sand considered is higher, because it is likely to be less uniform and less angular than the sands investigated by Lindenberg *et al.* (1981), which would make the soil less likely to be susceptible to static liquefaction.
o The approximated in-situ void ratio is not definitely above the (assumed) wet critical void ratio. On the basis of this analysis, static liquefaction is not very probable.

Case history IV:

o The zone most critical to static liquefaction is very probably situated in a pleistocene layer. The cone resistances found in the most critical zone, which consisted of silty fine to medium fine sands, were not extremely low, as should be expected in truly static liquefiable sands, at that depth. The soil profile displays great inhomogeneity (interlaterment with cohesive soils), which makes static

liquefaction less probable.
o The adopted value for the wet critical void ratio was based on findings on other sands. These sands are not very likely to have the same wet critical void ratios as the sand considered. The sands, on which the wet critical void ratio criterion has been based (Lindenberg *et al.* (1981)), are likely to be more uniform, thus the maximum and minimum void ratios are likely to have been higher. Hence, the actual wet critical void ratio of the sand considered will be lower than Lindenberg's, which would make the soil more likely to be susceptible to static liquefaction.
o The approximated in-situ void ratio is below the (assumed) wet critical void ratio. On the basis of this analysis, static liquefaction is not probable.

§ 1.6 Conclusions

The evaluation of the four case histories presented here has been performed, unfortunately forced, at a very low level. A lack of necessary data, like critical, maximum and minimum void ratios, meant that many parameters had to be estimated.

Nevertheless, the application of the proposed method of analysis (see Volume 2, Chapter 2) to the case histories has proven to be sound, although the results, in the four studied case histories, are indicative only. In all case histories in which failure did occur, it seems not likely to have been caused by static liquefaction. Possibly the development of active banks has lead to extensive failure in these cases. This thought is strengthened by the stair-like failure profiles encountered (see also Figure 29 on page 32).

The results may be useful as an indication of the likelihood of occurrence of static liquefaction and hence a possible flow slide. The occurrence cannot be excluded however, because no accurate measurements of the critical void ratio and in-situ void ratio were available. Thus, the critical void ratio criterion could not be evaluated.

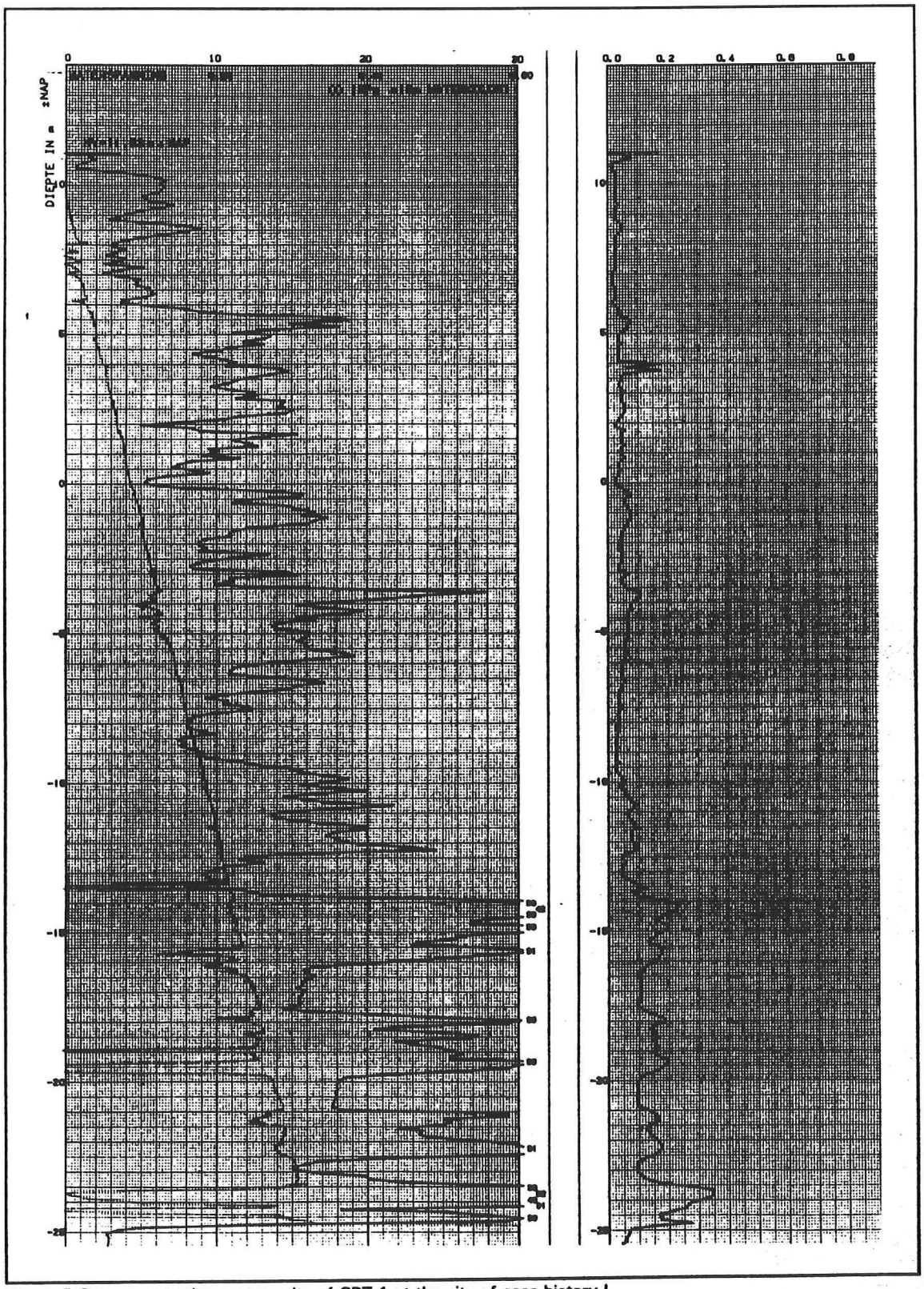

Figure 5 Cone penetration test results of CPT 1 at the site of case history I

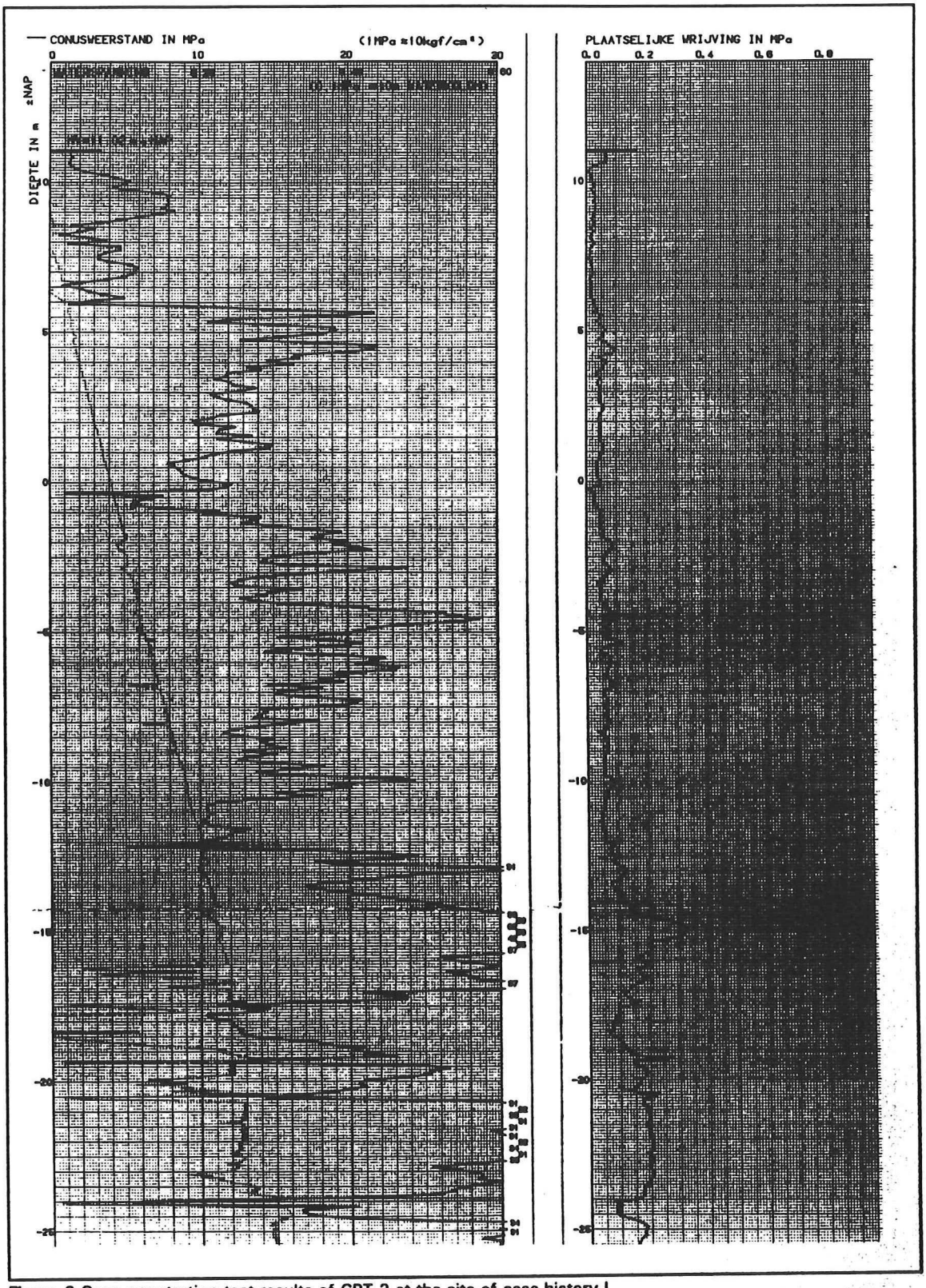

Figure 6 Cone penetration test results of CPT 2 at the site of case history I

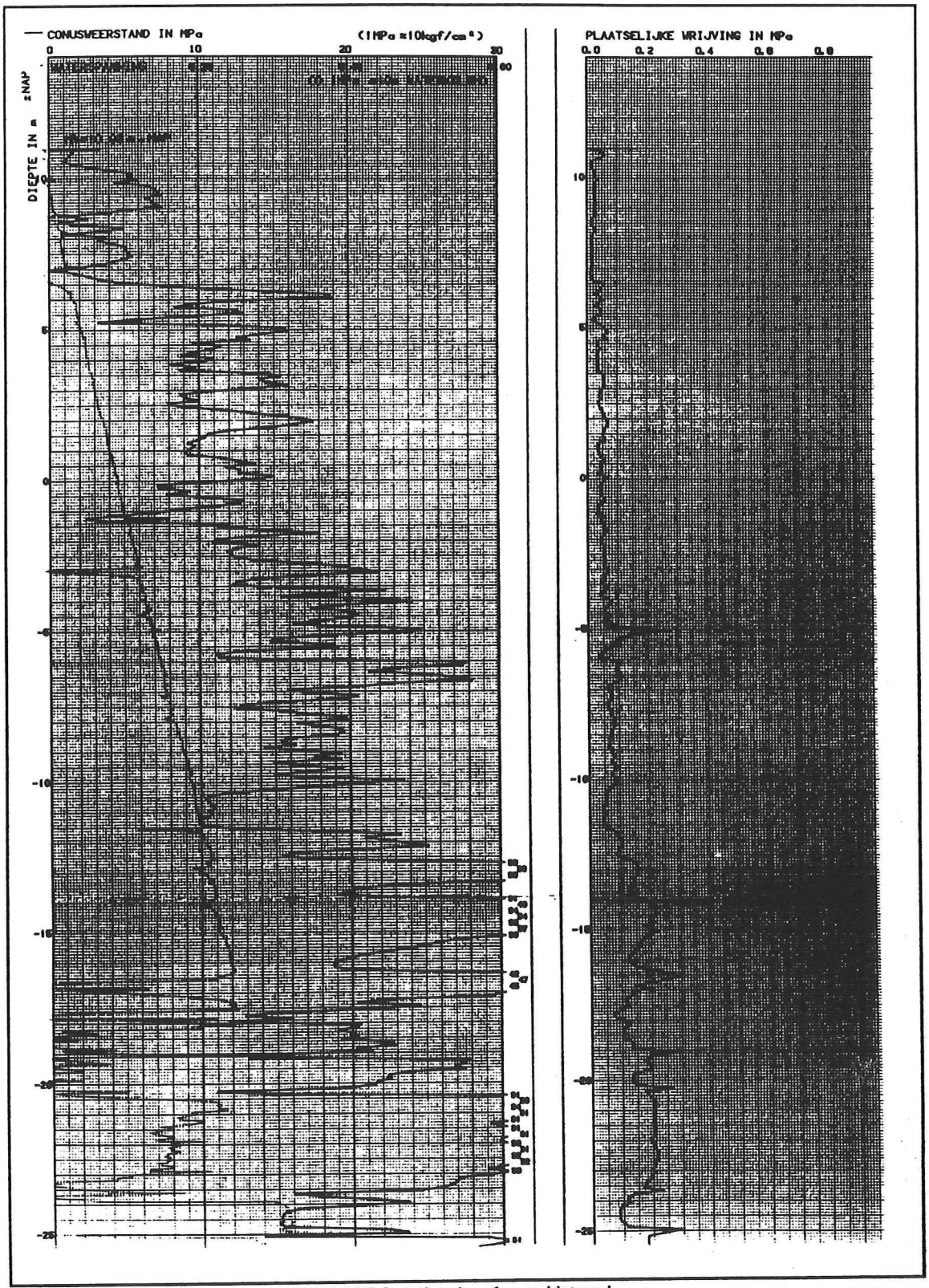

Figure 7 Cone penetration test results of CPT 3 at the site of case history I

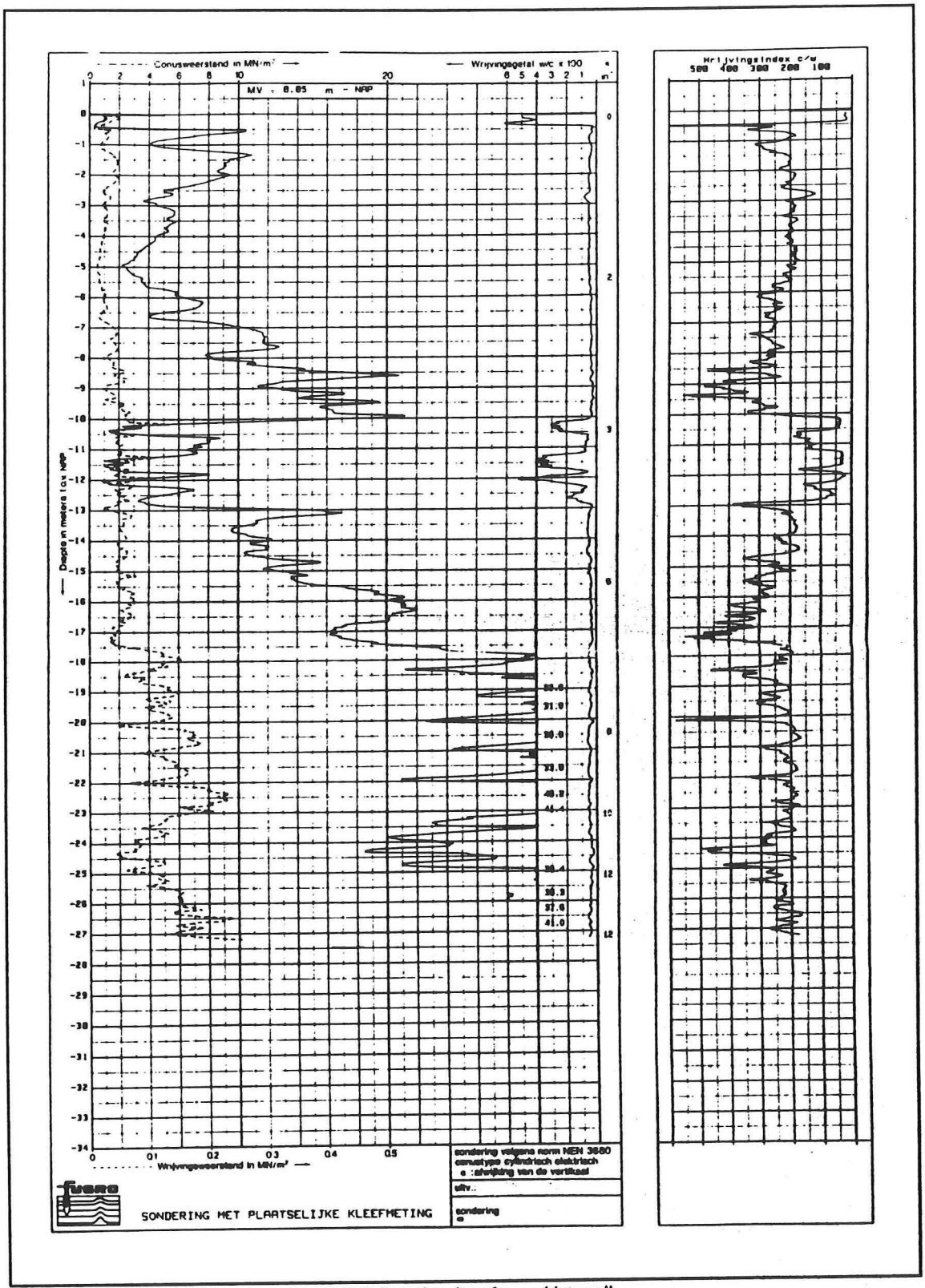

Figure 8 Cone penetration test results of CPT 1 at the site of case history II

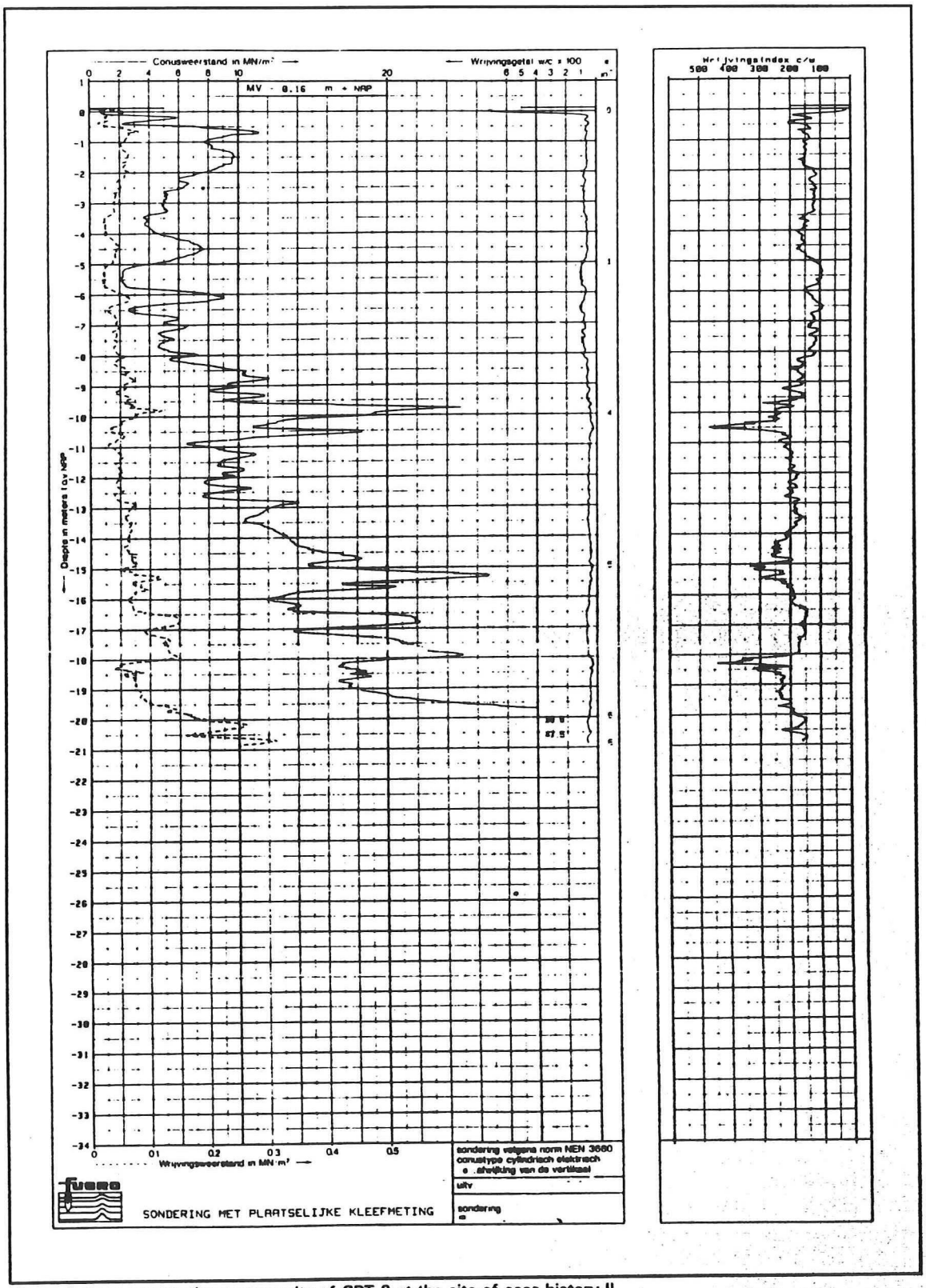

Figure 9 Cone penetration test results of CPT 2 at the site of case history II

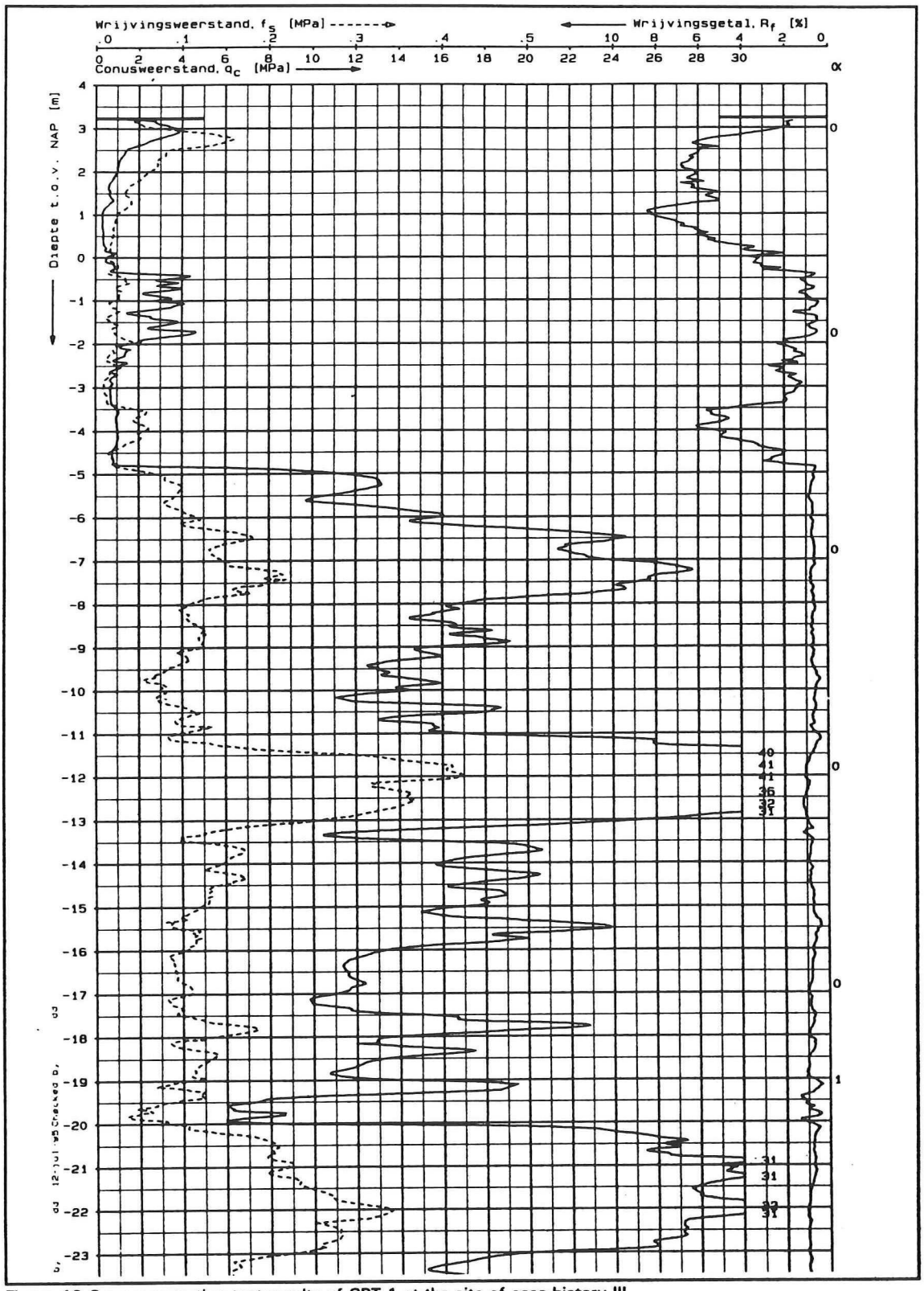

Figure 10 Cone penetration test results of CPT 1 at the site of case history III

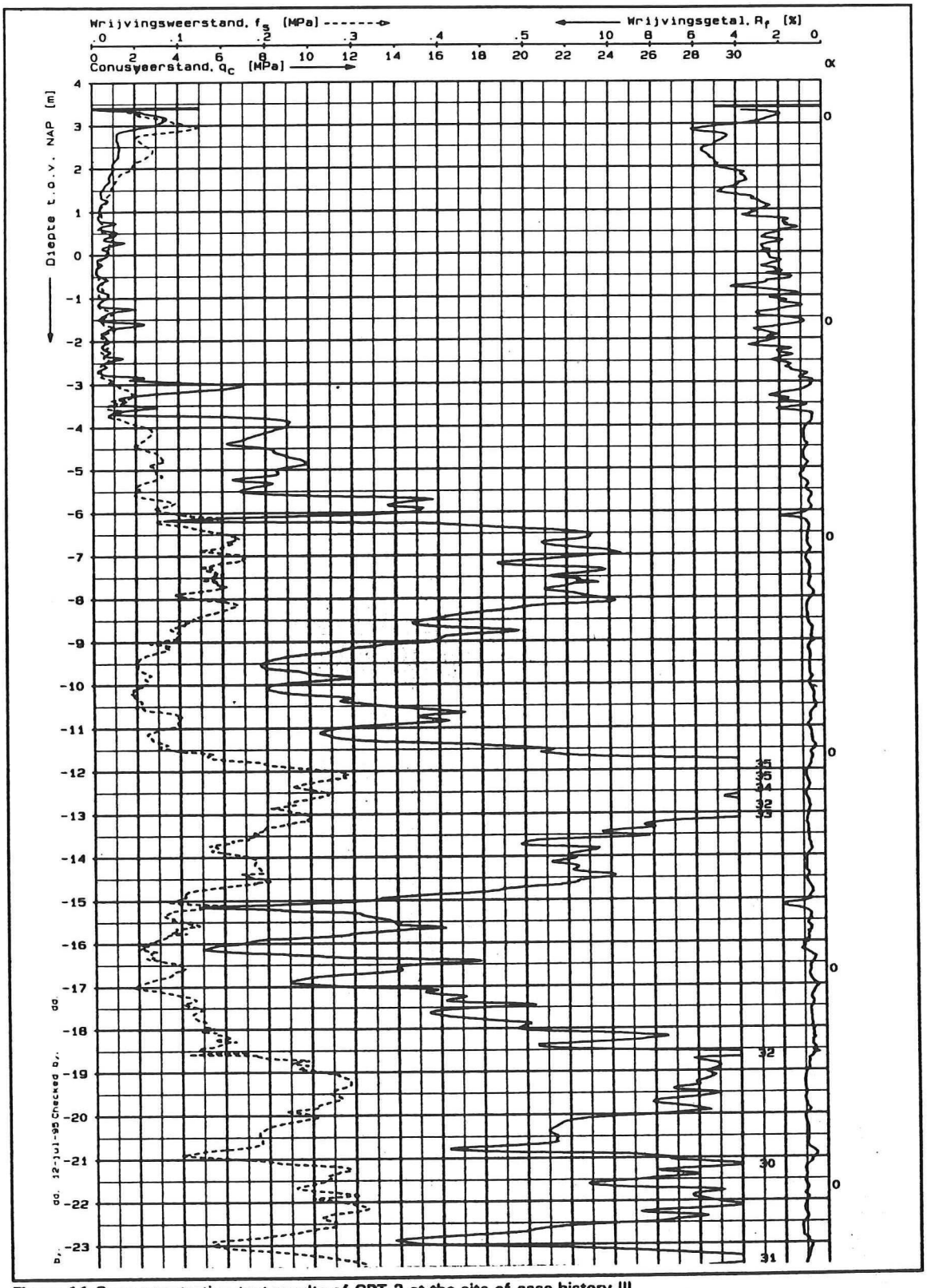

Figure 11 Cone penetration test results of CPT 2 at the site of case history III

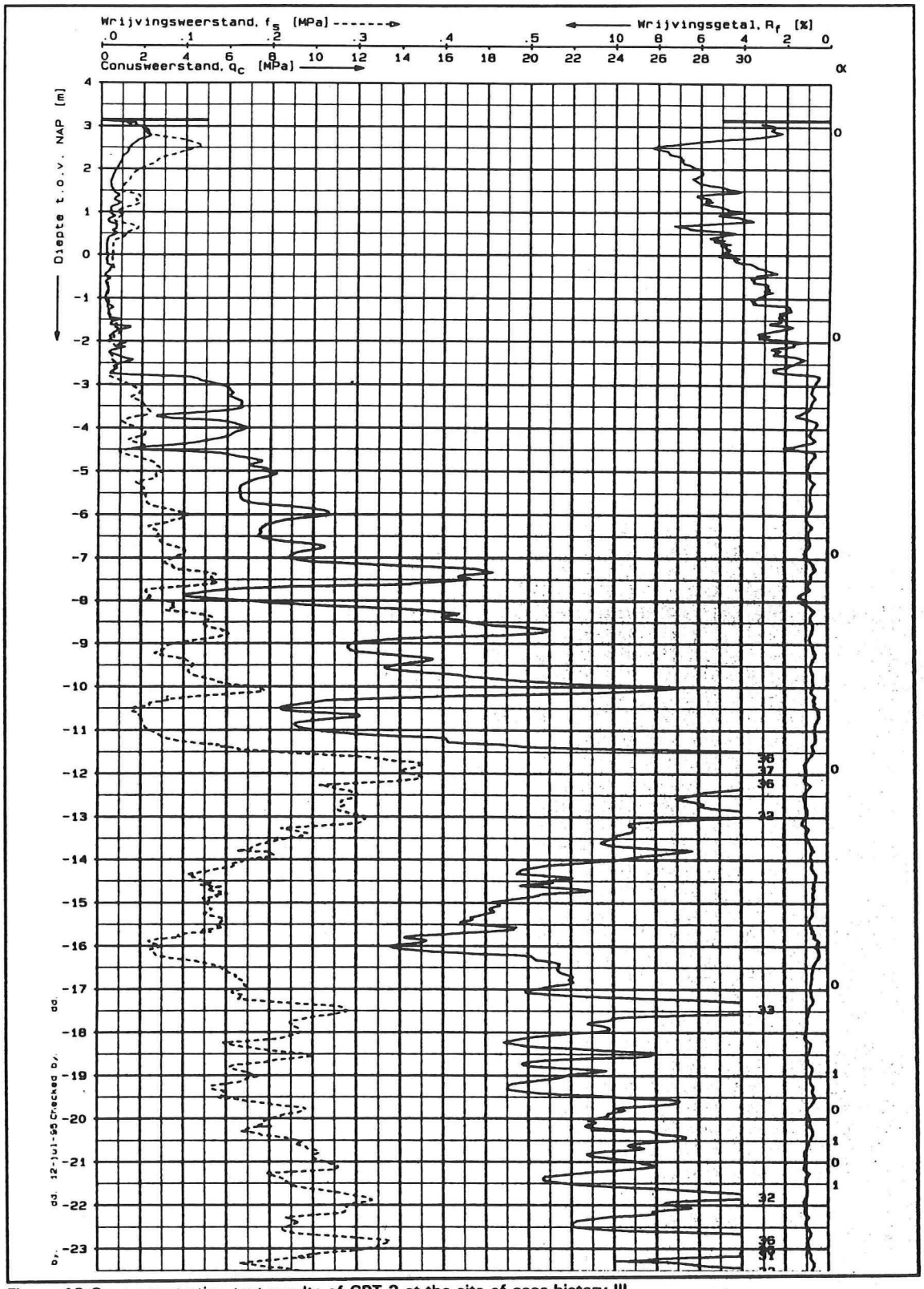

Figure 12 Cone penetration test results of CPT 3 at the site of case history III

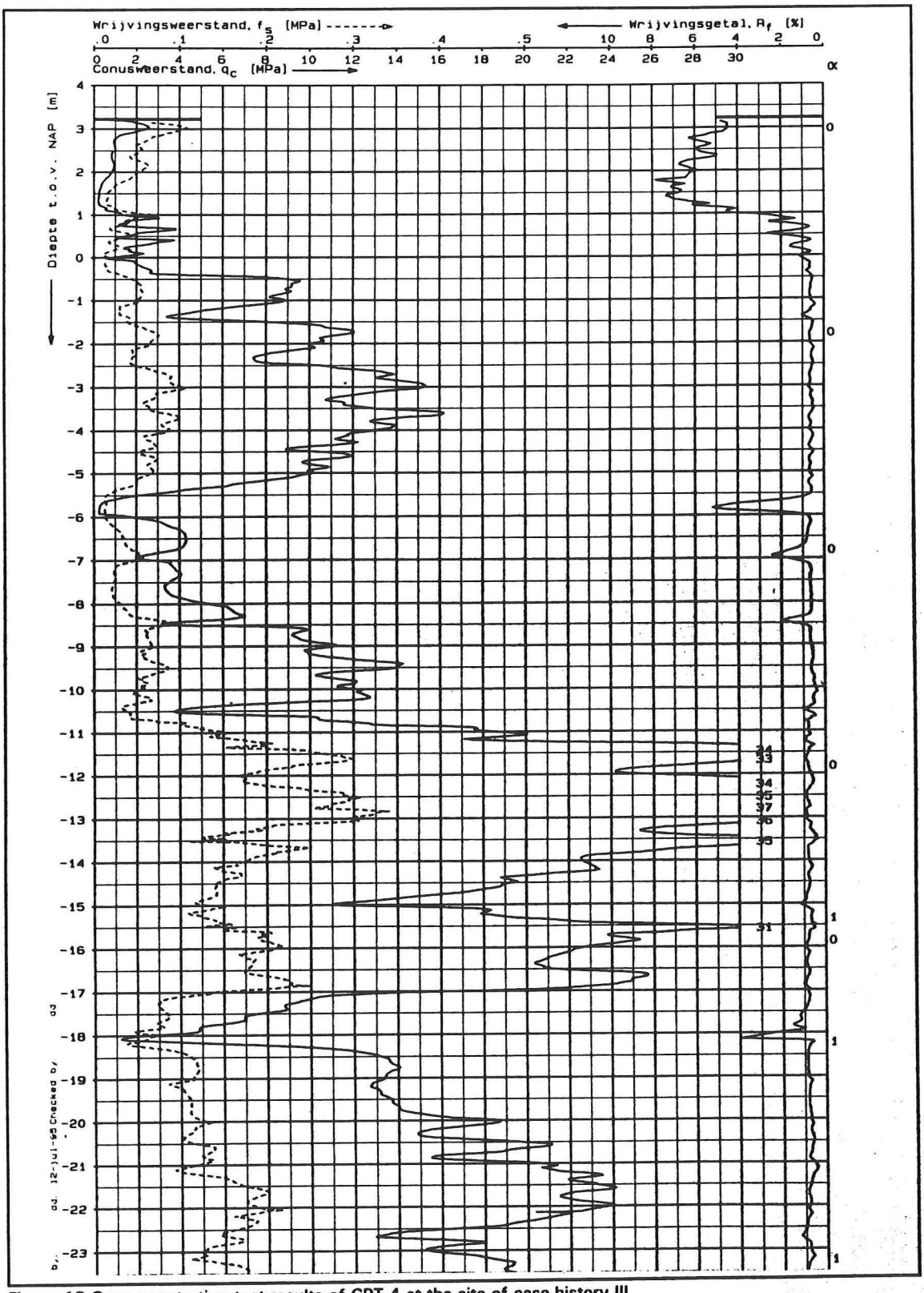

Figure 13 Cone penetration test results of CPT 4 at the site of case history III

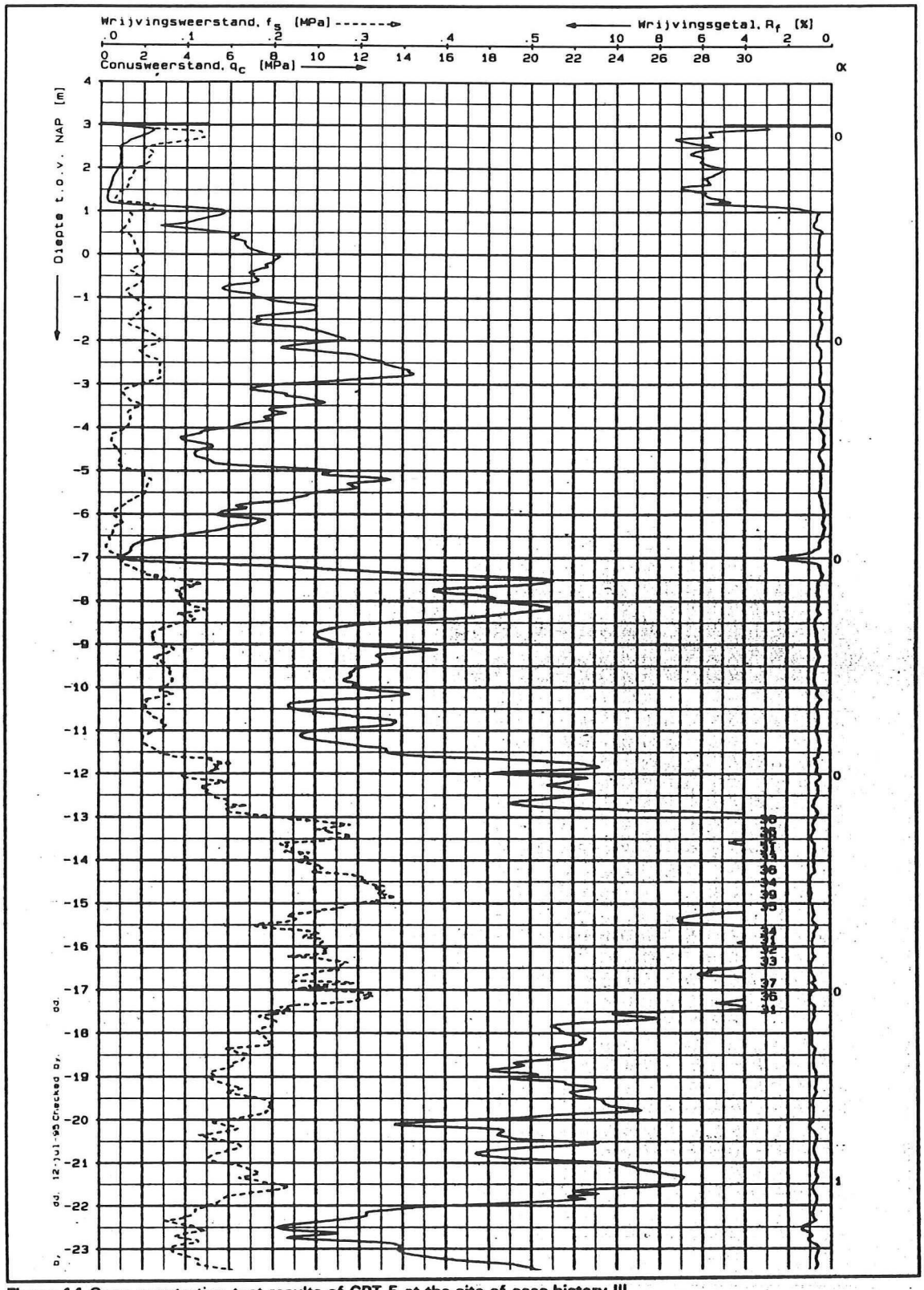

Figure 14 Cone penetration test results of CPT 5 at the site of case history III

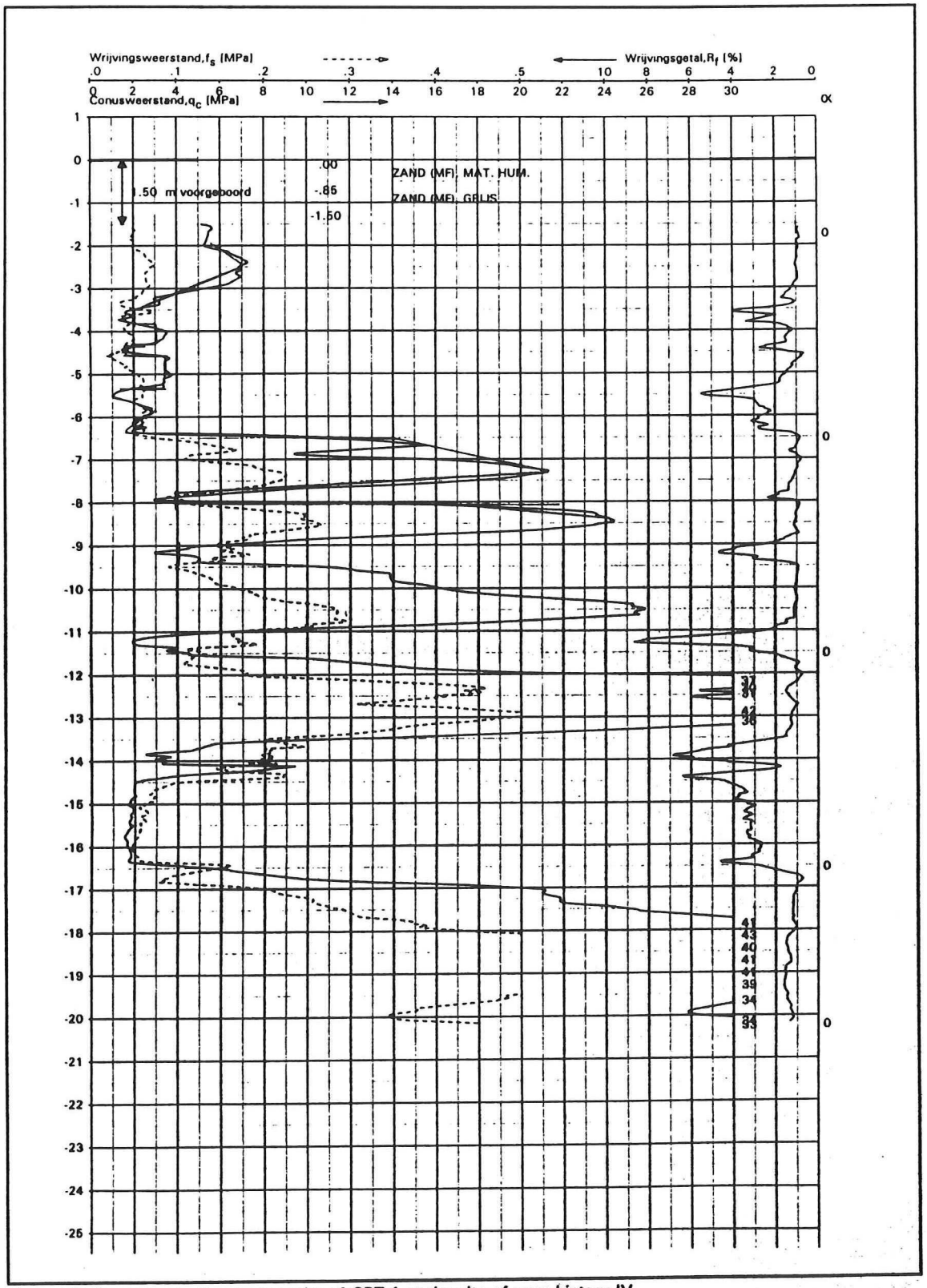

Figure 15 Cone penetration test results of CPT 1 at the site of case history IV

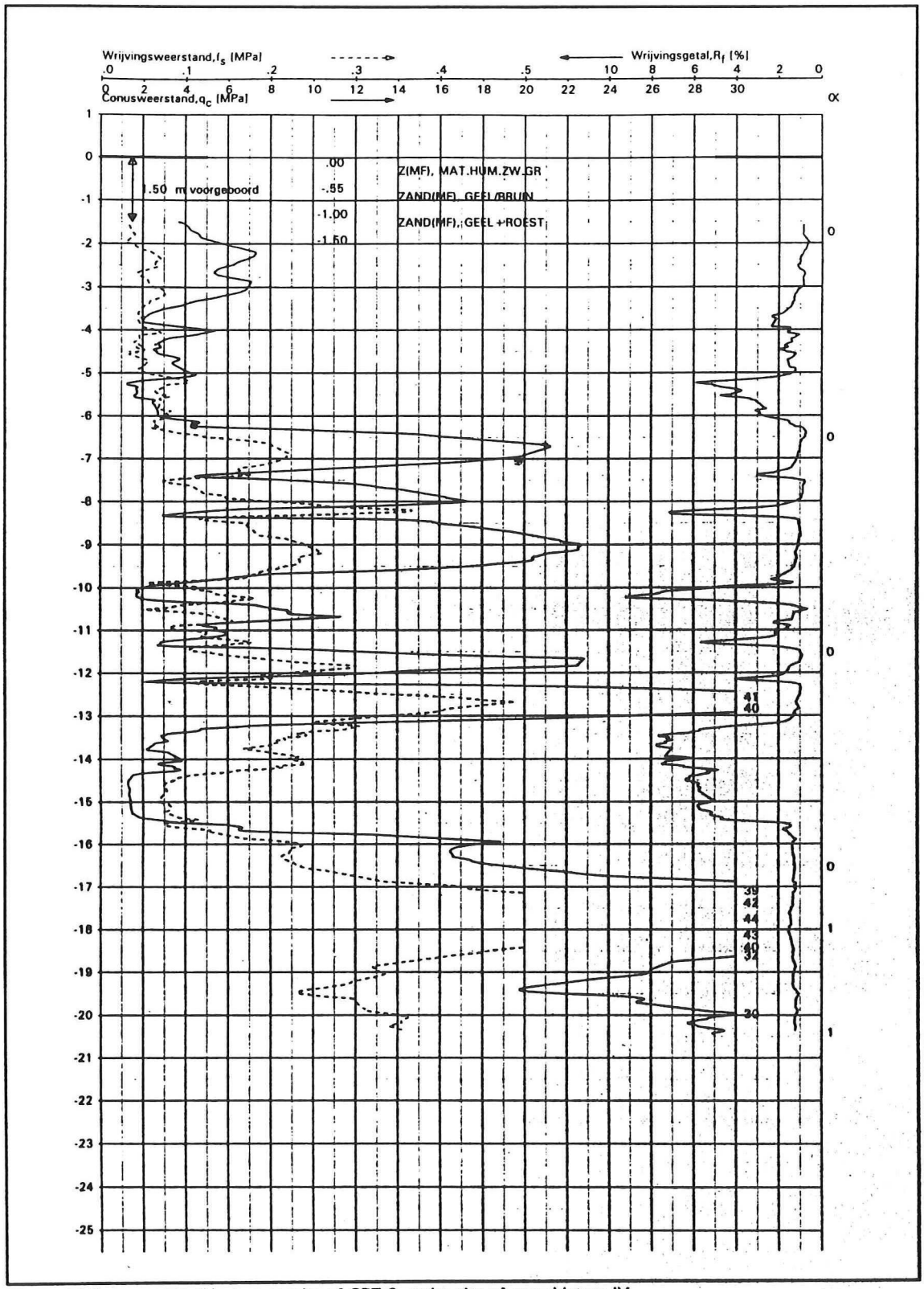

Figure 16 Cone penetration test results of CPT 2 at the site of case history IV

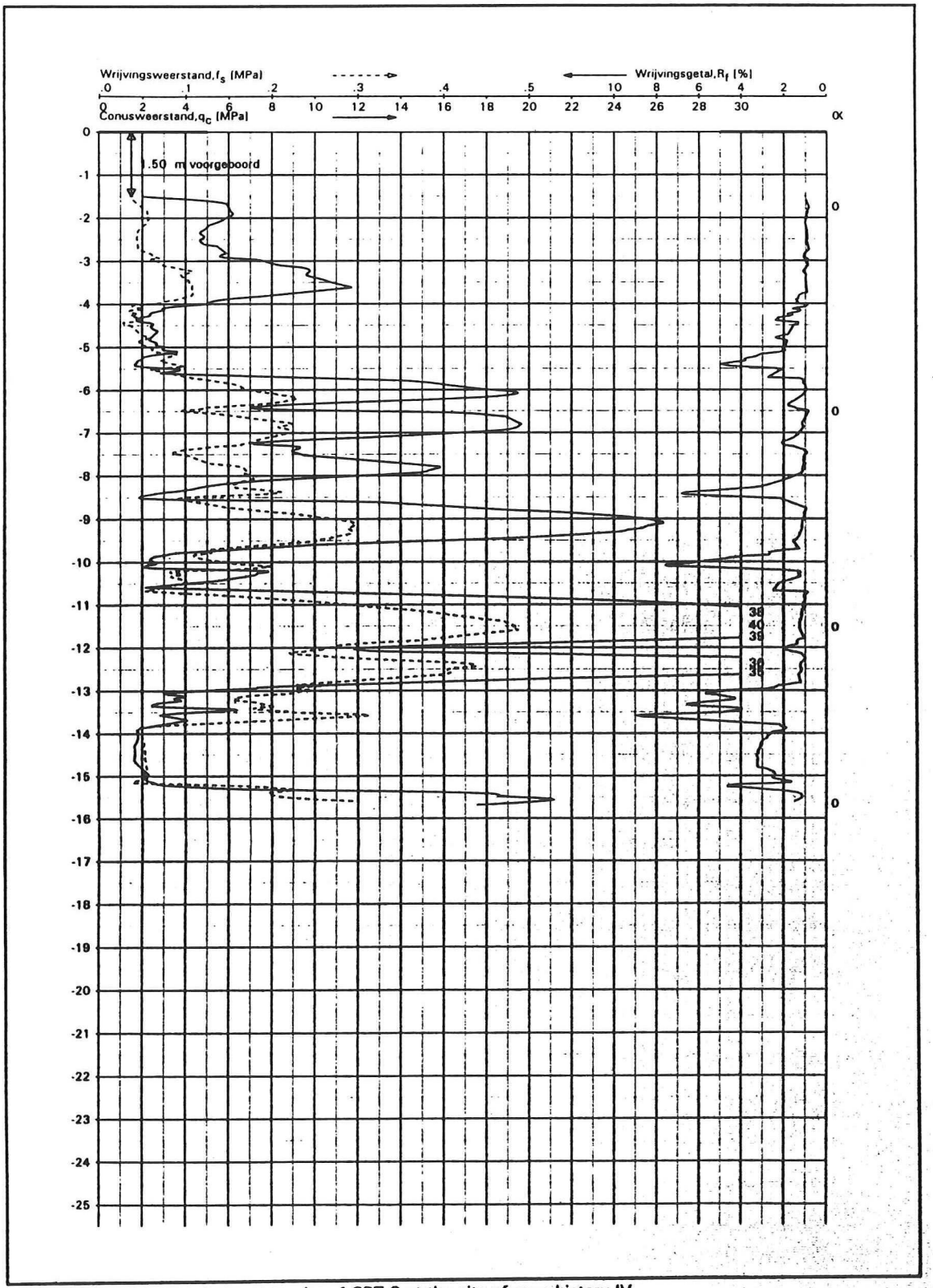

Figure 17 Cone penetration test results of CPT 3 at the site of case history IV

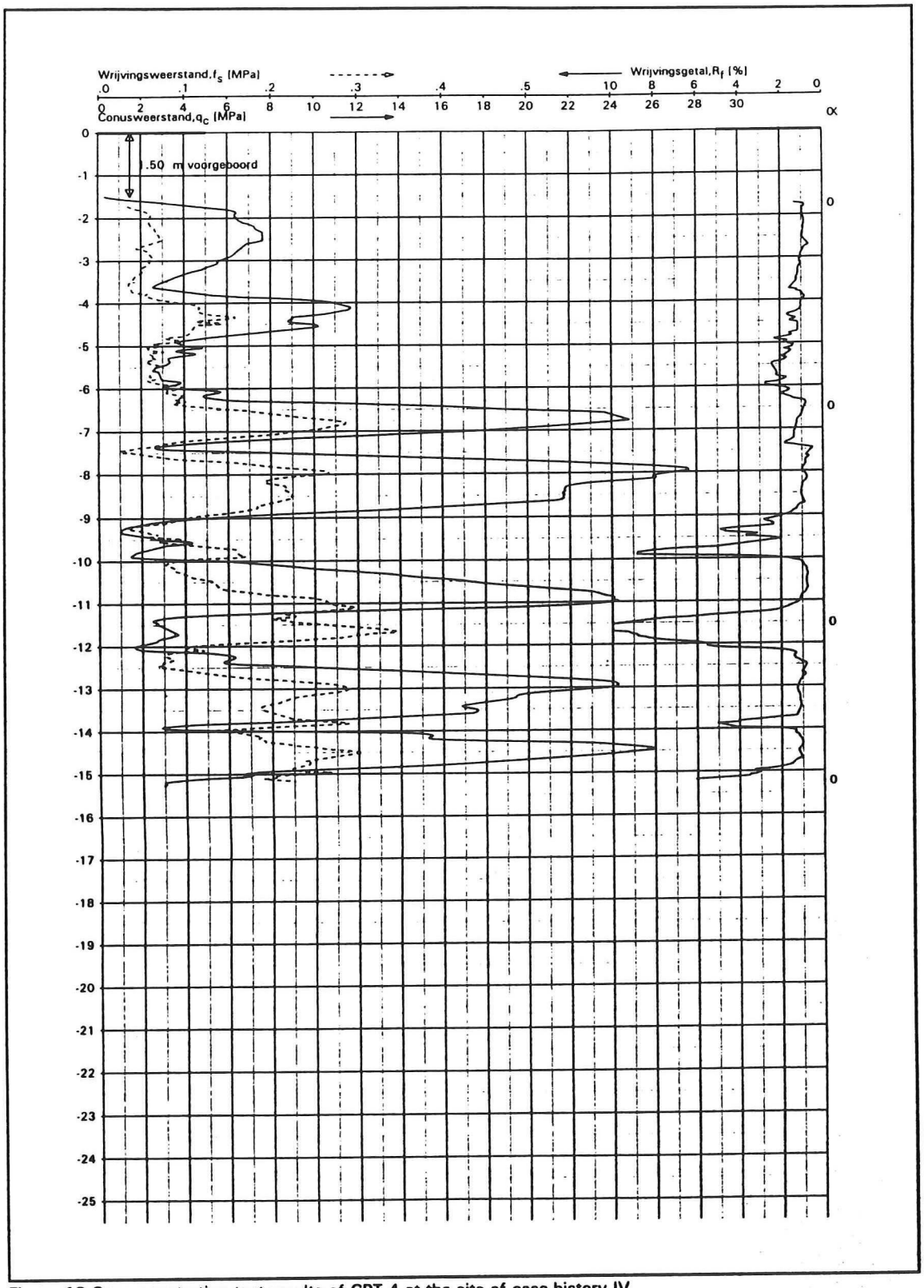

Figure 18 Cone penetration test results of CPT 4 at the site of case history IV

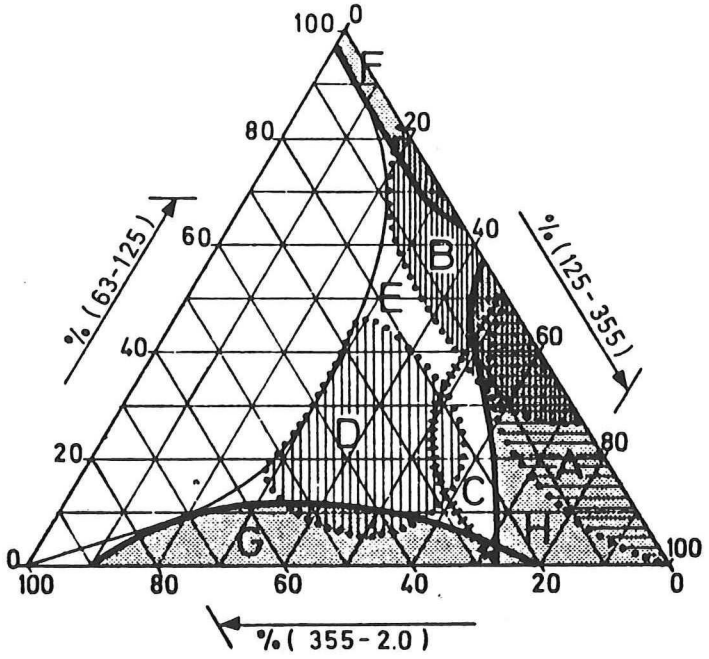

A = Little loamy eolian sand (drift sand, young coversand and older eolian sand)

B = Loamy eolian sand (old coversand and similar sand) incidental: fluvial sand)

C = Brooksand, fine river sand

D = Well graded (loamy) natural deposits (among others: solifluction material, "claysand", fluvio-glacial material)

E = Loam (sand fraction; no boundaries indicated)

F = Extremely fine basin sand

G = Coarse river sand

H = Estuarine and sea-sand, sand from coastal areas (shallow-sand, beach and dune sand)

Figure 19 Eight characteristic sandy deposits of The Netherlands after SCW (1975)

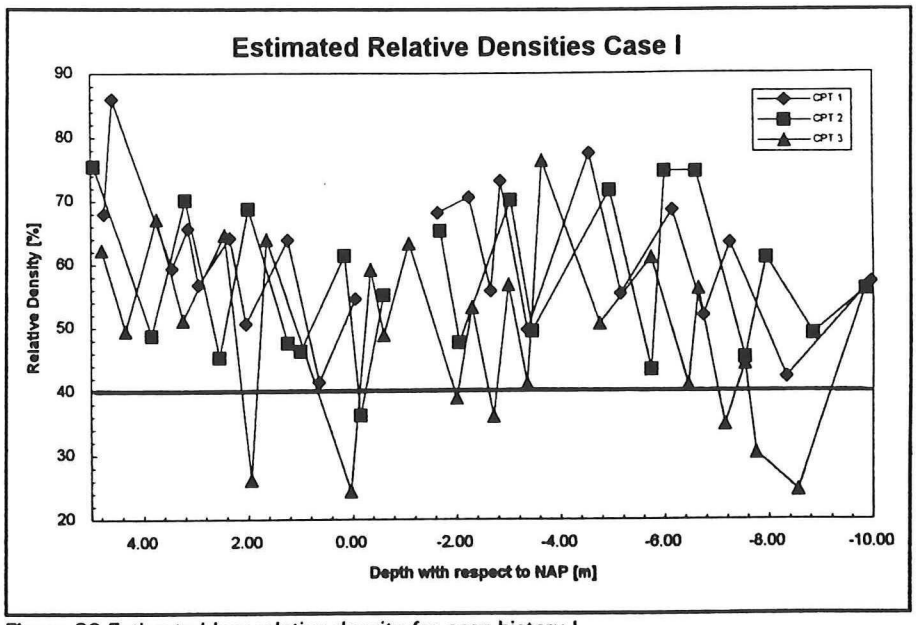

Figure 20 Estimated low relative density for case history I

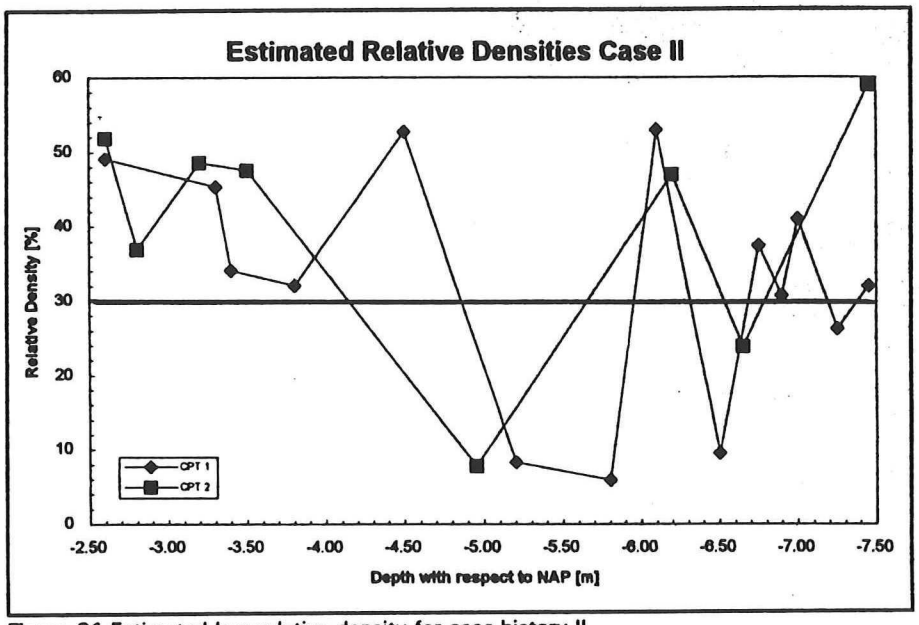

Figure 21 Estimated low relative density for case history II

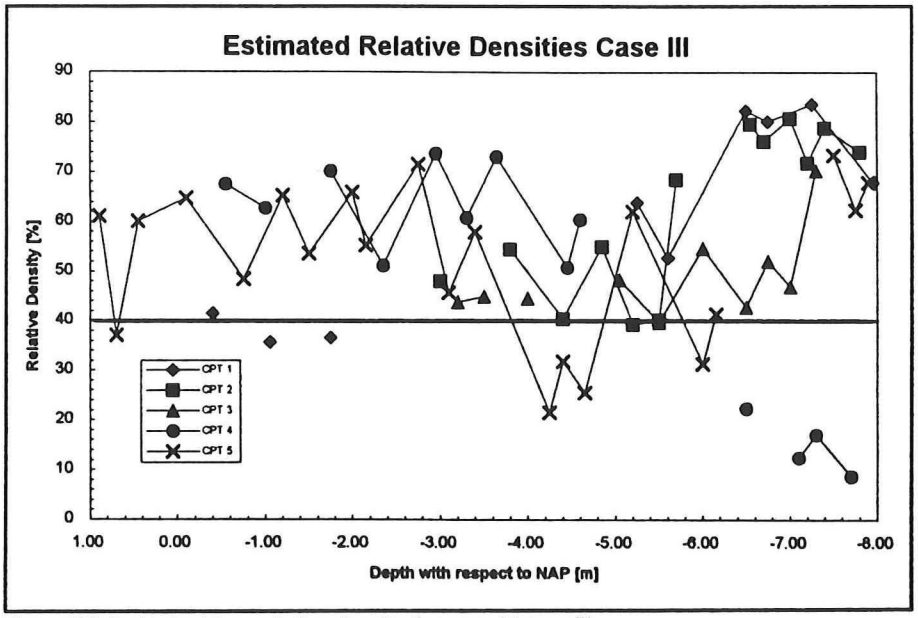

Figure 22 Estimated low relative density for case history III

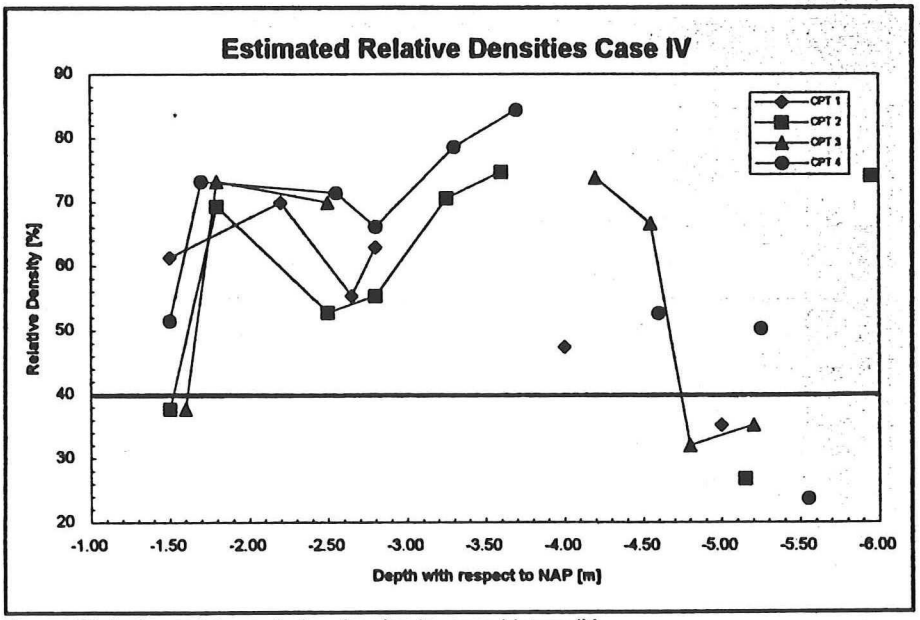

Figure 23 Estimated low relative density for case history IV

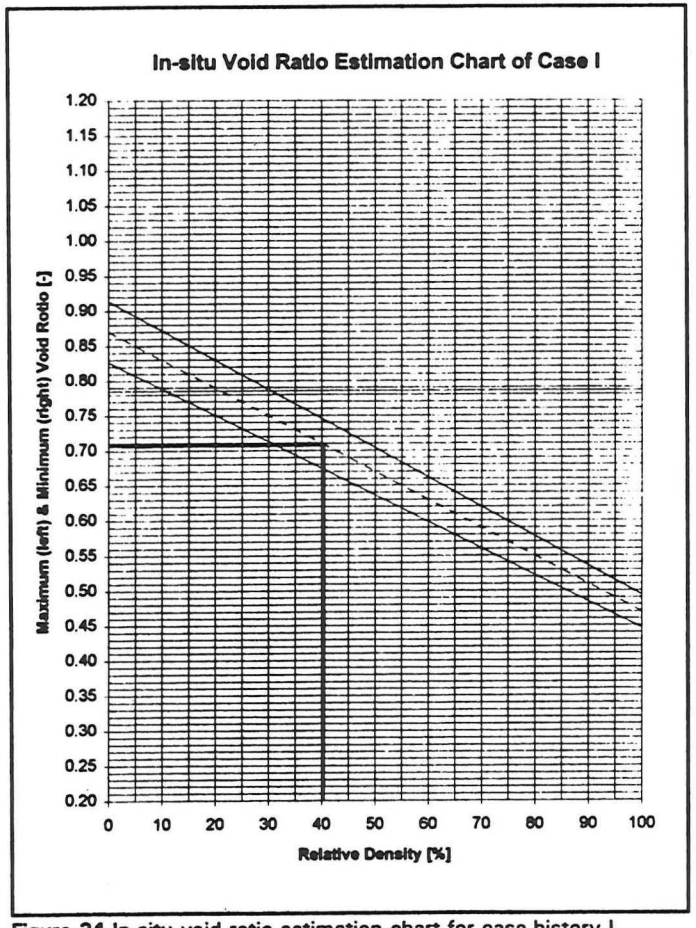

Figure 24 In-situ void ratio estimation chart for case history I

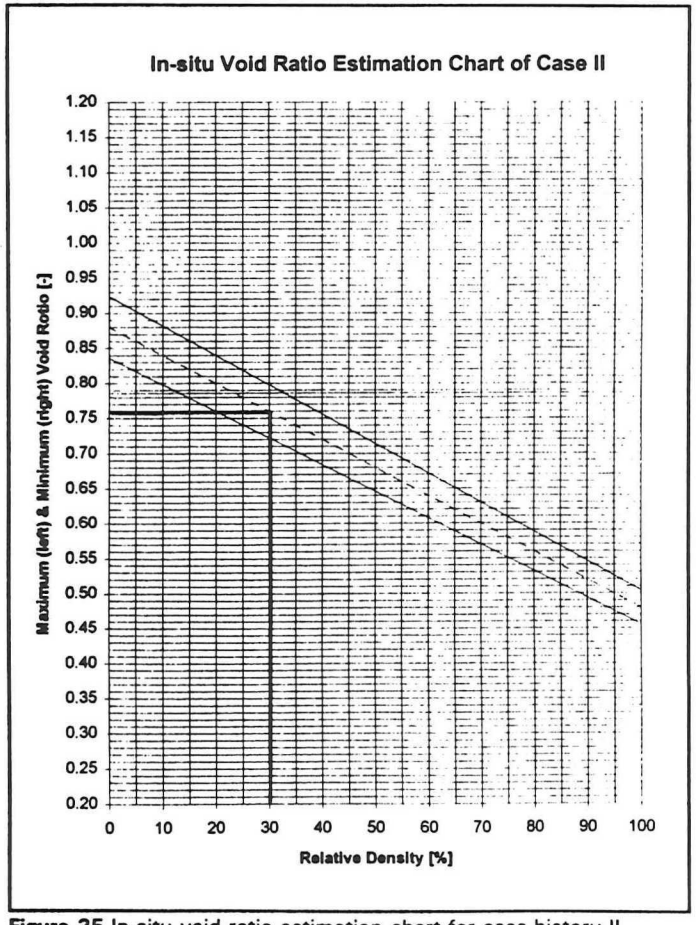

Figure 25 In-situ void ratio estimation chart for case history II

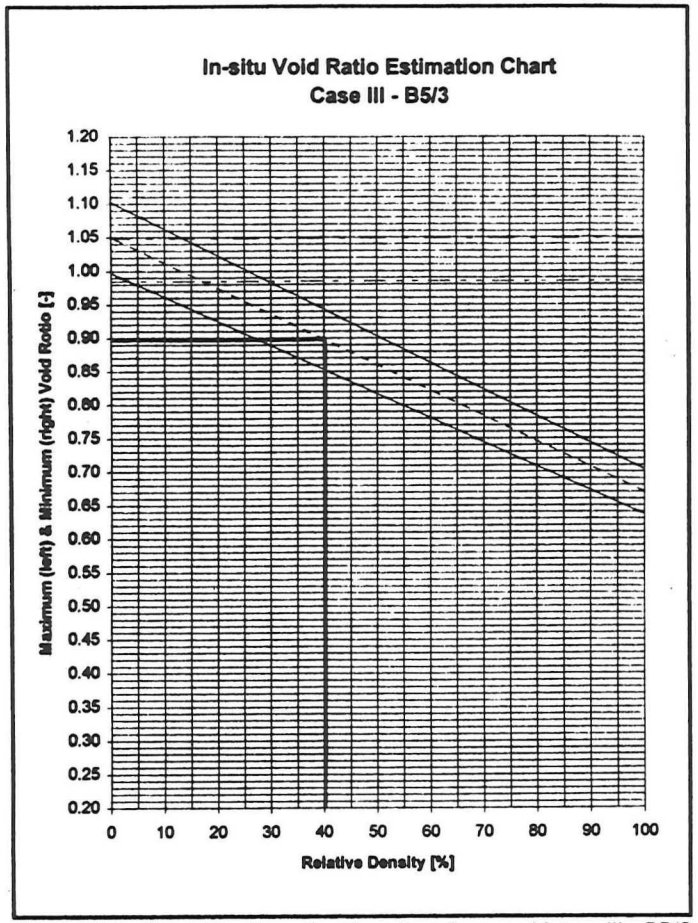

Figure 26 In-situ void ratio estimation chart for case history III - B5/3

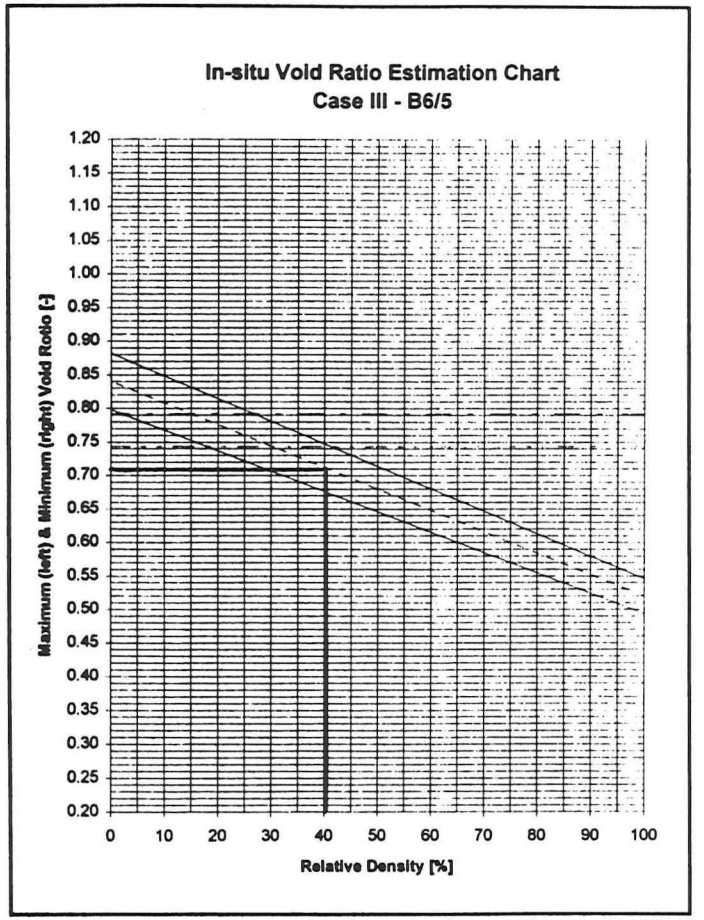

Figure 27 In-situ void ratio estimation chart for case history III - B6/5

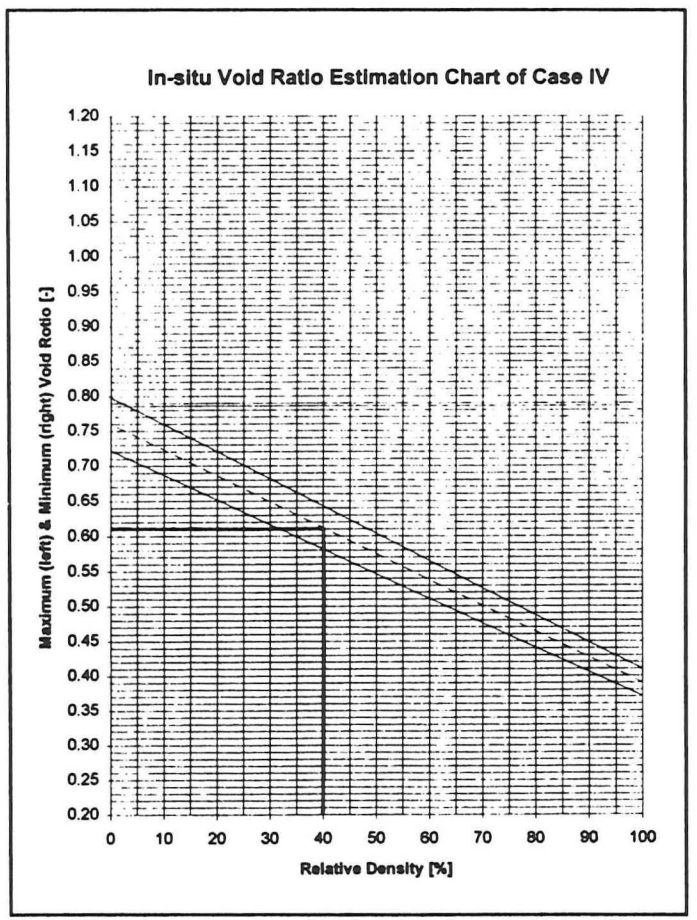

Figure 28 In-situ void ratio estimation chart for case history IV

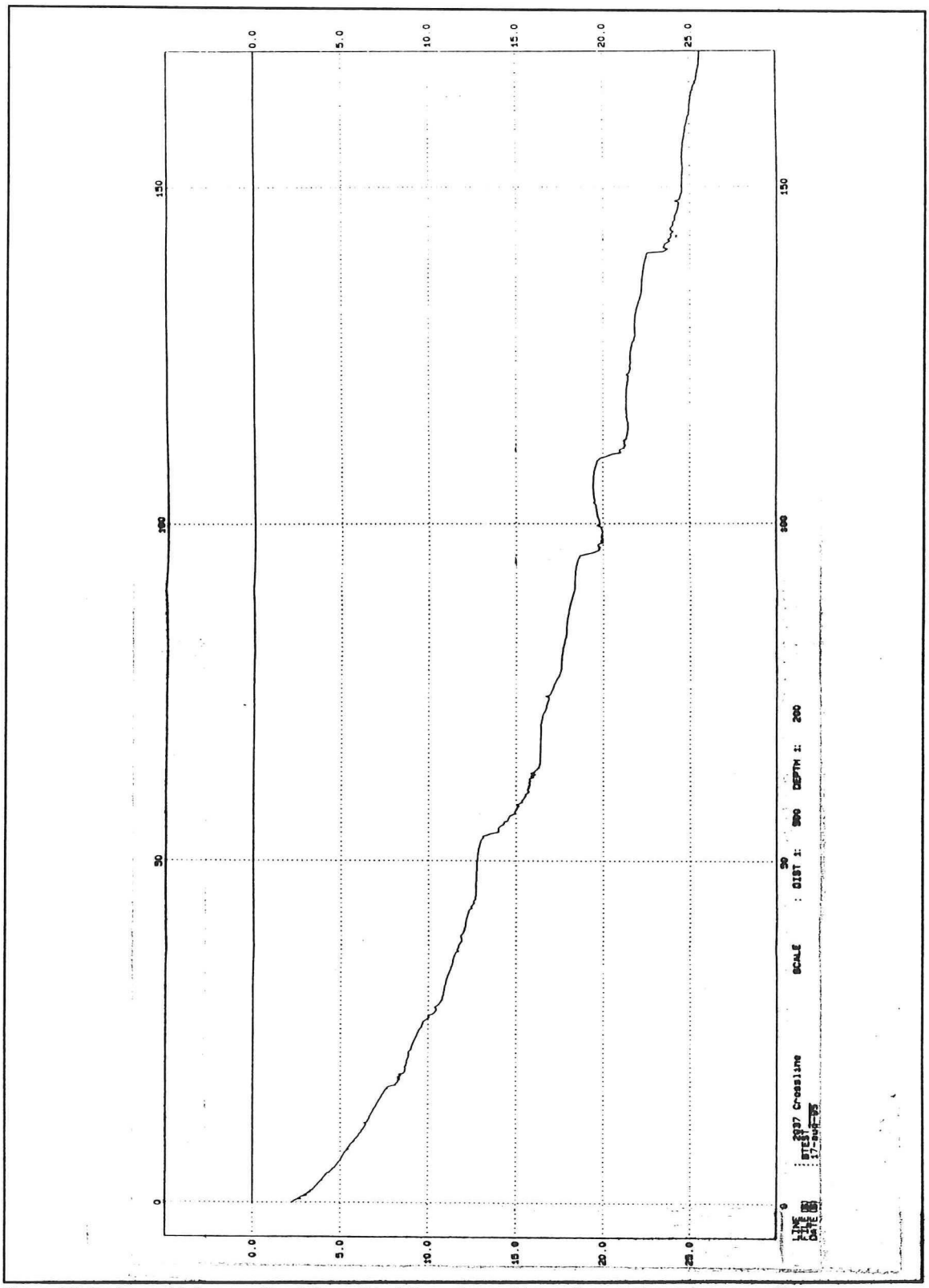

Figure 29 Registered failure profile of flow slide failure of case history II: note the stair-type profile

2 Combined Permeability & Fluidization Tests

§ 2.1 Introduction and Aim of the Tests

As one may conclude from the previous appendix, knowledge of the critical void ratio is vital in static liquefaction potential analyses. Also, one may conclude that determination of the critical void ratio in a triaxial apparatus, both 'wet' and 'dry', is very difficult.

When studying Van der Schrieck's lecture notes (1996), my attention was drawn to a graph in which the porosity of different sands were plotted against their permeabilities. The research from which this graph is derived, showed the critical void ratio to be approximately equal to the void ratio (and permeability) at the fluidization limit, increasing with lower permeabilities or a smaller particle size. The original tests were conducted within the framework of research on the cutting forces in sands.

At first glance, fluidization and the liquefaction problem may not seem to be related to the same mechanisms, completely. One may expect that fluidization, which may be established at any void ratio in any sand, as long as the head difference applied is large enough, is the result of high pore pressures lifting the grains. Liquefaction, on the contrary, may be seen as a continues process of softening, as a result of induced pore pressures.

However, the two are not that different, if fluidization is looked upon as the opposite of liquefaction. In other words, instead of grains moving toward a denser packing, causing a rise in pore pressure, the pore pressure is increased deliberately while monitoring the development of the equilibrium void ratio, closely, until the grain skeleton structure is lost.

The aim of the test series conducted within the framework of this graduate study program was twofold. First, it was meant to verify that an estimation of the (wet) critical density may be derived from a simple permeability test. Second, it was meant to work out a relative simple test procedure, as opposed to the current test procedures in static liquefaction analyses, to estimate the critical void ratio as well as the maximum and minimum void ratios. This last additional information would be useful for estimating the in-situ void ratios from CPT-approximated relative densities. Unfortunately no samples were available from the case history sites that were studied.

§ 2.2 The Permeability Apparatus

In fact, for the combined permeability & fluidization test, an ordinary permeability apparatus is used. The only adjustment made, was the extension of the head measuring tubes, to accommodate the high head differences. The diameter of the test cylinder was 60 *mm*, which made the inside area equal to 2,827.43 mm^2 ($\approx$ 2.827 * 10^{-3} m^2). A schematic view of the apparatus used is given in Figure 30 on page 34.

Tap water penetrates the specimen from below. The sixth head measuring tube indicates the pressure at the bottom of the specimen. The top of the apparatus serves as an overflow from which the water runs off to the sink. The first head measuring tube indicates the height of the water-level at the top of the test cylinder, which equals the hydrostatic pressure in the specimen.

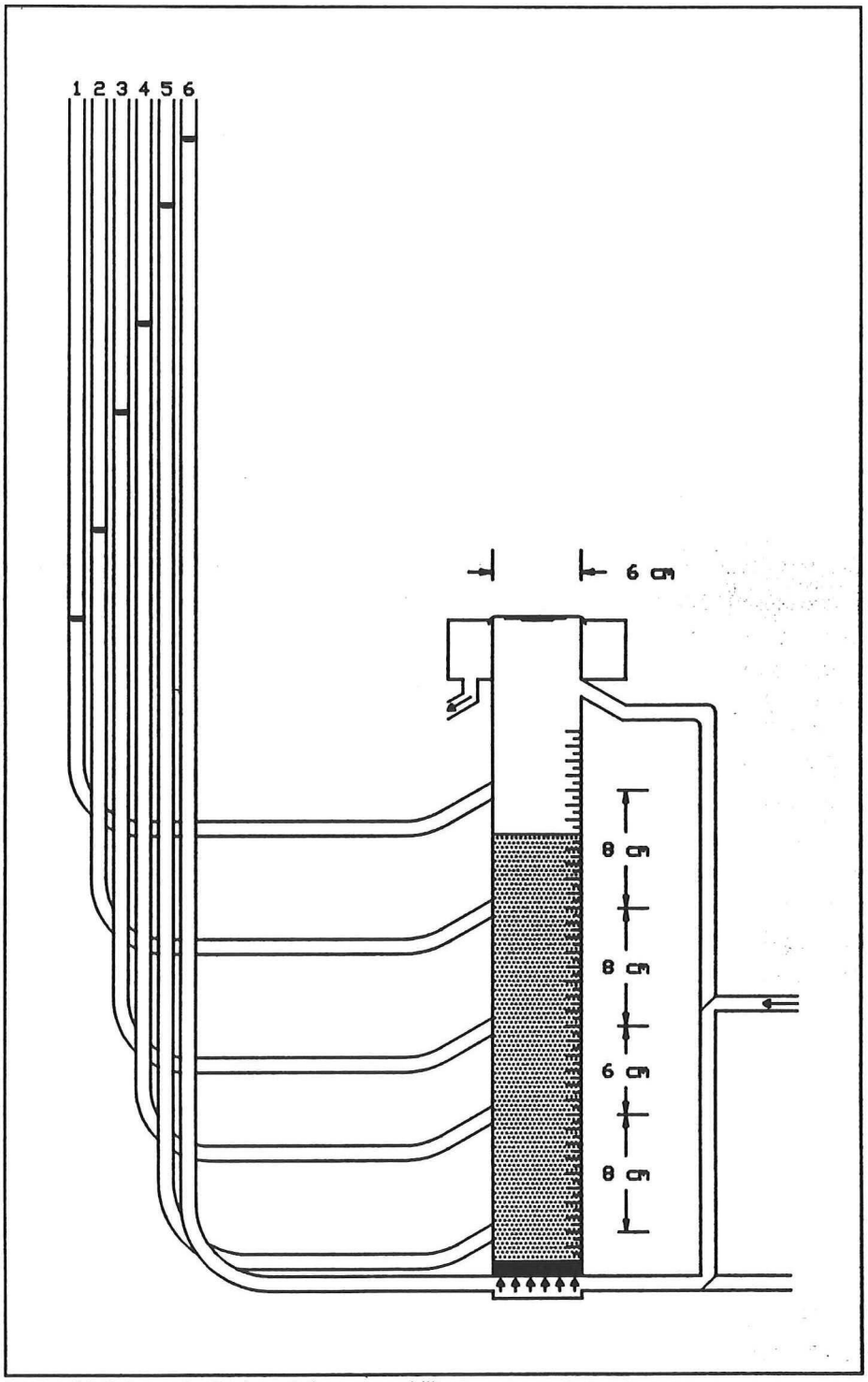

Figure 30 Schematic display of the permeability test apparatus

The four remaining head measuring tubes are connected to the test cylinder at different distances apart. Multiple head measuring tubes allow for differentiated permeability measurement which enables one to evaluate the uniformity of the void ratio over the height of the specimen and a mean permeability value.

§ 2.3 Description of the Test Procedures

A combined permeability & fluidization test is divided into two phases. Phase I is conducted to establish the permeability-void ratio path between the local maximum and minimum void ratios. Phase II is conducted to find the *fluidization limit* and permeability properties at fluidization. Each combined permeability & fluidization test was carried out in a series of steps, which will be described in this paragraph.

STEP 1: A weighted quantity of granular material must be carefully deposited in the test cylinder layer by layer, avoiding any disturbances. It is important to patiently let the individual particles settle layer by layer to avoid separation of the different fractions, as much as possible. If the material contains a high percentage of fines, it is advisable to mix some sand with a little water first, before pouring it into the test cylinder, if necessary through a funnel. Else, the finer particles may adhere to air bubbles and remain at the water surface. During sedimentation, the water level in the test cylinder must be high enough to prevent scour when adding a sand stream. Preferably, it must be low enough, at all times, to not overflow the test cylinder top. To establish the maximum void ratio, a constant upward gradient may be imposed on the settling sand.

STEP 2: A first estimation of the maximum obtainable void ratio is made by measuring the hight of the specimen in the test cylinder, after all particles have settled. Now, the weight of the material in the cylinder as well as the volume it takes are known. With the assumption that the specific volumetric weight of the particles, ρ_s, equals 2.650 kg/m^3 (Van Niekerk (1995) found deviations of less than a few percent on eight characteristic Dutch sands), the void ratio may be calculated from:

$$\gamma_{max,\,sed} = \frac{W_{dry,\,specimen}}{V_{max,\,sed}} \quad [kg/m^3]$$

$$e_{max,\,sed} = 1 - \frac{\gamma_{max,\,sed}}{\rho_s} \quad [-]$$

STEP 3: After measuring the maximum void ratio obtainable through very careful sedimentation, the specimen is fluidized by increasing the head difference. After full fluidization, the head difference is decreased gradually until all particles have settled again. At this time, the time needed to let the pore pressures return to hydrostatic level is measured. This period is called the *relaxation time* of the system. When hydrostatic pressure is reached, the maximum hight of the specimen is measured again to see whether an even looser packing was possible, than was established by sedimentation. The calculation procedure equals the one, mentioned above.

STEP 4: At this point, the actual permeability test commences. To the specimen a head difference of approximately 10 cmwc is applied. When the flow through the specimen is stationary (the relaxation time serves as an indication here), the amount of water flowing through the specimen during a certain time is measured, several times. A measuring glass and a stop-watch were used. After several measurements, indicating a stationary flow, the head differences at different spacings along the test cylinder are noted down, as well as the height of the specimen.

STEP 5: Next, the specimen is compacted by carefully rapping and vibrating the test cylinder at equal distances apart, starting at the lower end of the cylinder, to decrease the void ratio as uniform as possible over the height of the specimen. Any noticeable events, like excess pore pressures during rapping, are noted down. If the head difference excesses 15 cmwc, the head difference must be adjusted back to approximately 10 cmwc, to avoid turbulent flow. The steps 4 and 5 are repeated until it is not possible to compact the specimen any further.

STEP 6: To estimate the minimum void ratio obtainable, a negative head difference is applied and the test cylinder is given a final vibrating session. The minimum void ratio is calculated from the minimum height of the specimen in the same manner as the maximum void ratio, as mentioned above. A smaller test cylinder diameter gives less accurate results concerning the permeability. However, lower void ratios are obtainable because the vibrations have more impact.

STEP 7: At this point, the actual fluidization test commences. Gradually, a head difference of approximately 20 cmwc is applied to the specimen. Light rapping of the test cylinder may help the individual particles to rearrange. When the flow through the specimen is stationary, the permeability and the void ratio are measured as mentioned above.

STEP 8: Next, the head difference is increased very carefully cmwc by cmwc. After each step, the permeability and void ratio are measured again, as well as the head differences along the specimen. Meanwhile, the specimen is scrutinized for any particle movement. When the fluidization limit is approached, piping may be noticed and the upper part of the specimen may partially liquefy. Full fluidization appears suddenly all along the specimen and is easily noticed.

STEP 9: Lastly, the resistance of the particles in full fluidization is measured. For this purpose, the whole specimen is fluidized to a maximum allowable height (without spilling any of the specimen). Then again, the permeability and head differences along the specimen are measured. A void ratio measurement is not significant at this stage.

§ 2.4 Selecting the Materials to be Tested

Grading of the specimen and angularity of the individual particles (of the main fractions) are suspected to be important parameters to influence the maximum, minimum void ratio and the void ratio at the fluidization limit (see following paragraphs). Therefore, it is important to have an indication of these parameters. The main aim of the research conducted within the framework of this graduate study was not to evaluate de exact influence of the parameters mentioned above. Therefore, it was decided to test materials with different attributes, but within Ishihara's (1986) boundaries for most liquefiable sands, in order to establish significant differences in fluidization behaviour, qualitatively.

Three essentially different sands were tested. Unfortunately, no samples were available from the case histories, discussed in Appendix 1. The first sand is referred to as "Rutten Sand". This sample was taken from fill sand from a road construction site along highway A15, The Netherlands. With respect to the other sands tested it was well graded with a typical high percentage of fines (see Appendix 3). On the basis of microscopic analyses, it was classified as "highly spherical, sub-angular". Its VVS angularity index was measured a value of 66.047 (see Appendix 4).

The second sand tested is referred to as "Scheveningen Sand". It originates from the beach at Scheveningen, The Netherlands. As was to be expected, this sand is more uniform than the Rutten Sand. Sieve analyses indicated that in fact the Scheveningen Sand was a mixture of different sands, judged by particle size and colour. To test the individual permeability and fluidization behaviour as well as the influence of uniformity, the two main fractions of the Scheveningen Sand (350 & 250 μm) and the different-coloured 175 μm fraction were tested separately. The finer fraction may actually be dune sand while the coarser fractions may be brought to shore during recent beach nourishments. The Scheveningen Sand was selected because of its uniformity and expected roundness. On the basis of microscopic analyses, it was classified as "highly spherical, sub-rounded". Its VVS angularity index was measured a value of 51.696 (see Appendix 4).

The third sand tested is referred to as "Silver Sand", because of its white colour. It is not known what the origin of the sand is. Most likely it was taken from a bounty beach of some tropical island in the Pacific Ocean. Silver sand was used because of its supposed angular nature, with respect to the aforementioned sands. Although on the basis of microscopic analyses it was classified as "lowly spherical, sub-angular", the VVS angularity index was measured a value of 47.706 (see Appendix 4). Obviously, the dominant fractions were less angular than the fractions judged through the microscope.

§ 2.5 Hypothesis on the Material Behaviour During Testing

As was proven by the test series, the maximum obtainable void ratio is not equal to the void ratio at fluidization. When gradually increasing the head difference over the specimen, the void ratio seeks to find an equilibrium such that the head difference over a particle balances its weight and the intergrain sliding friction. With the increasing void ratio and pore pressure gradient, the internal friction reduces to a level at which only the intergrain sliding friction forces contribute to the equilibrium. The weight is balanced by the pore pressure gradient. This can be understood when one realizes that the effective stress as well as the pore pressure at the bottom of the specimen are larger than close to the top of the specimen.

At this point the steady state (also: "critical state") or state of deformation at constant void ratio has been approached. The effect of delation has been reduced to zero and the remaining friction angle is represented as the sum of the intergrain sliding friction (ϕ_μ) and particle rearrangements (see Figure 31 on page 38). This state, by definition, is not the same as the state at which a specimen has the critical void ratio, but the two are very close at this point. If the head difference is increased just a little, the intergrain sliding forces are exceeded and total collapse occurs because the pore pressure gradient is kept at a constant level. With the recognition of the intergrain sliding friction, also the influences of grading and angularity has been clarified. The above is in accordance with the statements of Poulos *et al.* (1985).

§ 2.6 The Test Results

Figure 32 on page 39 shows the interpretation of the combined fluidization & permeability tests. The over all test results are presented in Figure 33 on page 41 through Figure 44 on page 46. The maximum and minimum obtainable void ratios in the permeability test cylinder are indicated as well as the linear trend on the logarithmic scale. The trends are assumed to be parallel. The last measured void ratio before fluidization has been indicated with a dotted line.

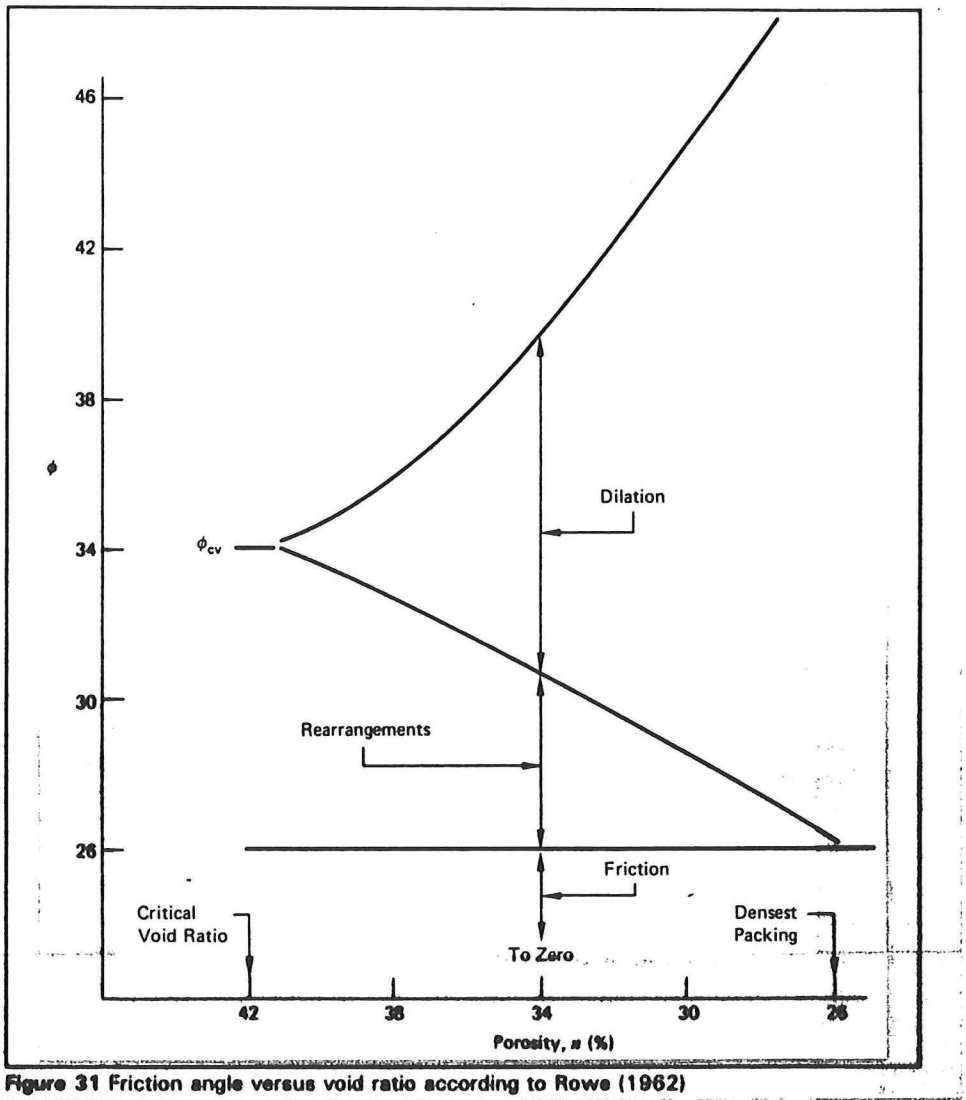

Figure 31 Friction angle versus void ratio according to Rowe (1962)

As we may conclude from Figure 32 on page 39, the fluidization limit displays some features that would have been expected of the critical void ratio too. The relatively well graded, fine and most angular Rutten Sand has the highest fluidization limit at approximately 0.82. The Scheveningen Sand has the lowest fluidization limit at approximately 0.72. The Silver Sand fluidization limit is in between the two at approximately 0.78.

Rapping the test cylinder lightly, while increasing the head difference, is considered to help the individual particles to rearrange. In accordance with the idea that the (wet) critical void ratio is approximated from below, no excess pore pressures were noticed while rapping.

Unfortunately, no critical void ratio test results were available to substantiate the agreement between the fluidization limit and the (wet) critical void ratio. Therefore no statement on the usefulness of this test can be made at this point. Although these tests take considerable time, they are relatively easy to conduct. The influence of in situ stress levels on the critical void ratio is not accounted for in this type of test.

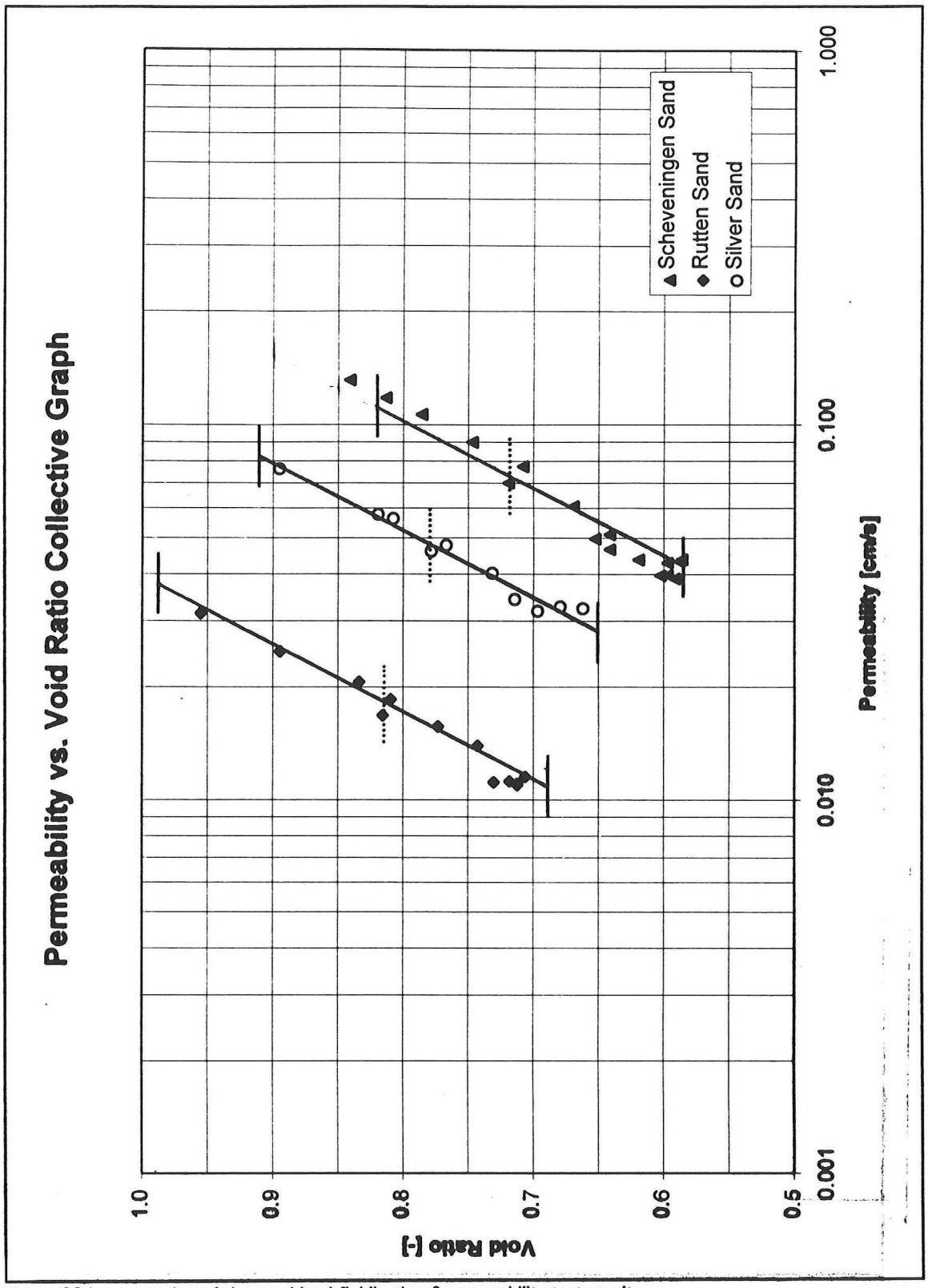

Figure 32 Interpretation of the combined fluidization & permeability test results

§ 2.7 Discussion and Validity of the Test Results

There are several factors that may have had their influence on the outcome of the combined fluidization & permeability test. Because all these factors of influence have been reasonably constant during the tests, comparison on the test results is considered possible. The validity of the absolute values must be doubted seriously.

1. The head difference was controlled by a very fine tunable valve connected directly to the tab. However, pressure fluctuations in the tab water were inevitably imposed on the specimen. It would have been better to use a buffer tank in which the water level may be controlled very easily.
2. Water from the tab contains a considerable amount of air and has a low temperature. During the test, the tab water warms up. As the water warms up, it can contain less air and air bubbles are formed in pores of the specimen. The influence of the air bubbles has not been quantified.
3. To get a clearer picture of the influence of different soil properties, more parameters must be varied. Amongst these are the particle size, gradation, angularity and the percentage of fines.
4. To establish a more precise fluidization limit, the head difference must be lowered and the particles must be allowed to settle again, after fluidization has occurred. From that point on, the head difference may be increased again until fluidization occurs. A couple of cycles may help to determine the exact void ratio at fluidization.
5. Darcy's law holds only for stationary flow. Non-stationary flow conditions like turbulence and piping cause inaccurate calculations of the permeability. The influence of non-stationary flow conditions on the fluidization limit has not been quantified.

Combined Permeability & Fluidization Tests.

Test 7: Rutten Sand.
Delft University of Technology, Soil Mechanics Laboratory, July 2, 1998.

Specific volumetric weight op grains:	rho_{sand}	2650 kg/m³
Diameter of test cylinder:	D_{cyl}	60 mm
Area of test cylinder:	A_{cyl}	2827 mm²
Weight at start:	W_{start}	2059 gram
Weight at end:	W_{end}	825 gram
Input weight:	W_{in}	1234 gram
Maximum height of specimen after sedimentation:	$h_{max\ sed}$	32.6 cm
Maximum volumetric weight after sedimentation:	$rho_{max\ sed}$	1338.8 kg/m³
Maximum porosity after sedimentation:	$n_{max\ sed}$	49.48 %
Maximum void ratio after sedimentation:	$e_{max\ sed}$	0.9794 -
Maximum height of specimen after fluidization:	$h_{max\ fluid}$	32.2 cm
Maximum volumetric weight after fluidization:	$rho_{max\ fluid}$	1355.4 kg/m³
Maximum porosity after fluidization:	$n_{max\ fluid}$	48.853 %
Maximum void ratio after fluidization:	$e_{max\ fluid}$	0.9551 -
Minimum height of specimen:	h_{min}	27.8 cm
Minimum volumetric weight:	rho_{min}	1589.9 kg/m³
Minimum porosity:	n_{min}	40.758 %
Minimum void ratio:	e_{min}	0.688 -
Approximate relaxation time to steady flow:	T_{relax}	± 10 min

	Discharge:											Head:						
No.	1	2	3	4	5	6	7	8	9	10	Time	h_1	h_2	h_3	h_4	h_5	h_6	h_{sand}
1	86	89	87	88							300	1.3	3.3	5.6	7.5	10.6	11.8	32.2
2	83	88	88								300	1.3	3.3	6.2	8.7	12.2	13.5	31.2
3	52	52	49								180	1.3	3.3	6.8	8.8	14.0	16.3	30.2
4	60	60	63								180	1.3	3.4	7.4	10.8	15.3	17.9	29.8
5	37	38	37	38							180	1.3	2.9	6.4	9.1	13.0	14.9	29.2
6	35	34	35								180	1.3	3.1	6.8	9.7	13.9	16.0	28.7
7	70	71	71								240	1.3	3.1	8.4	16.0	23.2	28.1	28.1
8	73	72	72								240	1.3	3.2	10.0	16.0	24.8	29.2	28.2
9	58	54	58	58							180	1.3	3.2	10.4	16.8	26.0	29.1	28.2
10	41	41	41	41							120	1.3	3.3	10.7	17.5	27.3	32.0	28.3
11	67	62	61	63							240	1.3	3.4	10.8	17.8	28.0	31.3	28.5
12	62	61	61								180	1.3	4.4	11.7	18.4	28.3	28.3	29.9
13	433	437									90	2.1	6.6	12.2	18.0	24.8	28.6	+++

Figure 33 CP&F test results (a): Rutten Sand

	Q_{max}	P_1	P_2	P_3	P_{max}	n	e	Obsevations
1	0.29	0.03	0.03	0.04	0.03	48.85	0.96	Excess pp when compacting / fines in suspension
2	0.28	0.02	0.02	0.03	0.02	47.21	0.89	Excess pp when compacting / fines in suspension
3	0.28	0.02	0.02	0.02	0.02	45.47	0.83	Excess pp / fines in suspension / air bubbles on top
4	0.28	0.02	0.02	0.02	0.02	44.73	0.81	Fines in suspension
5	0.20	0.01	0.02	0.02	0.02	43.60	0.77	Fines in suspension / head adjusted
6	0.19	0.01	0.01	0.01	0.01	42.62	0.74	Long pause
7	0.29	0.01	0.01	0.01	0.01	41.39	0.71	Long pause / rapped
8	0.30	0.01	0.01	0.01	0.01	41.60	0.71	Rapped
9	0.32	0.01	0.01	0.01	0.01	41.60	0.71	Rapped
10	0.34	0.01	0.01	0.01	0.01	41.80	0.72	-
11	0.35	0.01	0.01	0.01	0.01	42.21	0.73	-
12	0.45	0.02	0.01	0.02	0.02	44.92	0.82	-
13	4.83	0.21	0.18	0.20	0.20			Full fluidization

Notice:
In a small cylinder the *dry* maximum porosity was determined. This value appeared to be lower than the *wet* maximum porosity: 47,86% (void ratio: 0.918).

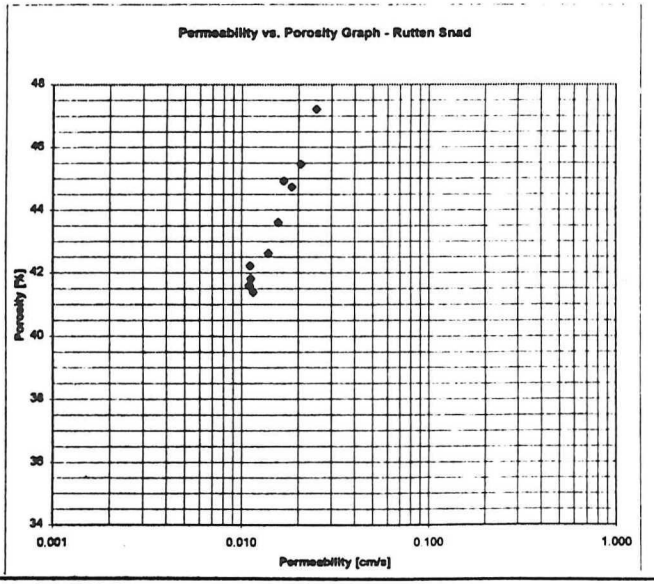

Figure 34 CP&F test results (b): Rutten Sand

Combined Permeability & Fluidization Tests.

Test 3: Scheveningen Sand.
Delft University of Technology, Soil Mechanics Laboratory, June 26, 1996.

Specific volumetric weight op grains:	rho_{solids}	2650 kg/m³
Diameter of test cylinder:	D_{cyl}	60 mm
Area of test cylinder:	A_{cyl}	2827 mm²
Weight at start:	W_{start}	1600 gram
Weight at end:	W_{end}	249 gram
Input weight:	W_{in}	1351 gram
Maximum height of specimen after sedimentation:	$h_{max,sed}$	32 cm
Maximum volumetric weight after sedimentation:	$rho_{max,sed}$	1493.2 kg/m³
Maximum porosity after sedimentation:	$n_{max,sed}$	43.653 %
Maximum void ratio after sedimentation:	$e_{max,sed}$	0.7747 -
Maximum height of specimen after fluidization:	$h_{max,fluid}$	32.9 cm
Maximum volumetric weight after fluidization:	$rho_{max,fluid}$	1452.3 kg/m³
Maximum porosity after fluidization:	$n_{max,fluid}$	46.186 %
Maximum void ratio after fluidization:	$e_{max,fluid}$	0.8248 -
Minimum height of specimen:	h_{min}	28.6 cm
Minimum volumetric weight:	rho_{min}	1670.7 kg/m³
Minimum porosity:	n_{min}	36.955 %
Minimum void ratio:	e_{min}	0.5862 -
Approximate relaxation time to steady flow:	T_{relax}	± 5 min

	Discharge:											Head:						
No.	1	2	3	4	5	6	7	8	9	10	Time	h_1	h_2	h_3	h_4	h_5	h_6	h_{gem}
1	84	83	84	85	83	83	85	85	85	84	60	1.3	5.8	9.4	11.9	15.1	18.8	32.7
2	83	84	83	85	84	84	84	84	84	85	60	1.3	6.2	10.3	13.1	16.5	18.0	32.2
3	85	84	85	83	85	86	86	85	85	85	60	1.3	5.9	11.0	14.3	18.3	20.1	31.5
4	84	84	84	82	86	86	82	84	85	84	60	1.3	6.4	11.0	16.2	20.5	22.8	30.8
5	86	85	85	85	85						60	1.3	5.1	12.0	17.1	23.3	28.0	32.1
6	85	84	84	85	84						60	1.3	3.8	8.9	12.8	17.8	18.3	29.6
7	84	84	84	83	84	83					60	1.3	4.3	11.2	15.8	20.8	21.5	28.8
8	84	83	84								120	1.3	4.3	10.0	14.0	17.3	20.0	28.8
9	86	86	87	87							120	1.3	4.4	11.2	16.8	20.8	23.8	28.7
10	84	84	84	84	84						60	1.3	4.4	11.7	16.8	22.2	24.7	28.8
11	88	88	88	88							60	1.3	4.5	12.5	18.0	24.0	28.0	28.9
12	72	72	70	70	70						60	1.3	4.8	12.7	18.7	25.8	28.0	28.2
13	80	78	77	78	78						60	1.3	4.8	12.8	18.8	28.7	30.0	28.6
14	88	86	87	86	86						60	1.3	5.2	12.8	18.8	28.2	31.0	28.8
15	118	116	118	118	118						60	1.3	5.8	13.6	19.6	27.8	31.3	31.0
16	192	191	187	185							60	1.3	7.7	14.6	20.0	28.8	29.7	33.2
17	418	420	418								30	7.2	12.1	17.4	21.8	27.8	30.6	+++

Figure 35 CP&F test results (a): Scheveningen Sand

	Q_{mean}	P_1	P_2	P_3	P_{mean}	n	e	Obsevations:
1	1.40	0.12	0.12	0.11	0.12	44.86	0.81	Excess pp when compacting
2	1.40	0.12	0.11	0.10	0.11	44.00	0.79	Excess pp when compacting
3	1.42	0.10	0.09	0.08	0.09	42.76	0.75	Excess pp when compacting
4	1.41	0.08	0.07	0.09	0.08	41.46	0.71	Excess pp when compacting
5	1.42	0.08	0.08	0.08	0.08	40.10	0.67	Excess pp when compacting
6	0.91	0.05	0.05	0.05	0.05	39.08	0.64	Excess pp / piping / head adjusted
7	0.89	0.05	0.04	0.04	0.04	37.39	0.60	No excess pp / piping
8	0.70	0.06	0.04	0.03	0.04	36.95	0.59	No excess pp / piping
9	0.81	0.05	0.04	0.03	0.04	37.17	0.59	-
10	0.90	0.05	0.04	0.03	0.04	37.39	0.60	-
11	0.98	0.05	0.04	0.03	0.04	37.61	0.60	-
12	1.18	0.05	0.04	0.04	0.04	38.25	0.62	Piping
13	1.31	0.05	0.05	0.05	0.05	39.08	0.64	Piping / air bubbles
14	1.45	0.04	0.05	0.05	0.05	39.49	0.65	Negative pp
15	1.95	0.07	0.07	0.07	0.07	41.84	0.72	Upward moving front
16	3.23	0.13	0.13	0.13	0.13	45.69	0.84	Negative pp / upper 10 cm liqified
17	13.93	0.66	0.67	0.74	0.69			Full fluidization

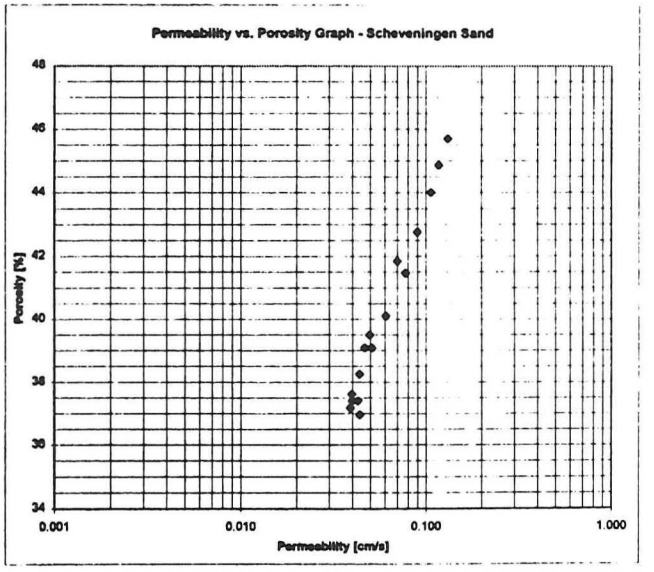

Figure 36 CP&F test results (b): Scheveningen Sand

Combined Permeability & Fluidization Tests.

Test 4: Scheveningen Sand, 0.35 mm-diameter fraction (uniform, round).
Delft University of Technology, Soil Mechanics Laboratory, June 26, 1996.

Specific volumetric weight op grains:	rho_{solids}	2650 kg/m³
Diameter of test cylinder:	D_{cyl}	60 mm
Area of test cylinder:	A_{cyl}	2827 mm²
Weight at start:	W_{start}	1971 gram
Weight at end:	W_{end}	647 gram
Input weight:	W_{in}	1324 gram
Maximum height of specimen after sedimentation:	$h_{max\ sed}$	33 cm
Maximum volumetric weight after sedimentation:	$rho_{max\ sed}$	1418 kg/m³
Maximum porosity after sedimentation:	$n_{max\ sed}$	46.453 %
Maximum void ratio after sedimentation:	$e_{max\ sed}$	0.8675 -
Maximum height of specimen after fluidization:	$h_{max\ fluid}$	33.3 cm
Maximum volumetric weight after fluidization:	$rho_{max\ fluid}$	1408.2 kg/m³
Maximum porosity after fluidization:	$n_{max\ fluid}$	46.835 %
Maximum void ratio after fluidization:	$e_{max\ fluid}$	0.8845 -
Minimum height of specimen:	h_{min}	29 cm
Minimum volumetric weight:	rho_{min}	1614.7 kg/m³
Minimum porosity:	n_{min}	39.087 %
Minimum void ratio:	e_{min}	0.6411 -
Approximate relaxation time to steady flow:	T_{relax}	± 5 min

	Discharge:											Head:						
No.	1	2	3	4	5	6	7	8	9	10	Time	h_1	h_2	h_3	h_4	h_5	h_6	h_{open}
1	183	180	180	180	180						60	1.2	6.5	11.7	15.5	20.8	23.5	33.3
2	116	117	114	116	116						60	1.2	4.8	9.1	12.4	16.8	18.6	32.0
3	120	116	116	112	116	116					60	1.2	5.1	10.9	15.2	20.5	23.3	31.0
4	231	228	230	231	230						120	1.2	5.2	13.3	19.4	28.5	29.5	30.0
5	70	68	73	71	69						60	1.2	4.3	9.7	13.7	18.2	20.1	29.4
6	63	62	62	62	62						60	1.2	4.1	8.8	13.8	18.3	20.2	29.2
7	66	65	64	64	64						60	1.2	4.2	10.2	14.6	19.4	21.7	29.3
8	77	77	77								60	1.2	4.6	11.6	16.9	22.6	25.5	29.4
9	68	68	68	67	69						60	1.2	4.9	12.7	18.7	25.7	28.4	29.5
10	95	95	94	95	94						60	1.2	5.1	13.3	19.4	28.7	30.0	29.7
11	207	207	207								120	1.2	5.4	13.4	19.2	27.1	30.5	30.1
12	227	228	230								120	1.2	5.6	13.7	19.5	27.7	31.6	30.6
13	142	145	138	140	143	142					60	1.2	6.4	13.8	19.7	27.6	31.0	31.2
14	680										30	7.9	13.4	18.6	22.8	28.6	32.0	+++

Figure 37 CP&F test results (a): Scheveningen 350 μm

	Q_{mean}	P_1	P_2	P_3	P_{mean}	n	e	Obsevations:
1	3.01	0.16	0.17	0.16	0.16	46.94	0.88	Excess pp when compacting / piping
2	1.94	0.12	0.12	0.13	0.13	44.78	0.81	Excess pp when compacting / head adjusted
3	1.94	0.10	0.10	0.09	0.10	43.00	0.75	Excess pp when compacting
4	1.92	0.08	0.07	0.07	0.07	41.10	0.70	-
5	1.17	0.07	0.06	0.06	0.07	39.90	0.66	Head No. 6 fluctuates / head adjusted
6	1.04	0.07	0.05	0.05	0.06	39.48	0.65	-
7	1.07	0.06	0.05	0.05	0.06	39.69	0.66	-
8	1.28	0.06	0.06	0.05	0.05	39.90	0.66	-
9	1.46	0.06	0.05	0.05	0.05	40.10	0.67	Negative pp when rapping the cylinder
10	1.58	0.06	0.06	0.05	0.06	40.50	0.68	-
11	1.73	0.06	0.06	0.06	0.06	41.29	0.70	-
12	1.90	0.07	0.07	0.07	0.07	42.25	0.73	-
13	2.36	0.08	0.08	0.09	0.09	43.36	0.77	Air-bubble blow outs at top of specimen
14	18.67	0.91	0.99	0.98	0.96			Full fluidization

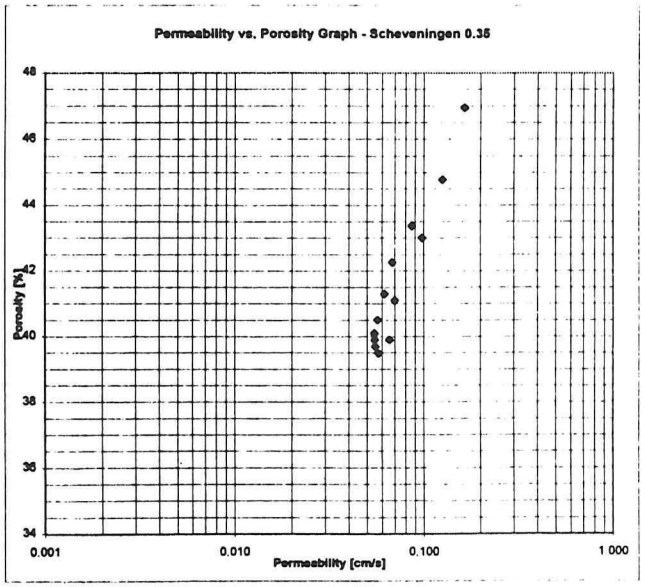

Figure 38 CP&F test results (b): Scheveningen Sand 350 μm

Combined Permeability & Fluidization Tests.

Test 5: Scheveningen Sand, 0.25 mm-diameter fraction (uniform, round).
Delft University of Technology, Soil Mechanics Laboratory, June 28, 1996.

Specific volumetric weight op grains:	rho_{solids}	2650 kg/m³
Diameter of test cylinder:	D_{cyl}	60 mm
Area of test cylinder:	A_{cyl}	2827 mm²
Weight at start:	W_{start}	1830 gram
Weight at end:	W_{end}	497 gram
Input weight:	W_{in}	1333 gram
Maximum height of specimen after sedimentation:	$h_{max,sed}$	33 cm
Maximum volumetric weight after sedimentation:	$rho_{max,sed}$	1428.6 kg/m³
Maximum porosity after sedimentation:	$n_{max,sed}$	46.089 %
Maximum void ratio after sedimentation:	$e_{max,sed}$	0.8549 -
Maximum height of specimen after fluidization:	$h_{max,fluid}$	33 cm
Maximum volumetric weight after fluidization:	$rho_{max,fluid}$	1428.6 kg/m³
Maximum porosity after fluidization:	$n_{max,fluid}$	46.089 %
Maximum void ratio after fluidization:	$e_{max,fluid}$	0.8549 -
Minimum height of specimen:	h_{min}	28.5 cm
Minimum volumetric weight:	rho_{min}	1654.2 kg/m³
Minimum porosity:	n_{min}	37.577 %
Minimum void ratio:	e_{min}	0.602 -
Approximate relaxation time to steady flow:	T_{relax}	± 5 min

	Discharge:											Head:						
No.	1	2	3	4	5	6	7	8	9	10	Time	h_1	h_2	h_3	h_4	h_5	h_6	h_{mean}
1	202	200	200	202	202	203					180	1.3	3.8	6.3	8.8	11.4	12.7	32.8
2	200	200	199	200	202	205					180	1.3	4.0	7.0	9.5	12.7	14.2	32.1
3	200	208	199	202	199	202					180	1.3	4.0	7.3	10.1	13.6	15.2	31.6
4	200	199	204	201	200	195					180	1.3	4.0	7.6	10.8	14.4	16.2	31.0
5	199	200	200	201							180	1.3	4.3	8.8	12.7	17.4	19.5	30.2
6	136	132	133	134	132	130					180	1.3	3.8	7.3	10.1	13.6	15.1	29.5
7	130	131	129	134	127	130					180	1.3	3.7	7.6	10.7	19.6	16.0	29.0
8	135	136	137	135	135						180	1.3	3.9	8.5	12.3	16.6	19.2	28.9
9	163	164	162	164	164	164					180	1.3	4.2	9.7	14.0	18.5	21.8	28.8
10	189	191	189	189	190						180	1.3	4.7	11.2	16.2	22.6	25.1	28.8
11	160	163	161	160	162						120	1.3	4.8	12.9	18.1	27.3	29.8	28.8
12	162	160	163	162	162						120	1.3	4.8	13.0	18.2	27.4	31.2	29.0
13	173	174	174	173							120	1.3	5.6	13.1	18.3	27.4	30.0	29.2
14	86	90	89	94	95						60	1.3	5.6	11.6	16.0	21.6	25.0	29.8
15	190	189	189	189	190						120	1.3	5.0	11.4	16.8	24.5	28.0	30.0
16	138	142	134	133	140	139	137				60	1.3	6.6	14.2	19.7	26.4	28.8	31.0
17	153	143	142	142	143	141					60	1.3	6.8	14.3	20.0	26.8	29.3	31.4
18	172	170	180	178	188						60	1.3	7.7	15.0	20.4	27.0	29.7	32.7
19	360	360									60	8.2	13.5	18.7	22.7	28.1	31.1	+++

Figure 39 CP&F test results (a): Scheveningen 250 μm

	Q_{mean}	P_1	P_2	P_3	P_{mean}	n	e	Obsevations:
1	1.12	0.11	0.10	0.13	0.11	45.76	0.84	Excess pp when compacting / instantanious liq
2	1.12	0.10	0.09	0.11	0.10	44.58	0.80	Excess pp when compacting / instantanious liq
3	1.12	0.09	0.08	0.10	0.09	43.70	0.78	Excess pp when compacting
4	1.11	0.08	0.08	0.09	0.08	42.61	0.74	Excess pp when compacting
5	1.11	0.07	0.08	0.07	0.07	41.09	0.70	Excess pp when compacting / head adjusted
6	0.74	0.06	0.06	0.06	0.06	39.69	0.66	Little excess pp
7	0.72	0.02	0.05	0.05	0.04	38.65	0.63	-
8	0.75	0.05	0.04	0.05	0.05	38.44	0.62	Unexpected compaction
9	0.91	0.05	0.04	0.05	0.05	38.23	0.62	Unexpected compaction
10	1.05	0.05	0.04	0.05	0.05	38.23	0.62	-
11	1.34	0.05	0.05	0.05	0.05	38.44	0.62	-
12	1.35	0.05	0.05	0.05	0.05	38.65	0.63	-
13	1.45	0.05	0.05	0.05	0.05	39.07	0.64	-
14	1.52	0.08	0.07	0.07	0.07	39.90	0.66	-
15	1.59	0.08	0.08	0.07	0.08	40.70	0.69	-
16	2.29	0.10	0.09	0.08	0.09	42.61	0.74	Piping
17	2.40	0.10	0.09	0.09	0.09	43.34	0.76	-
18	2.90	0.12	0.11	0.11	0.12	45.59	0.84	-
19	6.50	0.34	0.34	0.35	0.35			Full fluidization

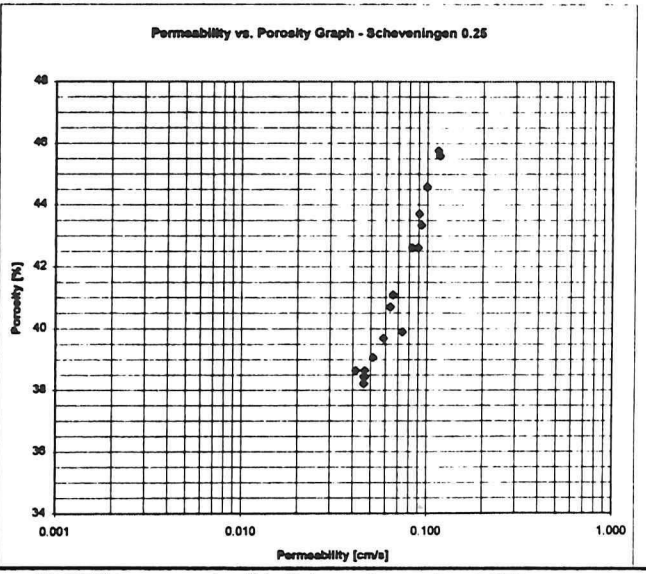

Figure 40 CP&F test results (b): Scheveningen Sand 250 μm

Combined Permeability & Fluidization Tests.

Test 6: Scheveningen Sand, 0.175 mm-diameter fraction (uniform, round).
Delft University of Technology, Soil Mechanics Laboratory, June 28, 1996.

Specific volumetric weight op grains:	rho_{solids}	2650 kg/m³
Diameter of test cylinder:	D_{cyl}	60 mm
Area of test cylinder:	A_{cyl}	2827 mm²
Weight at start:	Wt_{start}	1887 gram
Weight at end:	Wt_{end}	585 gram
Input weight:	Wt_{in}	1282 gram
Maximum height of specimen after sedimentation:	$h_{max,sed}$	33 cm
Maximum volumetric weight after sedimentation:	$rho_{max,sed}$	1374 kg/m³
Maximum porosity after sedimentation:	$n_{max,sed}$	48.152 %
Maximum void ratio after sedimentation:	$e_{max,sed}$	0.9287 -
Maximum height of specimen after fluidization:	$h_{max,fluid}$	32.7 cm
Maximum volumetric weight after fluidization:	$rho_{max,fluid}$	1388.6 kg/m³
Maximum porosity after fluidization:	$n_{max,fluid}$	47.678 %
Maximum void ratio after fluidization:	$e_{max,fluid}$	0.9112 -
Minimum height of specimen:	h_{min}	28.4 cm
Minimum volumetric weight:	rho_{min}	1598.5 kg/m³
Minimum porosity:	n_{min}	39.754 %
Minimum void ratio:	e_{min}	0.6598 -
Approximate relaxation time to steady flow:	T_{relax}	± 10 min

	Discharge:											Head:						
No.	1	2	3	4	5	6	7	8	9	10	Time	h_1	h_2	h_3	h_4	h_5	h_6	h_{mean}
1	78	80	80	81	81	80					120	1.2	3.7	6.6	8.8	11.8	13.2	32.7
2	81	81	82	81	82	82	81				120	1.2	4.0	7.6	10.4	14.0	15.5	31.8
3	80	79	81	81	80	82					120	1.2	4.1	8.2	11.3	15.1	17.1	31.1
4	80	78	80	80	80	81					120	1.2	4.0	8.7	12.3	16.8	18.9	30.4
5	57	57	58	57	58	58	57				120	1.2	3.8	7.8	10.7	14.4	15.6	29.7
6	58	57	57	57	57						120	1.2	3.8	8.8	12.4	16.8	18.1	28.8
7	54	54	53	53	53	52	53				120	1.2	3.8	8.0	12.7	17.4	19.6	28.4
8	61	61	61	61	61						120	1.2	4.0	10.0	14.3	19.7	22.1	28.5
9	66	65	66	66	66						120	1.2	4.0	10.6	15.2	21.2	24.0	28.5
10	74	74	74	74							120	1.2	4.1	11.5	16.9	23.7	27.0	28.6
11	66	63	66	66	66						120	1.2	4.2	12.4	18.4	26.2	29.5	28.6
12	50	50	51	51	50	51	51				60	1.2	4.8	12.4	18.4	25.5	28.7	28.3
13	53	54	53	54	52	53					60	1.2	4.9	12.8	18.7	26.3	28.8	28.4
14	63	62	63	62	62						60	1.2	6.3	13.8	19.6	26.6	29.3	31.4
15	94	92	91	92							60	1.2	7.2	14.5	19.8	26.3	29.0	32.5
16	219	222	223	220	220						120	1.2	7.7	14.8	20.0	26.4	29.4	32.8
17	470	466									60	6.4	13.1	18.2	22.3	27.8	30.8	+++

Figure 41 CP&F test results (a): Scheveningen 175 μm

	Q_{mean}	P_1	P_2	P_3	P_{mean}	n	e	Obsevations:
1	0.67	0.06	0.06	0.07	0.06	47.68	0.91	Excess pp when compacting / instantanious liq
2	0.68	0.05	0.05	0.05	0.05	45.85	0.85	Excess pp
3	0.67	0.05	0.05	0.05	0.05	44.98	0.82	Excess pp
4	0.66	0.04	0.04	0.04	0.04	43.72	0.78	Excess pp / head adjusted
5	0.48	0.04	0.03	0.03	0.03	42.39	0.74	Little excess pp
6	0.47	0.03	0.03	0.03	0.03	40.59	0.68	-
7	0.44	0.03	0.03	0.02	0.03	39.75	0.66	Unexpected compacting
8	0.51	0.03	0.03	0.02	0.03	39.98	0.67	-
9	0.54	0.03	0.02	0.02	0.02	39.98	0.67	-
10	0.62	0.03	0.02	0.02	0.02	39.98	0.67	-
11	0.71	0.03	0.02	0.02	0.03	39.98	0.67	-
12	0.84	0.03	0.03	0.03	0.03	41.60	0.71	-
13	0.89	0.03	0.03	0.03	0.03	41.80	0.72	-
14	1.37	0.06	0.05	0.05	0.05	45.51	0.84	Rapped / piping
15	1.54	0.07	0.06	0.06	0.06	47.35	0.90	Piping / fluidized partly when rapped / start fluid
16	1.84	0.08	0.08	0.07	0.08	47.99	0.92	Piping / very near fluidization limit
17	7.79	0.42	0.40	0.43	0.42			Full fluidization

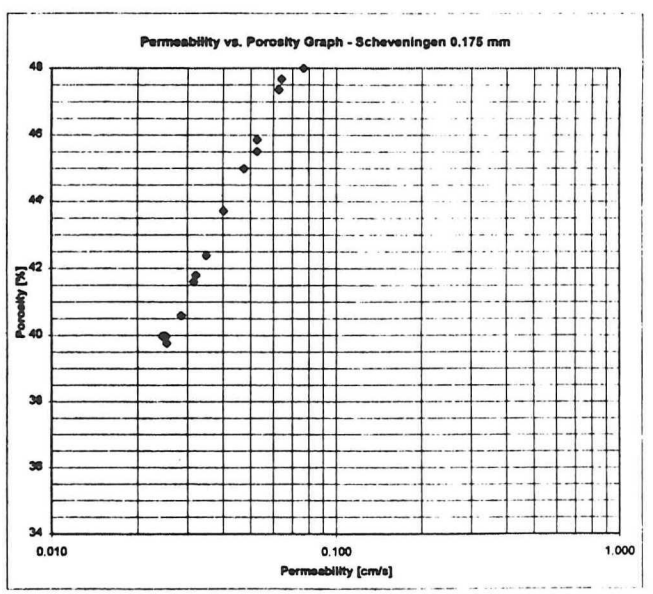

Figure 42 CP&F test results (b): Scheveningen 175 μm

Combined Permeability & Fluidization Tests.

Test 8: Silver Sand (angular).
Delft University of Technology, Soil Mechanics Laboratory, July 2, 1998.

Specific volumetric weight op grains:	rho_{solids}	2650 kg/m³
Diameter of test cylinder:	D_{cyl}	80 mm
Area of test cylinder:	A_{cyl}	2827 mm²
Weight at start:	W_{start}	1630 gram
Weight at end:	W_{end}	345 gram
Input weight:	W_{in}	1285 gram
Maximum height of specimen after sedimentation:	$h_{max,sed}$	32.5 cm
Maximum volumetric weight after sedimentation:	$rho_{max,sed}$	1398.4 kg/m³
Maximum porosity after sedimentation:	$n_{max,sed}$	47.231 %
Maximum void ratio after sedimentation:	$e_{max,sed}$	0.895 -
Maximum height of specimen after fluidization:	$h_{max,fluid}$	32.7 cm
Maximum volumetric weight after fluidization:	$rho_{max,fluid}$	1389.8 kg/m³
Maximum porosity after fluidization:	$n_{max,fluid}$	47.553 %
Maximum void ratio after fluidization:	$e_{max,fluid}$	0.9067 -
Minimum height of specimen:	h_{min}	28.3 cm
Minimum volumetric weight:	rho_{min}	1605.9 kg/m³
Minimum porosity:	n_{min}	39.398 %
Minimum void ratio:	e_{min}	0.6501 -
Approximate relaxation time to steady flow:	T_{relax}	± 5 min

	Discharge:											Head:						
No.	1	2	3	4	5	6	7	8	9	10	Time	h_1	h_2	h_3	h_4	h_5	h_6	h_{mean}
1	238	232	238								300	1.2	4.1	7.0	9.3	12.1	13.5	32.5
2	240	240									300	1.2	3.9	7.5	10.5	14.7	16.4	31.2
3	148	146	144	148							180	1.2	4.0	8.6	12.5	17.2	19.2	30.3
4	195	197	195								240	1.2	4.0	9.5	14.2	19.7	21.3	29.7
5	74	76	75	75							180	1.2	3.0	6.8	9.7	12.9	13.9	28.8
6	74	73	73								180	1.2	3.2	6.2	10.3	13.8	14.4	28.5
7	208	203	205								240	1.2	4.3	11.8	17.7	25.1	28.0	29.1
8	237	228	232								240	1.2	4.6	12.6	18.7	26.6	30.0	29.4
9	218	219	228	225							180	1.2	5.4	13.1	18.9	26.2	29.4	30.5
10	179	182	178	179							120	1.2	5.6	13.6	19.1	26.4	29.6	31.0
11	210	210									20	7.0	12.2	17.6	21.8	27.3	30.6	+++

Figure 43 CP&F test results (a): Silver Sand

	Q_{mean}	P_1	P_2	P_3	P_{mean}	n	e	Obsevations:
1	0.79	0.08	0.07	0.08	0.08	47.23	0.90	Excess pp when compacting
2	0.80	0.05	0.06	0.06	0.06	45.03	0.82	Excess pp when compacting
3	0.81	0.05	0.04	0.05	0.05	43.40	0.77	Excess pp when compacting/ air bubbles on top
4	0.82	0.04	0.04	0.04	0.04	42.26	0.73	Air bubbles on top
5	0.42	0.04	0.03	0.03	0.03	40.45	0.68	Air bubbles on top / head adjusted
6	0.41	0.03	0.04	0.02	0.03	39.82	0.66	Long pause
7	0.86	0.03	0.03	0.03	0.03	41.07	0.70	Long pause / rapped
8	0.97	0.03	0.03	0.03	0.03	41.67	0.71	Rapped / piping
9	1.23	0.05	0.05	0.05	0.05	43.77	0.78	Rapped / piping / fluidized
10	1.49	0.08	0.08	0.05	0.08	44.68	0.81	Many air bubbles in specimen
11	10.50	0.54	0.53	0.55	0.54			Full Fluidization

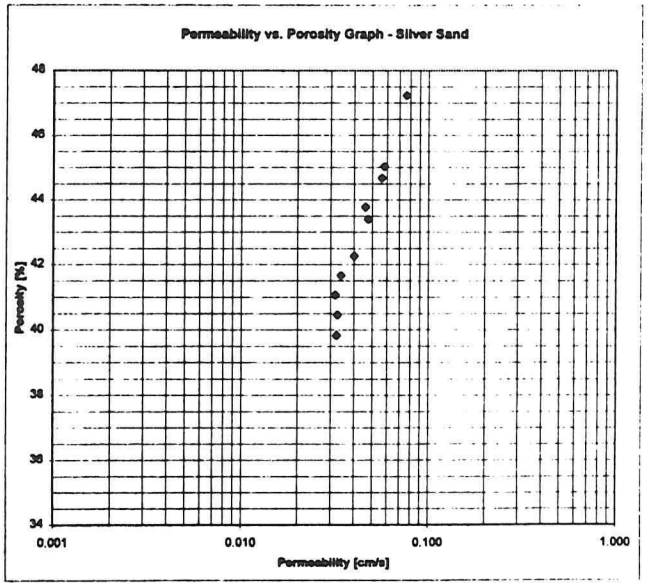

Figure 44 CP&F test results (b): Silver Sand

3 Sieve Analyses on Permeability & Fluidization Test Samples

To learn more about the composition of the samples testes in the permeability apparatus, sieve analyses were performed on all three main samples, within the framework of this graduate study. The sieve series NEN 480 were used, comprising the following sieves:

63 μm
90 μm
125 μm
180 μm
250 μm
500 μm
710 μm
1.0 mm
2.0 mm

The **sieve curves** are presented in Figure 45. The full sieve analyses data are presented in Figure **46 on page** 48 through Figure 48 on page 49.

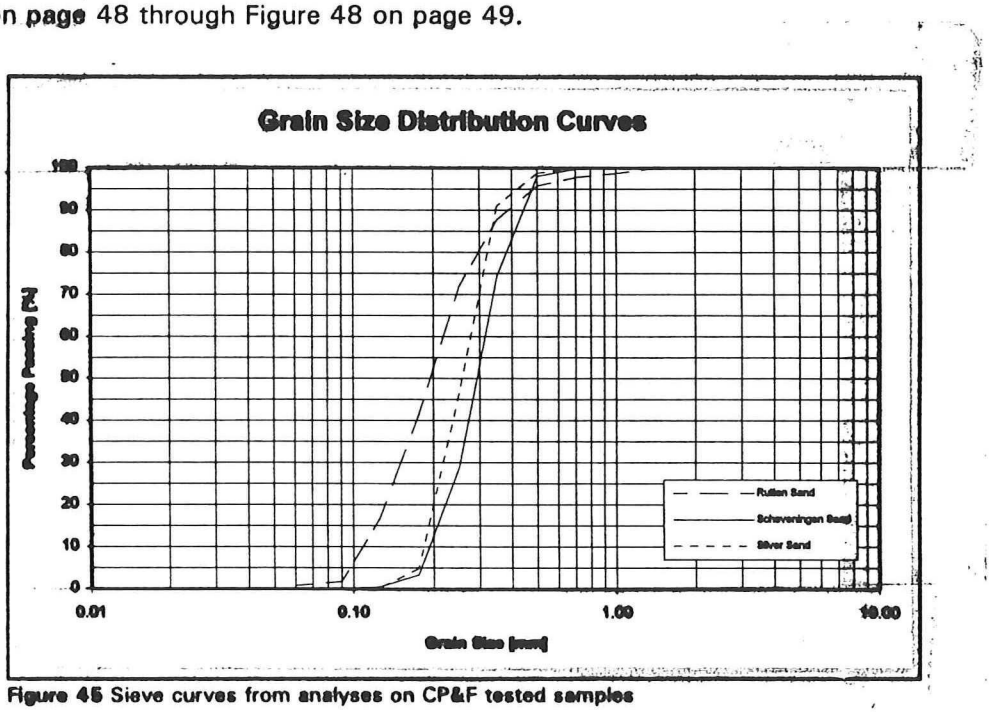

Figure 45 Sieve curves from analyses on CP&F tested samples

Sive Analyses on Sands Used in Combined Permeability & Fluidization Tests.

Sive Analysis 3: Rutten Sand
Delft University of Technology, Soil Mechanics Laboratory, June 25, 1996.

Weight Sand + Jar	586.11	gram
Weight Jar	161.58	gram
Weight Sand	424.53	gram

Sive	Weight Sive + Sand	Weight Sive	Weight Sand	% of Total	Corrected %	Cumulative %
1.400	378.84	378.29	0.55	0.13	0.13	99.87
1.000	369.14	364.36	4.78	1.13	1.13	98.74
0.710	394.08	390.00	4.08	0.96	0.96	97.78
0.500	401.61	392.87	8.74	2.06	2.06	95.72
0.350	374.70	340.78	33.92	7.99	8.00	87.72
0.250	442.19	375.13	67.06	15.80	15.82	71.90
0.175	498.87	368.47	130.40	30.72	30.76	41.14
0.125	456.33	351.89	104.44	24.60	24.63	16.51
0.090	349.44	286.88	62.56	14.74	14.76	1.75
0.063	346.52	342.42	4.10	0.97	0.97	0.78
-	351.23	347.91	3.32	0.78	0.78	0.00
	Sum Percentages			100	100	

Figure 46 Sieve data of CP&F tested Rutten Sand

Sive Analyses on Sands Used in Combined Permeability & Fluidization Tests.

Sive Analysis 2: Scheveningen Sand
Delft University of Technology, Soil Mechanics Laboratory, June 25, 1996.

Weight Sand + Jar	919.28	gram
Weight Jar	161.52	gram
Weight Sand	757.76	gram

Sive	Weight Sive + Sand	Weight Sive	Weight Sand	% of Total	Corrected %	Cumulative %
1.400	378.53	378.35	0.18	0.02	0.02	99.98
1.000	365.01	364.34	0.67	0.09	0.09	99.89
0.710	390.95	390.14	0.81	0.11	0.11	99.78
0.500	406.31	393.02	13.29	1.75	1.75	98.03
0.350	519.99	340.95	179.04	23.63	23.64	74.39
0.250	720.64	375.29	345.35	45.58	45.59	28.80
0.175	561.35	368.63	192.72	25.43	25.44	3.35
0.125	373.98	351.99	21.99	2.90	2.90	0.45
0.090	289.67	287.02	2.65	0.35	0.35	0.10
0.063	343.01	342.47	0.54	0.07	0.07	0.03
-	348.14	347.92	0.22	0.03	0.03	0.00
	Sum Percentages			100	100	

Figure 47 Sieve data of CP&F tested Scheveningen Sand

Sive Analyses on Sands Used in Combined Permeability & Fluidization Tests.

Sive Analysis 4: Silver Sand
Delft University of Technology, Soil Mechanics Laboratory, July 2, 1996.

Weight Sand + Jar	710.00	gram
Weight Jar	276.00	gram
Weight Sand	434.00	gram

Sive	Weight Sive + Sand	Weight Sive	Weight Sand	% of Total	Corrected %	Cumulative %
1.400	378.30	378.30	0.00	0.00	0.00	100.00
1.000	364.34	364.30	0.04	0.01	0.01	99.99
0.710	390.77	390.01	0.76	0.18	0.18	99.82
0.500	397.29	392.97	4.32	1.00	1.00	98.82
0.350	374.97	340.88	34.09	7.85	7.85	90.97
0.250	568.00	375.35	192.65	44.39	44.38	46.58
0.175	549.62	368.62	181.00	41.71	41.70	4.88
0.125	372.12	351.93	20.19	4.65	4.65	0.23
0.090	287.01	286.95	0.06	0.01	0.01	0.22
0.063	343.17	342.33	0.84	0.19	0.19	0.02
-	347.87	347.77	0.10	0.02	0.02	0.00
	Sum Percentages			100	100	

Figure 48 Sieve data of CP&F tested Silver Sand

4 Angularity Analyses on Permeability & Fluidization Test Samples

§ 4.1 Introduction and Aim of the Tests

It is suspected that the shape of the particles effects the fluidization limit and (hence) the critical void ratio, considerably. One way to quantify the *angularity* (or *roundness*) of the particles is to measure the time different fractions need to travel through a standard-sized mildly sloping rotating cylinder. This test is called the *rolability test* (see SCW (1979)).

Other attempts to quantify the shape of particles, objectively, have made use of the flow behaviour of particles. The *sharpness index* is related to the time different fractions need to flow out of a standardized funnel and made relative to the times measured for glass beads (0) and stone crusher sand (100), in the same apparatus (Volders & Verhoeven, see SCW (1979)).

Less objective, but a lot quicker, are microscopic analyses. In the next two paragraphs, microscopic analyses and determination of the Volders & Verhoeven sharpness index of the samples used in the combined permeability & fluidization tests, will be discussed.

§ 4.2 Microscopic Analysis of the Particle Shape

Powers (1953) categorized different particle shapes considering sphericity (high or low) and angularity (very angular, angular, sub-angular, sub-rounded, rounded or well-rounded). On the basis of this categorization, the tested sands were identified with a 25 x 0.6/4.0 microscope, as follows:

Sand	Sphericity	Angularity	Remarks	Categorization
Rutten Sand	Medium-sized fraction spherical. Other fractions less spherical.	All fractions a little angular.	Contains many organic (black) particles. Conglomerates of particles. Different colours.	High sphericity, sub-angular. *HS 40*
Scheveningen Sand	Main fractions seem spherical.	Mostly sub-rounded particles.	No organic material. Different colours.	High sphericity, sub-rounded. *HS 60*
Silver Sand	A little flat particles.	More angular than other sands. Sub-angular particles.	No organic material. White transparent colour.	Low sphericity, sub-angular. *LS 40*

It appeared very difficult to judge the total sharpness of the sands as the share of each fraction could not be quantified through the microscope. Therefore, it was decided to quantify the angularity with the method proposed by Volders & Verhoeven (see next paragraph).

The sand collected at the Scheveningen beach appeared to consist of three main fractions, which differed in size and colour. These fractions were analyzed separately:

Sand	Sphericity	Angularity	Remarks	Categorization
Scheveningen 0.35	Spherical.	Sub-rounded particles.	No organic material. Different colours.	High sphericity, sub-rounded. *HS 60*
Scheveningen 0.25	Spherical.	Sub-rounded particles.	No organic material. Different colours.	High sphericity, sub-rounded. *HS 60*
Scheveningen 0.175	Little spherical.	Sub-rounded particles.	No organic material. Different colours.	Low sphericity, sub-rounded. *LS 60*

The general conclusion, that must be drawn from this microscopic particle shape analysis, is that all particles have approximately the same shape. No extreme round or extreme angular materials were tested. To be able to be more specific on the influence of angularity, it may be advisable to test specimens on their fluidization limit with the same grading, but with more differently shaped particles.

§ 4.3 Volders & Verhoeven Sharpness Index

The *sharpness index* proposed by Volders and Verhoeven is related to the times five separated fractions need to flow out of a standardized funnel. The weighted average is made relative to the times measured for glass beads (0) and stone crusher sand (100), in the same apparatus. The following fractions, from over dry soils, are tested in quantities of 120 and 80 grams, when available (see Figure 49) for a schematic display of the VVS apparatus):

63 μm - 125 μm
125 μm - 250 μm
250 μm - 500 μm
500 μm - 1.0 mm
1.0 mm - 2.0 mm

If less than 120 grams, but approximately 80 grams is available, quantities of 80 and 60 grams are tested. If less than 60 grams is available, the whole quantity is testes twice.

Each tested fraction is inserted into the standardized funnel in an identical way through an insertion funnel. Next, the slide gate is opened and the time is measured, which is needed to let the material flow into the receiving dish.

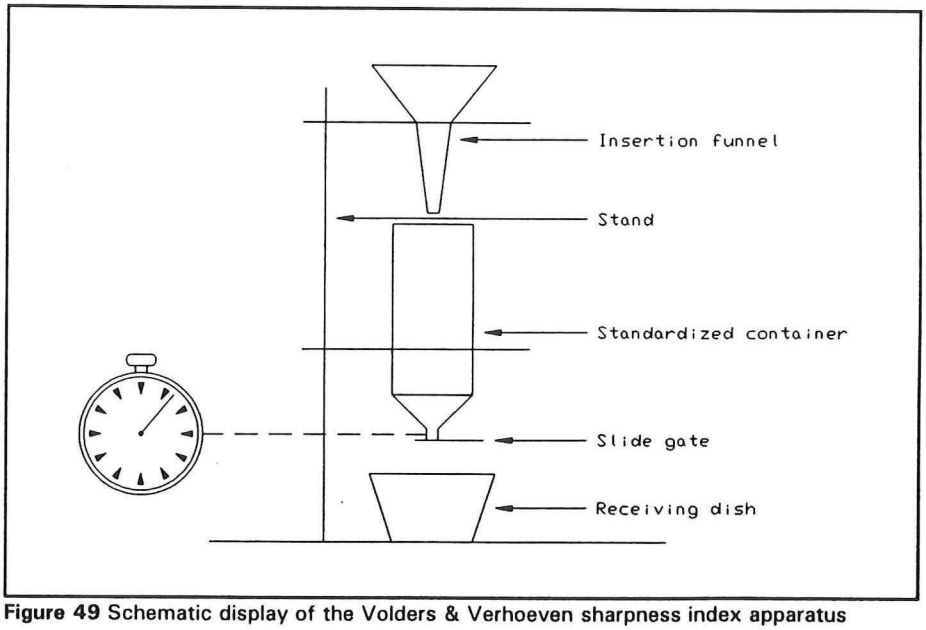

Figure 49 Schematic display of the Volders & Verhoeven sharpness index apparatus

The outflow time is made relative to the times needed for glass beads and stone crusher sand, before averaging for the successive tests per fraction (notation after Van Niekerk (1995)):

$$VVSI = 100\% \left[\frac{AOT_{wq} - AOT_{glb}}{AOT_{cs} - AOT_{glb}}\right]$$

in which AOT_{wq} is the average outflow time for the weighted quantities per fraction, glass beads and crusher sand (same weight quantities), respectively.

Next, to each fraction a weight is assigned, U_i, such that more weight is assigned to the finer fractions:

$$U_i = \left[\frac{1}{LL_i} - \frac{1}{UL_i}\right]\left[\frac{0.4343}{\log(UL_i) - \log(LL_i)}\right]$$

Together with the fraction size, $\%_i$, determined from sieve analyses, the overall sharpness index for the materials can be determined as follows:

$$VVS = \frac{\sum (\%_i\ U_i)}{\sum (\%_i + U_i\ /\ VVSI_{av})} \qquad for\ i = 1..5$$

For the three sands used in the combined permeability & fluidization tests, this procedure lead to the following sharpness indices. Note that now the Rutten Sand appears to be the most angular sand, which might be caused by the angularity of the finer fractions, and the Silver Sand is the least angular material:

Sand	VVS sharpness index
Rutten Sand	66.047
Scheveningen Sand	47.706
Silver Sand	51.696

5 Theoretical Maximum and Minimum Void Ratios of Spheres

The theoretical maximum and minimum void ratios are derived by considering the three-dimensional stacking of uniform distributed spheres. First, a repetitive unit is sought. Next, the volume of the box, defined by the moduli in three dimensions of the repetitive unit, is determined. The void ratios are calculated by dividing the box volume minus the volume of the spheres in the repetitive unit by the volume of the spheres, which is $4/3 * \pi * R^3$ per sphere, with R the radius of a sphere. For the loosest and the two densest packings the void ratios are thus determined (see also Figure 50).

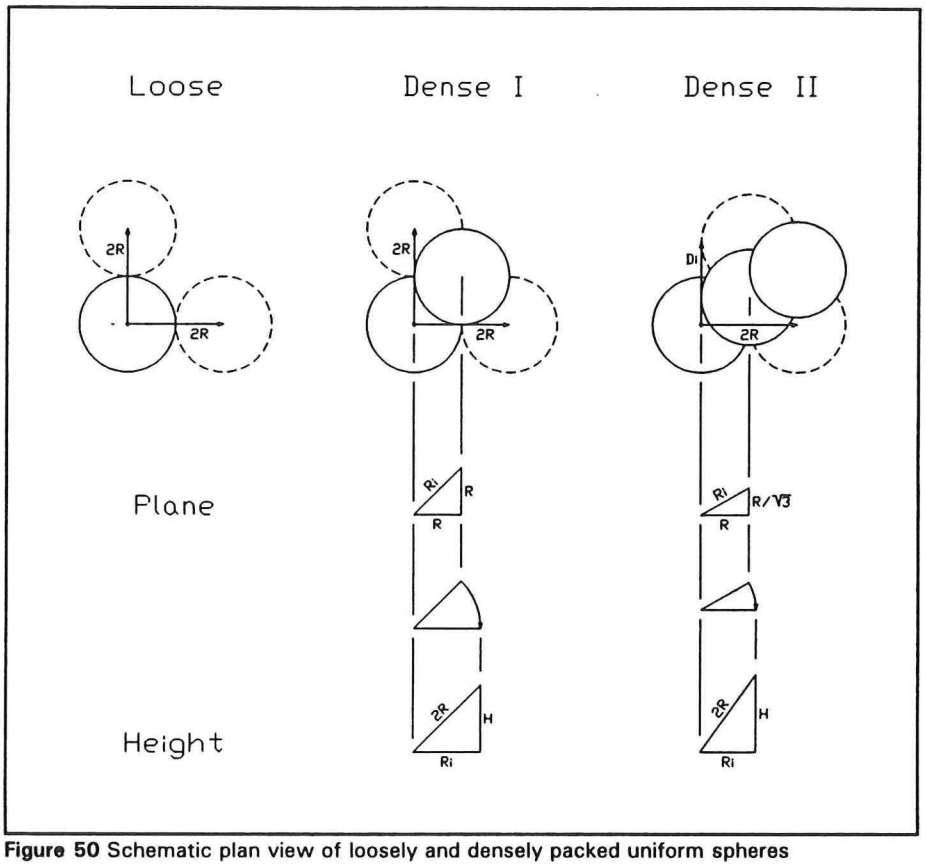

Figure 50 Schematic plan view of loosely and densely packed uniform spheres

Loosely packed: The repetitive unit for the most loosely packed state contains one sphere. Each sphere is situated at right angles to its neighbours. The moduli of a repetitive unit in three dimensions are all equal to $2R$. This leads to the following calculations:

$$V_{box,\ unit} = (2R)^3$$

$$V_{spheres} = \frac{4}{3}\ \pi\ R^3$$

$$e_{max} = \frac{V_{box,\ unit} - V_{spheres}}{V_{spheres}} = \frac{6}{\pi} - 1 \approx 0.91 \quad [-]$$

Densely packed I: The repetitive unit for the first densely packed state contains two spheres. Four spheres in the base plane are situated at right angles to their neighbours. The centerpoints of the spheres in the next layer coincide with the top of the square-based pyramid with constant rib, which has its base points at the centerpoints of the surrounding spheres in the base layer. The moduli of a repetitive unit in the base plane are equal to $2R$. The height of the unit equals two times the height of the pyramid, $2H$, which is $2R\sqrt{2}$. This leads to the following calculations:

$$V_{box,\ unit} = (2R)^2\ 2H = 8\ R^3\ \sqrt{2}$$

$$V_{spheres} = \frac{8}{3}\ \pi\ R^3$$

$$e_{min,\ I} = \frac{V_{box,\ unit} - V_{spheres}}{V_{spheres}} = \frac{3\sqrt{2}}{\pi} - 1 \approx 0.35 \quad [-]$$

Densely packed II: The repetitive unit for the second densely packed state contains three spheres. Three spheres in the base plane are situated with their centerpoints in a equilateral triangle. The centerpoints of the spheres in the next layer coincide with the top of the tetrahedron, which has its base points at the centerpoints of the surrounding spheres in the base layer. The moduli of a repetitive unit in the base plane are equal to $2R$ and Di, which is $R\sqrt{3}$. The height of the unit equals three times the height of the pyramid, $3H$, which is $R\sqrt{(4/3)}$. This leads to the following calculations:

$$e_{min,\ II} = \frac{V_{box,\ unit} - V_{spheres}}{V_{spheres}} = \frac{12\ R^3\ \sqrt{2}}{\pi} - 1 \approx 0.35 \quad [-]$$

Apparently, the two densely packed states have the same void ratios. The most loosely packed state and the second densely packed state are represented graphically in Figure 51 and Figure 52.

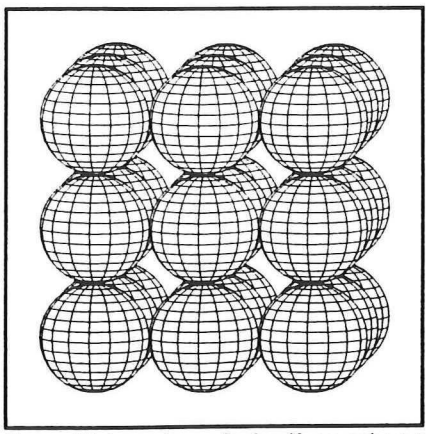

Figure 51 Loosely packed uniform spheres

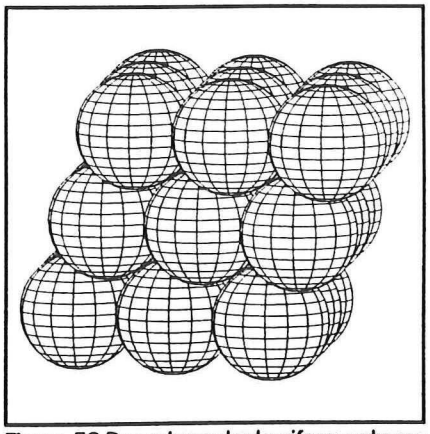

Figure 52 Densely packed uniform spheres

References

BOWELS J.E. (1992), *Engineering properties of Soils and their Measurement: International Editions*, 4th edition, Singapore: McGraw-Hill, Inc.

ISHIHARA K. (1986), *Stability of natural deposits during earthquakes*. Collected Papers Vol. **24**. Tokyo: University of Tokyo, Department of Civil Engineering.

NATIONAL GEOLOGICAL SURVEY (1984), Geological maps of The Netherlands and explanations. Haarlem: National Geological Survey.

NEDERLANDS NORMALISATIE-INSTITUUT (1993), *Dutch Standards (NEN), Geotechnics, TGB 1990 - Basic requirements and loads*. Delft: Nederlands Normalisatie-instituut.

NIEKERK A.A. VAN, *Establishing Complex Behaviour of Unbound Road Building Materials from Simple Material Testing (M.Sc. Thesis IP 44)*, Delft University of Technology, The Netherlands.

POWERS M. (1953), J SED PETR. 23: 117 - 119 (...)

SCHRIECK G.L.M. VAN DER (1996), *Baggertechniek deel V t/m VIII*. Lecture Notes. Delft: Delft University of Technology, Faculty of Civil Engineering.

SCW STUDY CENTRE FOR ROAD CONSTRUCTION (1975), *Classificatie van Zand*, Arnhem, The Netherlands.

SCW STUDY CENTRE FOR ROAD CONSTRUCTION (1979), *Various Properties of Natural Sands for Netherlands Highway Engineering*, Arnhem, The Netherlands.

YOUD T.L. (1973), *Factors controlling maximum and minimum densities of sands*, ASTM Special Technical Publications 523.